NOTICE

The quality of this microform is heavily dependent upon the quality of the original thesis submitted for microfilming. Every effort has been made to ensure the highest quality of reproduction possible.

If pages are missing, contact the university which granted the degree.

Some pages may have indistinct print especially if the original pages were typed with a poor typewriter ribbon or if the university sent us an inferior photocopy.

AVIS

La qualité de cette microforme dépend grandement de la qualité de la thèse soumise au microfilmage. Nous avons tout fait pour assurer une qualité supérieure de reproduction.

S'il manque des pages, veuillez communiquer avec l'université qui a conféré le grade.

La qualité d'impression de certaines pages peut laisser à désirer, surtout si les pages originales ont été dactylographiées à l'aide d'un ruban usé ou si l'université nous a fait parvenir une photocopie de qualité inférieure.

NL-339 (r. 88/04) c

Canada

A Multinuclear Magnetic Resonance Study of the Kinetics and Mechanisms of Dissociation of Cation Complexes with Ionophores

by Helen Patricia Graves Smith

a thesis presented at the University of Ottawa
in partial fulfillment of the requirements for the degree of Ph.D. in Chemistry

Department of Chemistry,
University of Ottawa,
Ottawa, Ontario.
Spring 1991

Christian Detellier
Research Supervisor

H.P. Graves Smith
Candidate

ISBN 0-315-68089-X

UNIVERSITÉ D'OTTAWA
UNIVERSITY OF OTTAWA

Table of Contents:

Acknowledgements:

Over the past few years I have benefited enormously from the guidance and teaching of my supervisor, Dr. Christian Detellier. I thank him for his efforts and patience as I have tackled these ideas in a bilingual environment. Our group has grown since my arrival in Ottawa. I have enjoyed the friendships, especially that of Dr. Kathleen M. Brière with whom I shared the path of graduate studies. Dr. Heather D. Dettman, Dr. Tony Williams and Mr. Raj Capoor of the NMR facility have all been helpful, especially Heather who endured my questions at nearly any hour of the day or night!

Girl Guides of Canada, FCAR (Fonds pour la Formation de Chercheurs et l'Aide à la recherche) and the faculty of Graduate Studies at the University of Ottawa are thanked for their financial support in the form of scholarships.

Mum and Dad have always supported my endeavours. I shared an apartment with my brother John for part of the time so he has been directly involved! I have always appreciated their support and encouragement. Finally, my husband Peter deserves a big vote of thanks, for his support, his patience, and his typing!

This thesis is dedicated to all of my family, and especially for my great aunt Auntie Nona who, like others of my elderly relations, did not have this wonderful opportunity for growth and learning through further education.

for Auntie Nona

Abstract

The behaviour of the cation - ionophore complexes in solution has been studied by ^{23}Na, ^{43}Ca and ^{13}C NMR. ^{23}Na NMR is an ideal tool for investigating the decomplexation of such complexes. The $(Na\text{-}DB24C8)^+$ and $(Na\text{-}18C6)^+$ complexes form quantitatively ($K_f > 10^5$) and may decomplex by either the dissociative or the metal associative interchange "M_{ai}" mechanisms. The $(Na\text{-}DB24C8)^+$ system follows the M_{ai} mechanism when either BPh_4^- or PF_6^- is the counter anion. The concentration of the counter anion does not influence the mechanism, but at higher concentrations the rate is slightly accelerated.

The $(Na\text{-}18C6)^+$ has been examined in AC (acetone), AN (acetonitrile), NM (nitromethane), PC (propylene carbonate), and PY (pyridine), with BPh_4^- as the counter anion. The dissociative mechanism is the only one operative in AC. The two mechanisms compete in AN, PC and PY. The kinetic parameters for the dissociative process have been calculated in these four solvents, while in PC the kinetic parameters of the M_{ai} mechanism were also accessible. An entropy-enthalpy effect was observed. In NM a kinetic study is precluded by the small difference in chemical shifts between free and complexed species.

The influence of the counter anion was studied by examining the changes which result when SCN^- replaces BPh_4^- for the $(Na\text{-}18C6)^+$ system in AC. With BPh_4^-, only the dissociative mechanism is operative, so if the presence of SCN^- were to change the mechanism this would be easily identifiable. Ion-pairing must be considered. All of the species were characterized, and the ion-pairing rate constants for the cation and complex were determined. The contributions to the observed rate constant could then be separated. The ion-paired complex, though 2.3±0.4 $kJ.mol^{-1}$ less stable, has a lower activation barrier (47.2±0.2 $kJ.mol^{-1}$ as compared to 49.5±0.2 $kJ.mol^{-1}$) and the faster rate of dissociation. ($(4.2\pm0.3)\times10^4 s^{-1}$ as compared to $(1.6\pm0.2)\times10^4 s^{-1}$) The presence of SCN^- accelerates the rate of the dissociative mechanism, rather than introducing another.

The ^{23}Na quadrupolar coupling constant is not accessible by ^{23}Na NMR. With the aid of ^{13}C NMR, and based on the assumption that the τ_{eff} measured for 18C6 is equivalent to the τ_c of the $^{23}Na^+$ it is complexing, a measure of the symmetry about the $^{23}Na^+$ is obtained. In AC, AN, and PC this environment is quite symmetrical (χ ~1.0-1.2 MHz). In PY the highly donating solvent competes with crown ether oxygens and in NM the high internal pressure of the solvent both lead to distortions of the complex from high symmetry and higher χ values result.

Lasalocid, a naturally-occurring ionophore, complexes with Na^+ cations. This compound can serve as both ligand and counter anion so the approach used for the $(Na\text{-}18C6)^+$ system gives some information, but does not describe it completely. The dissociative mechanism is operative in PY but other interactions are present. The tetra-carboxylic acid substituted 18crown6 ($18C6A_4$) was also studied in PY. Interactions between the Na^+ and $18C6A_4$ were observed by ^{23}Na NMR but were not quantified.

The ^{43}Ca nucleus is not as well-suited for NMR studies as ^{23}Na, since it is of low abundance and resonates at low frequencies. Despite these potential drawbacks an exploratory study in 50:50 AC:H_2O was made. The titration of $^{43}Ca^{++}$ by 18C6 could be followed, and the formation constant (K_f) was found to be 10±3.

List of Symbols and Abbreviations:

AC	acetone
AN	acetonitrile
DMC	dimethyl carbonate
DMF	dimethylformamide
DMSO	dimethyl sulphoxide
EtOH	ethanol
HMPA	hexamethyl phosphoramide
MeOH	methanol
NM	nitromethane
PC	propylene carbonate
PY	pyridine
THF	tetrahydrofuran

C222	cryptand-222
C222B	benzo-cryptand-222
18C6	18crown6
DB24C8	[4,4]-Dibenzo-24crown8
DC18C6	Dicyclohexyl-18crown6
GrA	Gramicidin A
Las	lasalocid A
X-537 A	lasalocid A

a_x	abundance of nucleus "x"
A^-	anion
AT	acquisition time
B	magnetic field
B_o	applied magnetic field
B_1	pulse of RF energy
C	crown ether
CW	continuous wave
D1	delay time
DN	Donor number
e	charge on the electron
E	energy
FID	free induction decay
FT	Fourier transform

ΔG^*	Gibb's free energy of activation
ΔG^*_{uni}	Gibb's free energy of activation for the dissociative mechanism
g	Landé splitting or g-factor
g_N	nuclear g-factor
h	Planck's constant
$\hbar$	Planck's constant / 2π
ΔH^*	enthalpy of activation
I	spin quantum number
K_f	formation constant
K_{CIP}	ion-pairing constant of the complexed ion
K_{IP}	ion-pairing constant of the solvated ion
$k_A + k_B$	pseudo-first order rate constants
k_A, k_{-1}, k_{-1}'	rate constant of dissociation
k_B, k_1	rate constant of formation
k_2	rate constant of the M_{ai} mechanism
$k_{-1,obs}$	observed rate of dissociation
k_B	Boltzmann constant (eq. 71)
M	magnetization
M^+	free cation
MC^+	cation-crown ether complex
m_e	mass of the electron
m_N	mass of the nucleus
N	number of active nuclei (eq. 14)
NOE	nuclear Overhauser effect
P_A, P_B	populations of sites A and B
P	angular momentum (eq. 2)
R_x	receptivity of nucleus "x"
R	gas constant
R	quantum number (eq. 2)
RF	radio frequency
S	observed signal height (eq. 14)
ΔS^*	entropy of activation
T	temperature
T_1^{-1}	spin-lattice, longitudinal relaxation rate
T_2^{-1}	spin-spin, transverse relaxation rate
$T_{2,obs}^{-1}$	observed transverse relaxation rate
$T_{2,inh}^{-1}$	inhomogeneity contribution to the transverse relaxation rate
$T_{2,ex}^{-1}$	exchange contribution to the transverse relaxation rate

$T_{2,ex,lim}^{-1}$	detectable limit to the exchange contribution to the transverse relaxation rate
$T_{2,q}^{-1}$	quadrupolar contribution to the transverse relaxation rate
$T_{1,q}^{-1}$	quadrupolar contribution to the longitudinal relaxation rate
$T_{1,DD}^{-1}$	dipole-dipole relaxation rate
W_x	rate constant for transitions (Fig. 6)
Z	charge number of the nucleus
$\nu_{\frac{1}{2}}$	linewidth at half-height (Hz)
ν	frequency of electromagnetic radiation
ϵ	dielectric constant
μ	magnetic moment
μ_B	Bohr magnetron
μ_N	nuclear magnetron
ϖ_o	Larmour precession
χ	quadrupolar coupling constant
δ_A,δ_B	chemical shifts of species A and B (in ppm)
τ	recovery time (eq. 19-21)
τ_c	correlation time
τ_A,τ_B	lifetime of species A and B
ν_A,ν_B	chemical shifts of species A and B (in Hz)
η	viscosity
ρ	$[ligand]/[cation]_T$
γ	gyromagnetic ratio

List of Tables:

List of Figures:

Chapter 1
Introduction

Ionophores are substances with the ability to promote the transfer of ions from an aqueous medium into a hydrophobic phase. The exact identities of these phases varies from a two-phase chloroform and water system to a lipid bilayer or a biological membrane. Almost simultaneously, in the 1960's, the ionophoric properties of certain naturally occurring compounds were discovered and synthetic compounds with similar capabilities emerged. The crown ethers provide a useful model for the study of the various factors which influence ionophoric activity. With a synthetic compound such as a crown ether the number of coordinating sites, their nature and their arrangement can be varied systematically.[1]

1.1 Biological and Pharmacological Aspects

1.1.1 Alkali and Alkaline-earth metals

The principal extracellular cation in mammalian cells is Na^+ (133-145mM), while the principal intracellular cation is K^+ (100-160mM).[3a] Sodium and calcium ions occur in similar fluids, such as extracellular muscle fluid and blood. Each of these ions has a multitude of regulatory or metabolic tasks and various passive and active carrier-like transport devices coupling its movement to that of another ion. All three are pumped "uphill" by ATP-driven pumps.[3b] Ionic gradients exist in most cell types. In the red blood cells of most species the concentration of K^+ is thirty times greater in the cell. The concentration of Na^+ is six times greater in the plasma. The gradients in skeletal muscle cells are larger.[3a] The cell membrane enzyme Na^+-K^+-ATPase hydrolyzes ATP in the presence of

Na^+, K^+ and Mg^{++} and thus regulates ion movements. It is the splitting of the ATP which provides the energy for the active transport of Na^+ and K^+.

Ca^{++} ions play an important regulatory role in most cellular processes. Muscle contraction is a well known example.[2] At rest Ca^{++} ions are pumped into the sarcoplasmic reticulum by Ca^{++}-ATPase, an enzyme similar to Na^+-K^+-ATPase. Upon excitation of the sarcoplasmic reticulum membrane, large amounts of Ca^{++} are released into the cytoplasm and a muscle contraction is triggered. The movements of Ca^{++} clearly show how binding affinity is important in regulatory roles.

1.1.2 Ionophores

Most of the transport phenomena in cells are usually due to biological carriers, such as Na^+-K^+-ATPase mentioned above. These carriers do not need to migrate physically in order to transport since they span the membrane. The ion interacts sequentially with specific sites on the enzyme as the latter undergoes conformational changes.[3a] The characteristics of the active site, such as configuration and conformation, make it selective for specific ions. A disruptive version of transport can be carried out by naturally occurring ionophores or antibiotics, which are metabolites of microorganisms. These compounds influence the cation transport across membranes by increasing their permeability to ions. Ionophores serve as passive carriers by diffusing back and forth across the membrane, transporting ions in each direction (as will be seen in Section 1.4).

Model ion channels based on peptide monomers of natural channels covalently linked to a carrier template such as a crown ether have been synthesized. The resulting ion channels can be incorporated into lipid bilayers to study their electrical properties.[3c-e] These synthetic channels have been characterized as not discriminatory with respect to Na^+ and K^+, though they do differentiate between anions and cations. Channel lifetimes for authentic systems are

in the millisecond range and these synthetic channels are also thus characterized. Variation in the amino acid sequencing in these channels, and the consequent changes in the nature of the channel provide insight into the role of each component in this natural channel structure. Structure-function relationships are expected to be more readily elucidated through the use of these channels.

The biological carriers, which regulate the specific ion concentrations and gradients, can be overwhelmed by the presence of antibiotic ionophores. As an example one can consider the function of mitochondria which is to convert the potential energy of different food materials into a usable form of energy for the cell, such as ATP. Their membranes are not usually penetrable by K^+ ions, but when valinomycin, an antibiotic ionophore, is incorporated, K^+ ions enter and the cell's energy is not used to make ATP.

Crown ethers are very simple compounds, easily synthesized, providing a simple model for the mechanistic role of naturally occurring ionophores. One of the mechanisms for the exchange of sodium cations between crown ether complexes discussed in this thesis (the M_{ai} mechanism) involves the approach of two positively charged species towards each other. This finding may be relevant to the observation that many ion channels, including one in canine cardiac sarcoplasmic reticulum, are occupied by more than one ion at a time.[3f] This is another example of circumstances where the charge-charge repulsions are overcome.

The gap between chemistry and biology is being bridged as channels are synthesized by the biologists using peptides[3c-e], and substituted crown ethers are incorporated into bilayer membranes by chemists[30]. The mechanisms and interactions for any particular system may provide the key to deciphering the action in another.

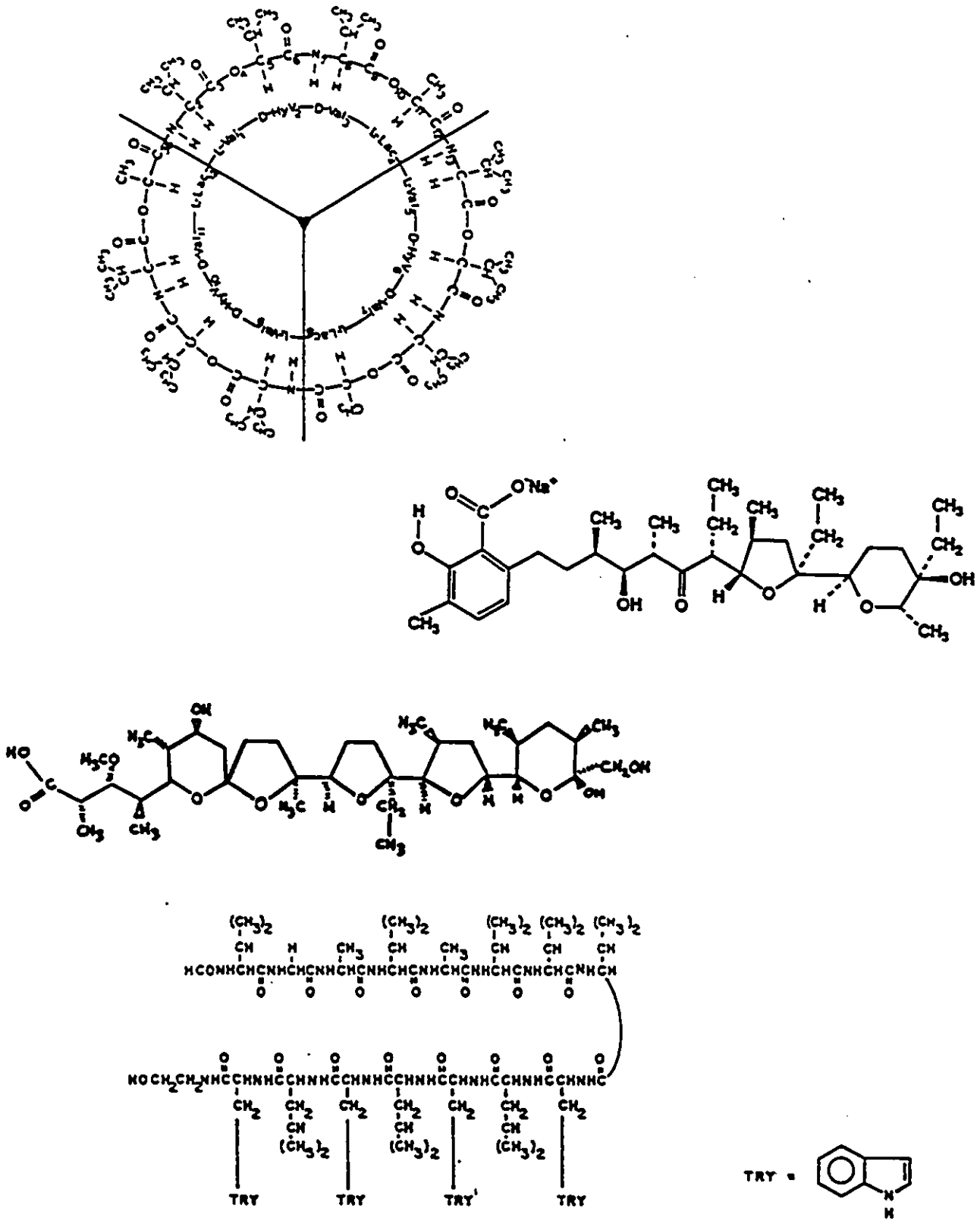

Figure 1: Naturally-occurring ionophores. (a) valinomycin; (b) lasalocid A; (c) monensin; (d) gramicidin A.

1.2 Chemical Applications of Ionophores

Ionophores are not just a subject of study in themselves but have uses for chemists studying other systems. One application of ionophores has been their role as the ion-selective components in liquid membrane electrodes. Cation-specific electrodes employing ionophores have been developed for Li^+, Na^+, K^+, NH_4^+ and Ca^{++} to name but a few.[1]

Synthetic organic chemists have put crown ethers to use. Inorganic salts such as NaOH, KOH or $KMnO_4$ are not readily soluble in nonpolar solvents like toluene, benzene or THF. When the crown ether whose cavity suits the cation is added, the salts dissolve. Pre-dissolving in MeOH, followed by evaporation leads to 1N solutions of NaOH or KOH in benzene if DC18C6 is used.[1]

1.3 Classes of Ionophores

The family of ionophores can easily be divided into different classes based upon origin and nature. For this study four groups are adequate, and examples for each class are given.

1.3.1 Natural neutral ionophores

Valinomycin is a neutral ionophore which forms a charged species when complexed with an alkali metal cation. It is a depsipeptide, meaning that it is built from alternating amino acid and hydroxy acid residues. (see Figure 1a)

1.3.2 Natural carboxylic ionophores

Lasalocid A (X-537A) and monensin are both anionic molecules which form neutral complexes with alkali metal cations. (see Figure 1b and 1c) They and the other ionophores in this class, are produced by *streptomyces* cultures. These open-chain polyether molecules are terminated by a carboxyl group at one end and by one or two hydroxyl groups at the other. Hydrogen bonding between the two ends forms the macrocycle. Monensin has shown a preference for complexing Na^+ over K^+ while lasalocid is much less selective, complexing most mono- and divalent cations.[1]

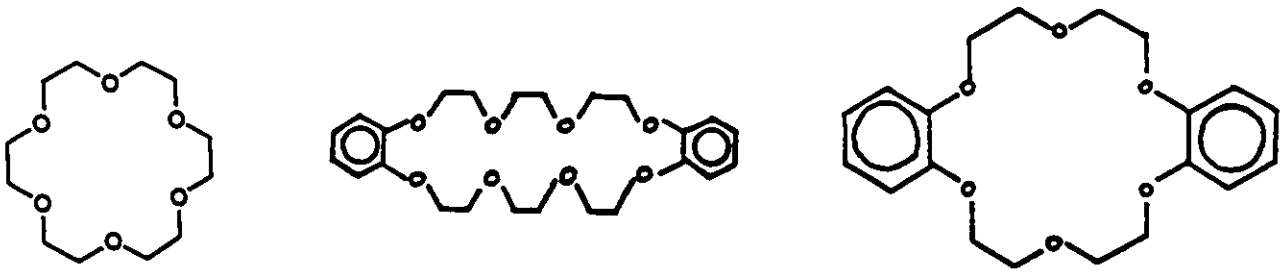

Figure 2: Crown ethers. (a) 18-crown-6; (b) [4,4]-DB24C8; (c) [3,3]-DB18C6.

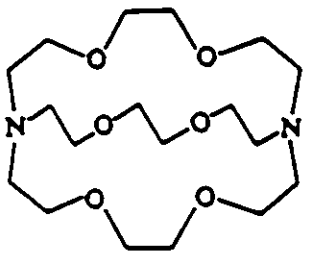

Figure 3: Cryptand. C222.

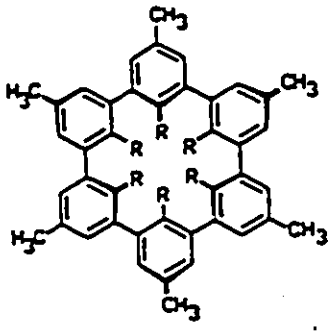

Figure 4: Spherand.

1.3.3 Synthetic ionophores

Within the class of synthetic ionophores are the crown ethers, the cryptands, the spherands and the podands. In 1967 Pedersen published the first report of crown ethers.[4,5] A small yield (~0.4%) of white crystals, silky and fibrous in structure, was not ignored but investigated. Pedersen had observed the apparent insolubility in hydroxylic solvents and was curious to know more. The compound's increased solubility in the presence of sodium ions was explained when the structure of the compound, DB18C6, was derived. The common names for these compounds are based on the side-ring substituents, the number of oxygen atoms in the main ring and the size of that ring (for example: DB18C6, 18C6, DB24C8). (see Figure 2) They are much less cumbersome than the IUPAC names and are given below:

18C6 = 1,4,7,10,13,16-hexaoxacyclooctadecane

[4,4]-DB24C8 = 6,7,9,10,12,13,20,21,23,24,26,27-dodecahydrodibenzo-[b,n][1,4,7,10,13,16,19,22] octaoxacyclotetracosin.

[3,3]-DB18C6 = 6,7,9,10,17,18,20,21-octahydodibenzo[b,k][1,4,7,10,13,16]-hexaoxacyclooctadecin.

The aromatic crown ethers are generally neutral, colourless compounds, which are sparingly soluble in water and alcohols, moderately soluble in aromatic solvents and very soluble in dichloromethane and chloroform. The saturated crown ethers in general are much more soluble in all solvents, and the majority are soluble in petroleum ethers too.[6] The fact that crown ethers complex alkali metal cations preferentially makes them unique. The relative sizes of the cations and the crown ether cavities are a factor in determining the stoichiometry of complexes. (see Table I) Gokel et al synthesized crown ethers possessing ligating arms, and called them lariat ethers. The flexible arm can overlay the cavity so that the complexed cation is further encapsulated.[7]

Table I: Some diameters of cations and the cavities of crown ethers.

cation	size (Å)	crown ether	size (Å)
Li^+	1.36	15C5	1.7 - 2.2
Na^+	1.94	18C6	2.6 - 3.2
K^+	2.66	21C7	3.4 - 4.3
Rb^+	2.94		
Cs^+	3.34		
Ca^{++}	1.98		
NH_4^+	2.86		

The crown ethers are part of the larger family of compounds called the coronands, to which cryptates also belong.[8] Jean-Marie Lehn et al synthesized the first one, C222, in the fall of 1968.[9] These compounds are commonly named by the number of oxygens in each of the three links between two N atoms (see Figure 3). Substituents are identified at the end of the name, as in benzo-cryptand-222 = C222B. These compounds, by nature, provide spherical recognition of ions and are characterized by high stability and selectivity, slow exchange rates and relatively effective isolation of the bound substrate from the surrounding environment and solvent molecules.

Donald J. Cram entered this field in 1970, publishing in 1973 the articles on spherands, another class of the coronand family.[10,11] Unlike crown ethers and cryptates which are not always in conformations where the cavity is evident and available, spherands were designed so that the oxygen atoms are permanently in an octahedral arrangement about a spherical cavity. (see Figure 4). Podands, the class of acyclic hosts, are not pre-organized for binding like the spherands and are the least likely to bind their most complementary guests as compared to the other classes. They must undergo the most conformational changes in order to be in a suitable configuration for complexation.

Of course, since the work of Pedersen, Lehn and Cram, for which they received the Nobel Prize in Chemistry in 1987, other classes of compounds which may complex ions have

been synthesized. These include the catenands[12] and a trefoil knot[13], though these synthetic wonders involve complexation during their synthesis more than afterwards.[14]

1.3.4 Quasi-ionophores

The ionophores in the previous three classes transport ions across liquid membranes by enclosing the cations, replacing the solvation shell by oxygen functions. They are carriers. Channel-forming molecules have been dubbed "quasi-ionophores".

Sarges and Witkop reported the structure of Gramicidin A (GrA) in 1965.[15] (see Figure 1d) It dimerizes by hydrogen bonding and spans the membrane bilayer. The channels may last as long as a minute or as short as 30 ms. Once formed sodium ions flow through at a rate of 10^7 ions/second. These channels are 4-5 Å in diameter and 20-30 Å long. Their dimensions vary with what is passing through them. If Cs^+ ions are occupying the channels they measure 5Å × 32Å, but they will become 6.8Å × 26Å if K^+ ions are passing though.[16]

1.3.4.1 NMR Studies on Gramicidin A

Urry et al have used several different nuclei in their studies of GrA.[17-20] One ^{13}C NMR study verified the incorporation of GrA into lecithin micelles[17] while another estimated binding constants for potassium and thallium ion binding and suggested that two ions may be accommodated in the channel under the conditions used for these studies.[18] The binding constants for cesium ions were determined using ^{133}Cs NMR T_1 values.[19] ^{39}K NMR relaxation times were used to calculate binding constants and channel conductances were calculated and compared for K^+, Na^+ and Rb^+.[20]

Hinton et al have used ^{205}Tl NMR in their investigations on GrA.[21,22] Once the binding of the Tl^+ was investigated that nucleus was used in competitive studies with alkali metal cations. A comparison between the equilibrium binding constants obtained by different techniques for a given system shows some variation. The use of differing theoretical models is one of the reasons cited to explain these variations.

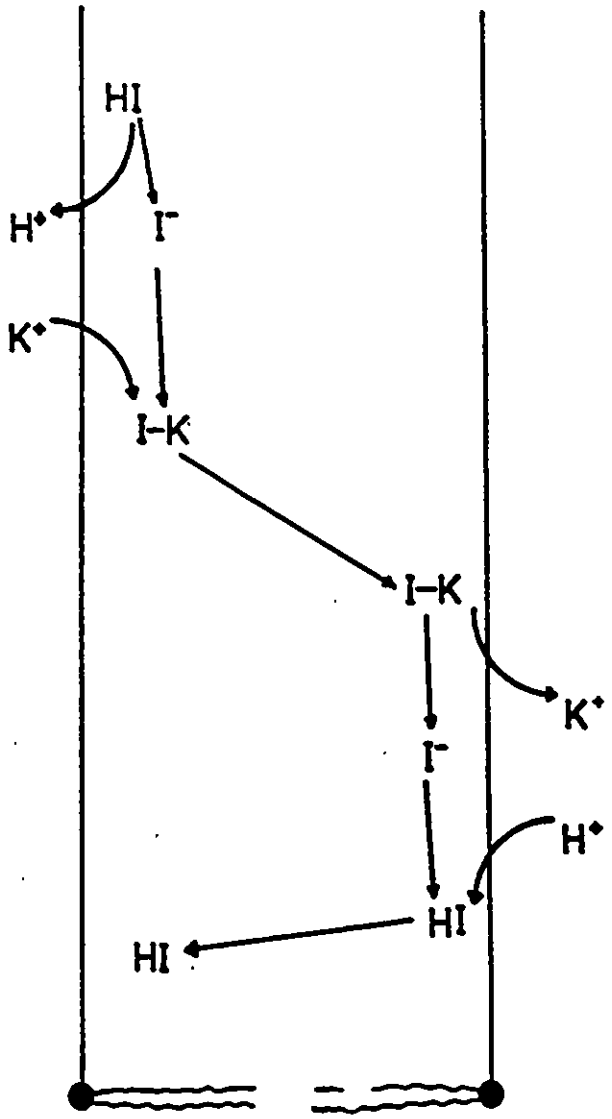

Figure 5: The transport of ions across a liquid membrane.

1.4 Transport across membranes

There are three methods of crossing a membrane. They may be traversed through pores, which are transient holes in the membrane. A hole can also be created by a defined molecule such as gramicidin. This is usually a channel with a polar interior and a nonpolar exterior. An ion carrier must have special characteristics in order to achieve its goal. Just like the channel, it needs a polar part to interact with the cation and a nonpolar part to solubilize it in the lipophilic membrane. This is usually obtained by facing the oxygen atoms towards the inside where they coordinate with the cation, leaving the more lipophilic portion of the molecule facing outwards.[23]

There are four steps in the transport of ions, with an ionic gradient, across a liquid membrane, by membrane-soluble ionophores. (see Figure 5) First the cation is complexed at the interface, then the complex diffuses across the membrane to the interface where decomplexation occurs. Finally the carrier diffuses back to the starting point in order to be ready to repeat the process.[24] This transports the ion in the direction of its gradient but, biologically, the both processes may be relevant. Through coupling with a proton transport in the opposite direction, in a pH gradient, this may be achieved. Fyles et al have studied this with carboxylic acid substituted crown ethers.[25] ^{23}Na, ^{39}K, and ^{7}Li NMR have been used to study the transport of these cations, mediated by monensin, across phospholipid bilayers.[26,27]

Synthetic channels, which incorporate crown ethers, and other membrane models have been reported.[28-32] Choy et al developed a carrier-containing membrane which has monensin in an octanol solution with a 0.1N NaOH solution on one side and 0.1N NaCl and 0.1N HCl on the other[28] but Behr et al actually formed a macrocyclic K^+ complex which provides a model for a K^+ channel.[29] It is a tetrasubstituted crown ether-K^+ complex which stacks in the crystal form in such a way that the characteristics of channels are fulfilled. Fyles et al have developed the channel formation further.[30,31] Their ion channel mimic uses a 18C6 hexa-acid as the framework to support the channel walls. Nakano et al[32] linked three

diaza-18C6 with dodecyl chains to allow the relay from ring to ring of the transported ion.

A model for the movement of an ion through a channel was proposed by Andersen[33] and involves five steps, as summarized in Table II. Cornélis and Laszlo used ^{23}Na NMR to identify specific cationic binding sites at the entrance of the GrA channel.[34] Fast exchange between a bound site on the GrA and the free ion was observed in an EtOH:H_2O (90:10) binary mixture. This is rapid compared to the transport process, but is believed to provide a 'reservoir' with respect to the slower diffusion from outer to inner sites.

Table II: The Five Steps in the Movement of an Ion through a Channel

1 DIFFUSION	towards the channel
2 ASSOCIATION	with the channel entrance
3 TRANSLOCATION	through the channel interior
4 DISSOCIATION	from the channel exit
5 DIFFUSION	away from the channel

1.5 NMR

Association and dissociation are important steps in both the transport of ions across a membrane (see Figure 5) and the movement of ions through a channel (see Table II). The understanding and knowledge of the mechanisms of these two processes is essential, and the study of model systems can provide the necessary details. There are several techniques which can be used to access this information, including nuclear magnetic resonance (NMR).[35] In Chapter 2, systems studied by NMR and by other techniques are discussed in more detail.

NMR was the principal tool used for this research. This technique is relatively young. In 1945 Bloch ran the first ^1H NMR experiment. Four years later the chemical shift effect was discovered. Being able to see more than one peak certainly increased the usefulness of this technique. In 1953 the first commercial NMR spectrometer entered the market, with the

capacity for ^{1}H NMR. ^{13}C NMR was not observed until 1957, but it took until 1965 for proton-decoupling of ^{13}C spectra to be both understood and accomplished. The following year the greatest step was made. Previously all spectrometers were continuous wave (cw), but in 1966 the first Fourier Transform (FT) NMR spectrometer was introduced. Since the early 1970's FT NMR spectrometers have become much more readily available and more affordable. This has allowed the field of NMR to flourish so that now higher field instruments, 2- and 3-D experiments, in vivo experiments and many fancy pulse sequences are all reality and the development continues.[36,37]

NMR spectroscopy, like any other form of spectroscopy, may be defined as the interaction between matter and electromagnetic radiation such that energy is either emitted or absorbed according to the Bohr frequency condition.

$$\Delta E = h\nu \qquad \text{equation 1}$$

where h is Planck's constant, v is the frequency of the electromagnetic radiation and ΔE is the difference in energy (normally quantized) between the initial and final states of the matter.

Modern chemical physics postulates that the total angular momentum of any isolated particle is quantized. It cannot have any arbitrary value and its magnitude (P) can be specified in terms of a quantum number, here it is R.

$$P = \hbar[R(R+1)]^{\frac{1}{2}} \qquad \text{equation 2}$$

$\hbar$ is Planck's constant (h) divided by 2π, and R may be either half-integral or integral. The modes of motion which contribute to the total angular momentum may be treated individually. Each could be assigned a quantum number specifying the angular momentum due to that particular mode of motion.

Since angular momentum is a vector quantity, its direction must be specified. Another quantum number, such as m_R, is used so that the angular momentum in the direction of z, P_z, is expressed as:

$$P_z = \hbar m_R \qquad \text{equation 3}$$

m_R has (2R+1) values being R, R-1, R-2 ... -R.

When discussing NMR, the most pertinent type of angular momentum is that of nuclear spin. It is the transitions between the nuclear spin energy levels which give rise to the NMR phenomenon. For nuclei other than ^1H, the spin angular momenta of the individual nucleons couple giving a total spin angular momentum which is characterized by the spin quantum number I.

$$P_I = \hbar[I(I+1)]^{\frac{1}{2}} \qquad \text{where } m_I = I, I-1, I-2 \ldots -I. \qquad \text{equation 4}$$

If a charged body moves, there is an associated magnetic field. On the atomic scale for when electrons and nuclei possess angular momentum there is a magnetic moment.

The Landé splitting factor (or g-factor) is included in order to quantitatively relate the magnetic moment (μ) and the angular momentum (P).

$$\mu = -g\mu_B P/\hbar \qquad \text{equation 5}$$

where μ_B is the Bohr magnetron, which is defined in equation 6:

$$\mu_B = \left(\frac{eh}{4\pi m_e}\right) = 9.27410 \times 10^{-24}\ J/T \qquad \text{equation 6}$$

where e is the charge on the electron and m_e is the mass of the electron.

Equations 5 and 6 are related to electrons but analogous equations may be formulated for nuclei. The spin motion of a nucleus and the nuclear magnetron (μ_N) are thus established, relating the magnetic moment to the mass (m_N) and charge number (Z) of the nucleus. The nuclear magnetron is based on the proton.

$$\mu \propto \left(\frac{Ze}{2m_N}\right) P \qquad \text{equation 7}$$

$$\mu_N = \left(\frac{eh}{4\pi m_p}\right) = 5.05095 \times 10^{-27} J/T \qquad \text{equation 8}$$

In order that other nuclei may be considered, once again a nuclear g-factor is introduced:

$$\mu = g_N \mu_N P/\hbar \qquad \text{equation 9}$$

Nuclear g-factors are not the usual way of referring to nuclear magnetic moments, gyromagnetic ratios (γ) are more common.

$$\gamma = \frac{g_N \mu_N}{\hbar} = \frac{\mu}{P} \qquad \text{equation 10}$$

When a nucleus is placed in a magnetic field (B), which is oriented along the z-axis, the magnetic moment has an energy (E):

$$E = -\mu_Z B \qquad \text{equation 11}$$

In terms of the gyromagnetic ratio (γ) the energy is:

$$E = -\gamma \hbar m_I B \qquad \text{equation 12}$$

with (2I+1) nondegenerate energy levels, each separated by $\gamma\hbar B$.

The appropriate electromagnetic radiation can induce transitions, the selection rule for which is $\Delta m_I = \pm 1$. The frequency of radiation (ν) thus becomes:

$$\nu = \frac{\gamma}{2\pi} B \qquad \text{equation 13}$$

Since the resonance frequency is proportional to the magnetic field either ν or B may be varied in order to achieve resonance.

The theory discussed so far, has dealt with individual nuclear spins, but any observed signal would be the total of the contributions of many nuclei. The observed signal area (S), when the applied field (B_o) and the temperature (T) are constant is:

$$S \propto \gamma^3 N[I(I+1)] \qquad \text{equation 14}$$

where N is the number of active nuclei present.

The receptivity of a nucleus represents its suitability for NMR and relates the natural abundance of the NMR-active nucleus as follows:

$$R_x = a_x \gamma_x^3 [I_x(I_x+1)] \qquad \text{equation 15}$$

Of more practical use is the receptivity relative to another nucleus, such as ^{13}C or ^{1}H. Equation 15 then becomes:

$$R_x^y = \frac{a_x \gamma_x^3 [I_x(I_x + 1)]}{a_y \gamma_y^3 [I_y(I_y + 1)]} \qquad \text{equation 16}$$

These equations form the basis for NMR. NMR is the principal technique used in this thesis. Fourier transform solution NMR is the specific type of NMR used.

1.5.1 Fourier Transform NMR

To summarize FT NMR in a few steps it can be said that:

1- The sample is irradiated with a brief burst of radio frequency energy at such a power that all the nuclei across a frequency range of tens of kHz are excited.

2- A sinusoidal current is induced in the receiver coil, and in the time after the RF pulse it decays. This is known as a free induction decay (FID).

3- Once the RF pulse finishes the nuclei relax to their Boltzmann distribution.

4- The FID plot of absorbtion versus time is Fourier transformed so an absorbtion versus frequency plot may be seen. This is the form similar to that seen on a Continuous Wave (CW) spectrum.

The brief burst of RF energy (B_1), known as a pulse, is perpendicular to the B_o. At resonance the effective B (B_e) is the same as B_1. If B_1 is the correct amplitude and duration, a 90° rotation of the magnetization (M) is produced. M will tend to realign with B_o once the pulse has stopped. The rate of this form of relaxation is the spin-lattice or longitudinal relaxation rate (T_1^{-1}).

T_2^{-1}, the spin-spin or transverse relaxation rate, depends upon the precession of M in the (x′,y′) plane of the rotating frame. Since there are inhomogeneities in the field there is a lack of coherence. Since observation is along the y′ axis only those components of the signal are viewed. This signal gradually decays to zero. In the FID, the period of the sine wave gives its frequency. Where more than one signal is present the FID represents a sum of sinusoids and is an interferogram.

The Bloch equations describe relaxation in terms of a first order kinetic process.

$$\frac{d(M_z - M_o)}{dt} = \frac{-(M_z - M_o)}{T_1} \qquad \text{equation 17}$$

$$\frac{d\,M_y}{dt} = \frac{-M_y}{T_2} \qquad \text{equation 18}$$

Integration gives:

$$M(t)-M_o = [M_z(0)-M_o]\ e^{-\tau / T_1} \qquad \text{equation 19}$$

This means that with a 90° pulse, $M_z(0)=0$ and:

$$M_z(t) = M_o(1- e^{-\tau / T_1}) \qquad \text{equation 20}$$

so after $t = 10T_1$, 99.995% of the signal is oriented with M_o.

1.5.2 T_1 Measurements

The T_1 can be a valuable piece of information. The technique which was used to measure T_1 values was the inversion-recovery technique.

$$(-180°-\tau-90°-AT-D1)_n \qquad \text{expression 21}$$

This means that the 180° pulse inverts the magnetization, which begins to relax during time τ. In order to observe the extent of relaxation a 90° pulse must be applied, which is followed by acquisition of the FID. The acquisition time plus the delay before the cycle is repeated (AT+D1) must total more than the time for $4T_1$ since the nuclei must be relaxed before another pulse is applied. The experiment involves the acquisition of at least seven spectra with different τ delays, since an equation with 3 parameters is being solved:

$$M_z(t) = M_o(\ 1-a\ e^{-\tau / T_1}) \qquad \text{equation 22}$$

$M_z(t)$ is measured for varying τ values so the three unknowns are: M_o, a and T_1.

1.5.3 T_2 Measurements

Under extreme narrowing conditions ($\varpi_o\tau_c << 1$), where ϖ_o is the Larmour precession frequency and τ_c is the correlation time of the nucleus, transverse relaxation times may be obtained, for a liquid, from the Lorentzian lineshape in the frequency domain.[38]

$$\nu_{\frac{1}{2}}\,(\text{Hz}) = \frac{1}{\pi T_{2,obs}} \qquad \text{equation 23}$$

For ^{23}Na NMR, for one species in solution, such as Na^+ (solvated), the $T_{2,obs}^{-1}$ contains an inhomogeneity contribution. Under extreme narrowing conditions, $T_{1,q}^{-1}$ should equal $T_{2,q}^{-1}$.

$$T_{2,obs}^{-1} = T_2^{-1} + T_{2,inh}^{-1} \qquad \text{equation 24}$$

1.5.3.1 Spin Echo Measurements

Spin echo techniques are one way to access T_2^{-1} relaxation rates. They force the system back to equilibrium rather than waiting for the nuclei to relax completely. The sequence is given below.

$$90°_x\text{-}(\text{-}\tau\text{-}180°_y\text{-}\tau\text{-echo})_n \qquad \text{expression 25}$$

The initial $90°_x$ pulse turns M_o into the y direction where the magnetization vectors begin to diverge. After time τ a $180°_y$ pulse (in the y phase) is applied which serves to invert the yz plane. After another time τ the magnetization vectors have converged. To minimize the effect of error on the 180° pulse it can alternate in sign (positive to negative etc.).

Magnetic field inhomogeneity is often the factor dominating $T_{2,obs}^{-1}$ but in the systems studied here in the $0< \rho <1$ region the contribution from exchange is by far the dominant factor and comparison between T_2^{-1} and T_1^{-1} values show that $T_{2,inh}^{-1}$ is usually small so for these systems spin-echo is not necessary.

1.5.4 Nuclear Overhauser Enhancement (NOE) Measurements

If there are components at appropriate frequencies, relaxation can occur by the dissipation of energy to the lattice. In solution dipole-dipole coupling provides a relaxation pathway. Refer to Figure 6. If X is irradiated the Boltzmann distributions are perturbed and the (3)→(1) and (4)→(2) transitions are saturated. W_2 and W_0 work to counteract the perturbation but $W_2 >> W_0$, so the net result is a depopulation of (3) and an overpopulation of (2). The link between A and X is established because the irradiation of X has yielded an increase in the signal A. The irradiation of X is also referred to as decoupling. The relationship between the NOE and dipole-dipole relaxation is given by equation 26:

$$NOE = \frac{M_A}{M^o_A} = 1 + \frac{\gamma_X \, T_{1,DD}^{-1}}{2\gamma_A \, T_1^{-1}} \qquad \text{equation 26}$$

where M_A is the equilibrium value when X is completely decoupled and M_A^o is the unperturbed value. The NOE is usually determined experimentally by comparing spectra with and without decoupling at the second nucleus.

Dipole-dipole relaxation is the most common mechanism for spin-½ nuclei. Under extreme narrowing conditions the dipole-dipole relaxation rate for two different types of nuclei within the same molecule, such as the ^1H and ^{13}C nuclei in 18C6, is expressed as:

$$T_{1,DD}^{-1} = \left(\frac{\mu_o^2}{4\pi} \right) \gamma_A^2 \gamma_X^2 \hbar^2 \tau_c r^{-6} \qquad \text{equation 27}$$

When the decoupler is in use it generates heat. Since there is an effect from temperature, interleaving of acquisitions for both modes of operation of the decoupler is often arranged in order to minimize it.

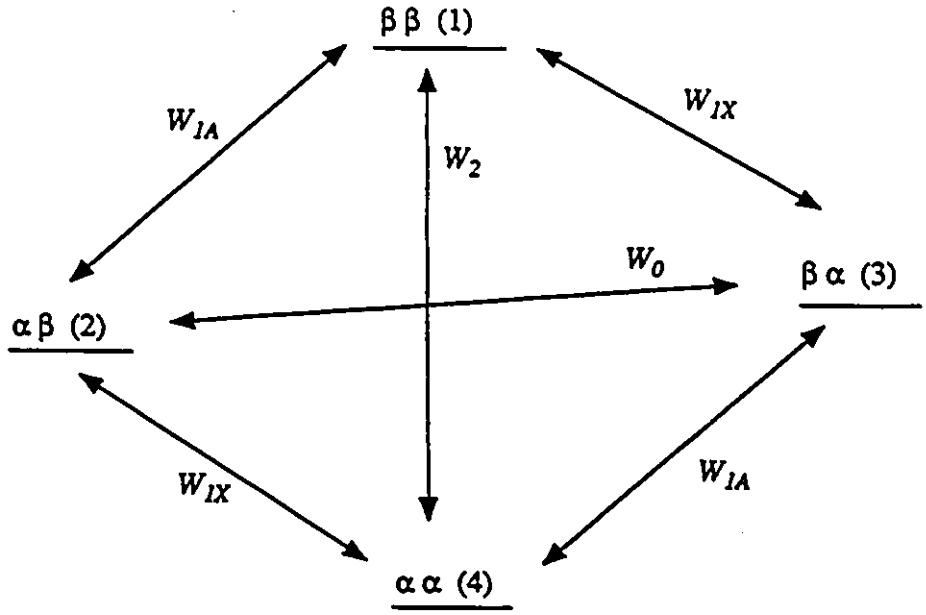

Figure 6: Transition rates of an AX spin system. $\Delta m = \pm 1$. '*W*' are rate constants.

1.5.4.1 The WALTZ sequence

In order to avoid problems with excessive power requirements for decoupling and the fact that certain techniques may result in both an NOE and decoupling, modern heteronuclear decoupling schemes were developed. Less power is required because the protons receive a continual stream of pulses rather than one long continuous burst of RF. The WALTZ-16 pulse sequence originated from the sequence given in expression 28, and is now typically done according to expression 29. The shorthand indicates the pulse length as a multiple of 90°, and the bars above indicate the inverse phase so, for instance, expression 28 would be (1,2,3).[38]

^{1}H: $(90°\text{-}180°\text{-}270°)_n$ expression 28

WALTZ-16: $(Q\bar{Q}\bar{Q}Q)_n$ where $Q = \bar{3}42\bar{3}1\bar{2}4\bar{2}3$ expression 29

1.5.5 The different nuclei

The nuclei used for the research presented in this thesis were: ^{13}C, ^{23}Na and ^{43}Ca. Their properties are given in Table III.[40]

A great deal of information can be obtained from ^{23}Na NMR.[41-43] It has high abundance and has a relatively high receptivity, which allows the use of dilute samples. Unlike ^{13}C and ^{1}H NMR the resulting spectra are a few broad lines. There are three actual quantities which are determined experimentally but they are the windows to much more. The three pieces of information are: the chemical shift (δ), the spin-spin relaxation rate (T_2^{-1}) and the spin-lattice relaxation rate (T_1^{-1}). The chemical shift range for ^{23}Na NMR has been of the order of 40ppm, but the signals of sodium cation and anion have been observed simultaneously on samples including metallic sodium and C222. The range effectively spans 80ppm. The nature of ^{23}Na chemical shift is not well understood. The chemical shift of Na^+ complexed by various antibiotic ionophores spans 25ppm and a similar phenomenon is observed with synthetic ionophores!

In general the lineshapes are Lorentzian and the linewidth at half-height ($\nu_{\frac{1}{2}}$) is related to T_2 (see equation 23). Under extreme narrowing conditions the T_1 and T_2 are equal, and the $\nu_{\frac{1}{2}}$ is an easy, accurate method of estimating T_1.

^{13}C NMR is a well-established nucleus which, despite its low abundance and low sensitivity, has found use on a regular basis and is one of the principal tools used by organic chemists for structural determinations. The ^{13}C spectra in this study were principally T_1 measurements, followed by NOE measurements. These measurements were used to access ^{23}Na quadrupolar coupling constants.

^{43}Ca NMR is not very popular because of the physical characteristics of the nucleus and economic reasons that arise in consequence. The natural abundance of ^{43}Ca is one of the lowest among the non-zero spin nuclei, and its sensitivity is not very high either. Usually lower sensitivity is overcome by enriched samples but for ^{43}Ca the cost is prohibitive.[44] ^{43}Ca NMR was used to try to see what this nucleus might yield in terms of information on 18C6

Table III: NMR Properties of ^{1}H, ^{13}C, ^{23}Na and ^{43}Ca.

	Natural abundance (%)	Spin	Gyromagnetic ratio γ (10^{7} rad T^{-1} s^{-1})	Quadrupole moment Q (10^{-28} m^{-2})	Receptivity relative to ^{13}C	Resonance frequency at 7.05 Tesla
^{1}H	99.985	1/2	26.7519	-	5.67×10^{3}	300.00
^{13}C	1.108	1/2	6.7283	-	1.00	75.429
^{23}Na	100	3/2	7.0761	0.12	525	79.346
^{43}Ca	0.145	7/2	-1.8001	-0.049	5.27×10^{-2}	20.188

systems and whether or not isotopically enriched samples were required for this type of study. It was hoped that even with low sensitivity it might still be possible to tell whether or not exchange was occurring at an observable rate on the NMR time-scale.

The chemical shift range for ^{43}Ca is of the order of 100ppm.[44] 18C6 has a shift of about -40ppm in MeOH relative to a Ca^{++}(aq) reference. Aqueous proteins have chemical shifts of about 10ppm. The chemical shift is influenced by concentration and choice of calcium salt.[45] Broad signals are usually observed since this is a quadrupolar nucleus.

1.6 The Purpose of the work

The $(Na\text{-}18C6)^+$ system has been studied by various techniques in order to obtain a wide range of information about it. The focus of this work has been to verify the roles of the different components of the system (temperature, concentration of the different species, the counter anion and the solvent) in order to more fully comprehend the mechanism by which this complex dissociates and the influences of each component upon the rate and/or mechanisms of dissociation. In order to access the ^{23}Na quadrupolar coupling constant, ^{13}C NMR will be used.

The role of the counter anion in the mechanism of decomplexation will be examined for the (Na^+-DB24C8) system. The study will be extended to other systems which will be examined in light of the results obtained for the $(Na\text{-}18C6)^+$ system. The Na^+ cation forms complexes with $18C6A_4$, a tetra-substituted carboxylic acid 18C6 derivative, and the naturally occurring ionophore Lasalocid A. These systems will be examined and a ^{43}Ca NMR study of the (Ca^{++}-18C6) system will be attempted.

Chapter 2
Introduction to Kinetics and Mechanisms

The study of the association and dissociation steps in the transport of ions involves the investigation of their mechanisms and kinetics. The formation of a complex between an alkali metal cation and crown ether involves the substitution of one or more of the solvent molecules from the inner coordination sphere of the cation by the ligand. In certain circumstances all of the solvent molecules will be expelled from the coordination sphere. These systems serve as useful models for the natural processes. The rates of these reactions span a range of times, and fortunately there is a wide range of techniques available to provide access to all of these time domains. Figure 7 gives the ranges of times available for a few of the currently available experimental techniques.[46] Flash photolysis is a versatile technique in that it is possible from the sub-picosecond range to the microsecond range and beyond. The useful NMR timescale is not continuous. Lineshape analysis is suitable for processes which are longer than 10^{-5} seconds. Correlation times span the picosecond to nanosecond time range. The gap in between ($\sim 10^{-9}$ to $\sim 10^{-5}$ seconds) is spanned quite effectively by ultrasonic methods. Few systems, if any, are suitable for study by both methods because of these different time windows. Data from similar systems are accessible but no system has been identified, and studied in detail by both methods.

2.1 Mechanism of Complexation

The overall rate constants for complex formation reactions with alkali ions are generally of the order of 10^8 to 10^9 $M^{-1}s^{-1}$, which are close to those of diffusion-controlled reactions.[47] These ions also have high solvation energies. For example, the ΔG_{298} of solvation for Na^+ in AC is 16.4 $kJ.mol^{-1}$ and for Li^+ it is 17.0 $kJ.mol^{-1}$, while for Et_4N^+ it is 10.0 $kJ.mol^{-1}$, all when the counter anion is picrate.[48] A stepwise reaction scheme is the way to account and satisfy these two characteristics. Almost every encounter is successful in diffusion-controlled complex formation, implying low activation barriers and a lack of ligand

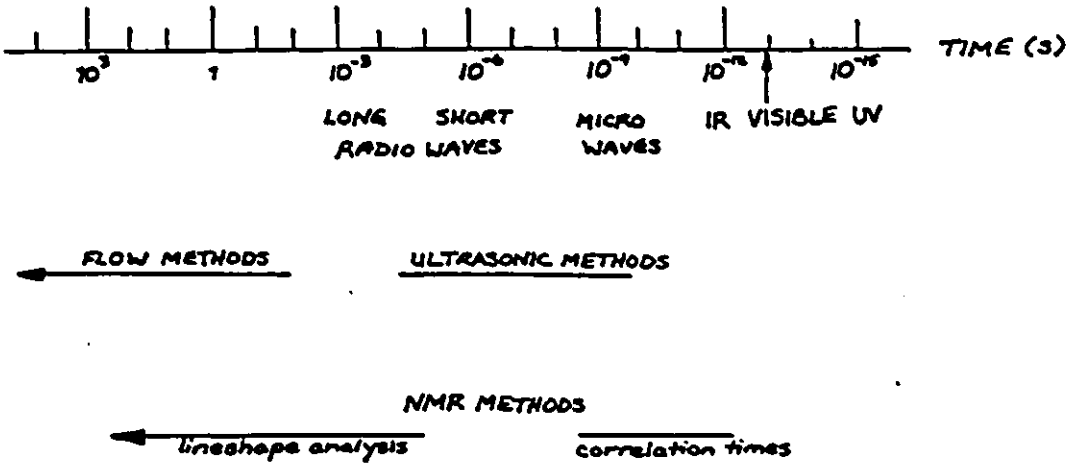

Figure 7: The relationship between experimental techniques on the time scale. Based on Figure 1 in reference 46.

specificity. The transition state is not one where the ligand and cation are "recognizing" one another. Rather, the cation interacts with accessible donor atoms and then the substitution for the other solvent molecules and any conformational changes occur rapidly to give the final, stable complex. Overall, the complexation and dissociation processes are:

$$M^{n+} + C_o \underset{k_{-1}}{\overset{k_1}{\rightleftharpoons}} (MC)^{n+} \qquad \text{equation 30}$$

A mechanism was proposed by Eigen in 1970[49] to account for the stepwise formation of the complex as it goes from being a solvent-separated metal ion-ligand pair to a contact pair and finally to a complex with the metal cation well embedded, in the case of a crown ether in the crown cavity. High activation energies are avoided by this stepwise formation called the Eigen-Winkler mechanism.[47]

$$M^+ + C_o \underset{k_{-o}}{\overset{k_o}{\rightleftharpoons}} M^+C_o \underset{k_{-a}}{\overset{k_a}{\rightleftharpoons}} M^+C_1 \underset{k_{-b}}{\overset{k_b}{\rightleftharpoons}} M^+C_2 \underset{k_{-c}}{\overset{k_c}{\rightleftharpoons}} \ldots \underset{k_{-m}}{\overset{k_m}{\rightleftharpoons}} M^+C_m \qquad \text{equation 31}$$

where M^+ and C_o are the fully solvated metal ion and ligand, M^+C_o is the outer-sphere complex, and M^+C_i is the metal ion coordinated through i of m ligand donor atoms. k_o and k_{-o} are diffusion controlled reactions.[47,50]

Ultrasonic absorption is the principal technique used for studying this type of system. The complexation of $(K^+,Na^+)SCN^-$ by 18C6 in DMF was investigated using both ultrasonic absorption and Raman spectroscopy.[51] DMF was used because it was desirable to distinguish between the desolvation step and the rearrangement of the ligand. In the Eigen-Winkler mechanism the rearrangement of the ligand is rate-determining but a second mechanism, where the complexation is rate-determining, was also proposed for this system. Chock's mechanism involved rapid conformational changes of the ligand to a suitable form for

complexation, followed by the complexation.[52] Both the Raman spectra, which were interpreted on the basis of SCN^- and 18C6 competing to complex the cation, and the ultrasonic data were best interpreted by the Eigen-Winkler mechanism. Further work on the same system varied some of the features in order to more fully understand the operative mechanism.[53] The solvent was changed to EtOH so that both the rapid relaxation process which was observed previously, and a slower process which had only been detected, could be characterized. The investigation found that Na^+ reacts with 18C6 in a single step in EtOH and a two-step process in DMF. The solvent therefore plays an important role based, not upon its dielectric constant but, possibly upon its donor number.

Also in DMF, $(Ba^{++}$-18C6) forms faster than $(K$-18C6$)^+$, despite their similar ionic radii, by the Eigen-Winkler mechanism.[54] The formation constants for several alkaline-earth - crown ether complexes were determined in MeOH, DMF and DMSO solutions but no mechanism identification was made.[55] DME is another relatively common solvent for complex formation studies.[56,57] The primary species in the $NaClO_4$-18C6 system is the ion-paired complex, but dimerization is also present.[56] 18C6 must compete with the solvent molecules in order to coordinate with the ion-paired $LiAsF_6$.[57] In MeOH the $NaClO_4$-18C6 system, as well as the Li^+ and K^+ systems, complex by the Eigen-Winkler mechanism.[58] No mention of ion-pairing was made. When 18C6 is added to $LiClO_4$ in DMC solutions more "free" ClO_4^- ions are observed because the 18C6 competes with the ion pairs.[59]

Ultrasonic absorption techniques are not the only ones used in the study of complexes and complex formation. Raman spectroscopy, which has been already mentioned, has provided structural information.[51,60] Computational methods have successfully reproduced the relative strengths of alkali metal - 18C6 complexes in aqueous solution ($K^+ > Rb^+ > Na^+$).[61] The relative free energy of binding of Na^+ and K^+ to 18C6 in MeOH have also been computationally determined and are in reasonable agreement with experimental values.[62] Theoretical calculations have also helped to interpret some of the experimental structural data. The Raman spectra of $(Na$-18C6$)^+$ are similar to the ones for $(K^+$-18C6) except that

two forms of 1:1 complex exist: the stable D_{3d} type and a less well characterized metastable form.[60] Wipff et al have an interpretation as to why both the C_i and D_{3d} forms of Na^+-18C6 are observed. (see Figure 8) Their calculations show that the lowest energy structure depends upon the dielectric constant of the solvent. The crystal structure and the structure in a low dielectric constant solvent are both C_i symmetry but in a more polar solvent the D_{3d} structure is of similar energy.[63] This work was extended to the reaction path and aimed to give an accurate complexation rate constant. It was relatively successful but did acknowledge that solvent molecules would have to be considered for a more accurate value.[64]

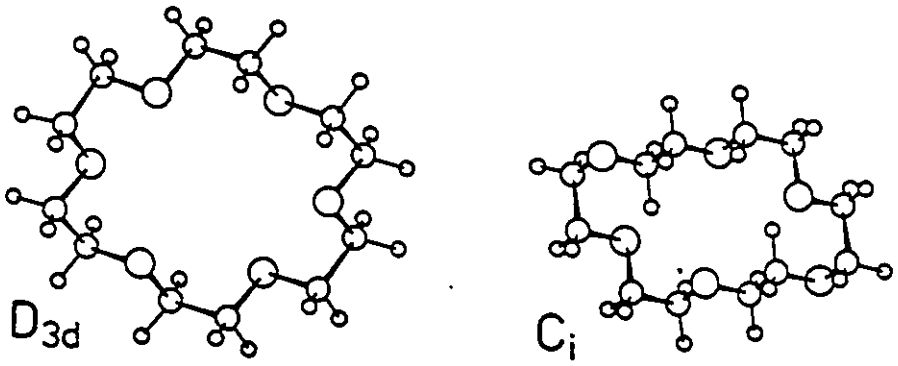

Figure 8: Conformers of 18C6 with D_{3d} and C_i symmetry.

Despite these studies to determine formation constants and to determine the mechanism of complexation, this fast process does not yield all of the possible information about any given system. This multistep process desolvates the cation and the ligand binds it in a stepwise manner, but the selectivity is not controlled here. The opposite reaction, the dissociation process is where selectivity is controlled.

2.2 Dissociation

Since complexation is a multistep mechanism which proceeds at a rate close to diffusion control, variation among systems is less clear. The dissociation process is the one where selectivity is achieved. For a range of alkali metal cation complexes with crown ethers

and cryptands, the rate of dissociation of each complex (k_{-1}) can be graphed with respect to its formation constant (K_f). (see equation 30) The plot of log k_{-1} as a function of log K_f (see Figure 9) gives a linear relationship. The formation rate constants of these complexes (k_1) are all within a factor of about 100 of the diffusion controlled rate. Changes in the solvent, cation and/or ligand are reflected in the dissociation rate constants. Dissociation processes must therefore be studied. Their rates are typically 10^{-5} to 10^{-2} seconds. As can be seen in Figure 7, NMR fits that time domain. While ultrasonic absorption studies focus upon the complexation process, the reverse process is studied by NMR.

The reaction profile in Figure 10 can be used as an aid to further understanding. The formation constant (K_f) is the ratio between the formation and the dissociation rates (k_1/k_{-1}). K_f is easily determined and k_1 is very fast. Often this is a way to estimate k_{-1}, and indirect access to it is provided by ultrasonic absorption results. NMR sees the global process rather than each individual step.

2.3 Dissociation rate constant from NMR

Using NMR, the dissociation rate constant can be accessed quite easily. The alkali metal cation is generally considered to occupy one of two possible sites, being either solvated (site A) or complexed (site B). If there is exchange of the cation between these two sites, the rates are characterized by k_A and k_B.

$$A \underset{k_B}{\overset{k_A}{\rightleftharpoons}} B \qquad \text{equation 32}$$

The lifetime (τ) of each species can be given as $\tau_A = 1/k_A$ and $\tau_B = 1/k_B$ respectively. The mean lifetime of the two sites (τ) relates the populations of each site (P_A and P_B) to the reaction rates.

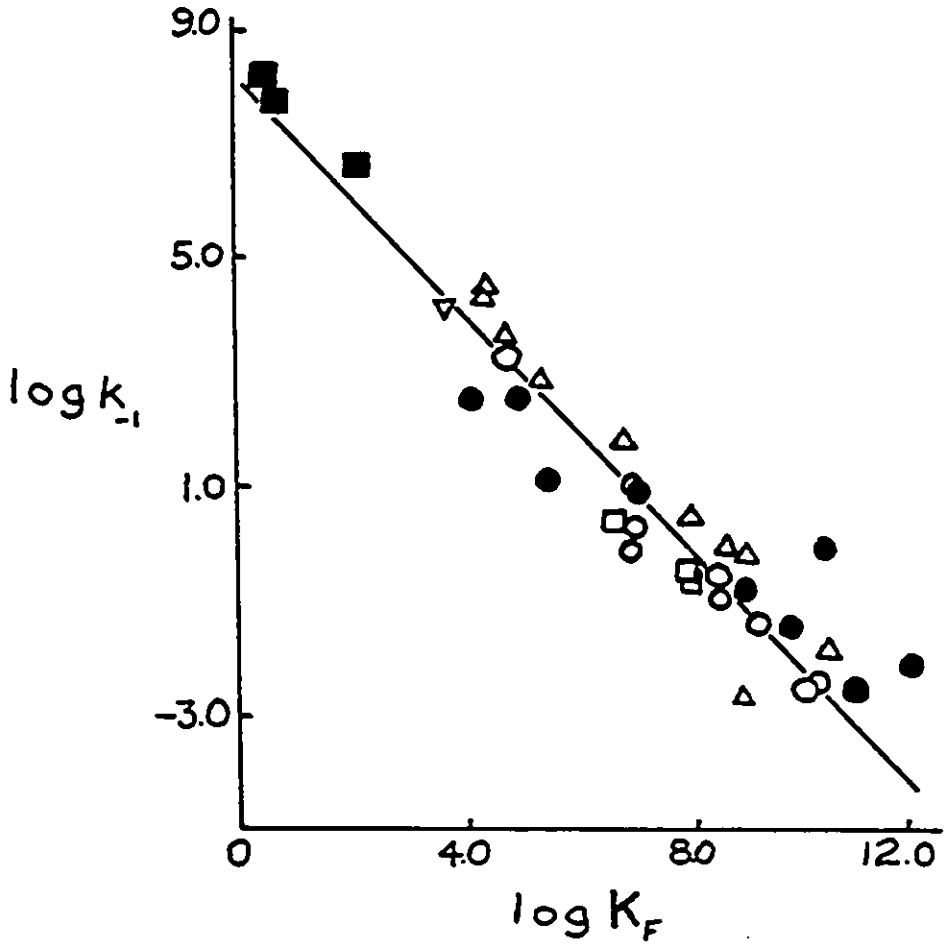

Figure 9: Log k_{-1} as a function of log K_f for a range of crown ethers and cryptands with alkali metal cations in several solvents at 298K. MeOH, cryptands:(Δ); PC, cryptands:(●); DMF, cryptands:(□); H_2O, crowns:(■); DME, crowns:(▽); EtOH, cryptands:(○). Based on Figure 3 in reference 65.

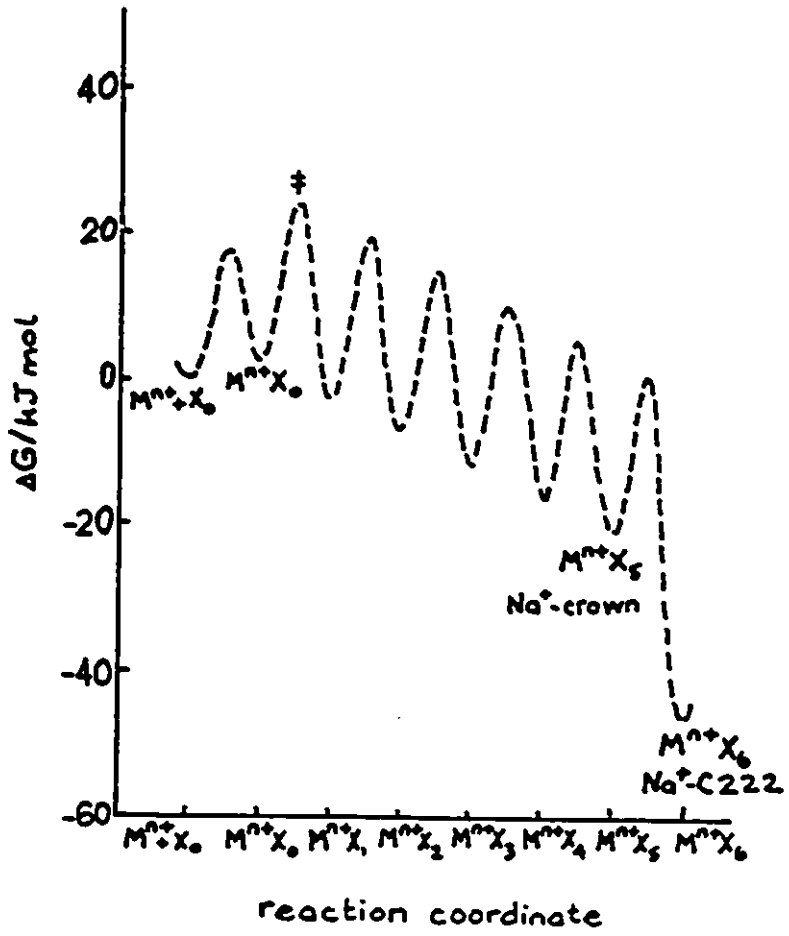

Figure 10: Reaction profile for stepwise complexation model. Based on Figure 3 in reference 48.

$$\tau = \frac{P_A}{k_B} = \frac{P_B}{k_A} = \frac{1}{k_A + k_B} \qquad \text{equation 33}$$

Shchori et al[66,67] proposed two mechanisms for simple two-site chemical exchange of the cation between the solvated and complexed sites, and showed how NMR provided access to them. The dissociation rates for the appearance of the solvated and complexed cation (see equation 30) can be expressed as:

$$d[M^+]/dt \quad = k_{-1}[MC^+] \quad = k_B[MC^+] \qquad \text{equation 34}$$

$$d[MC^+]/dt \quad = k_1[M^+][C] \quad = k_A[M^+] \qquad \text{equation 35}$$

The observed pseudo-first order rate constant expression is therefore:

$$k_A + k_B = k_1[C] + k_{-1} \qquad \text{equation 36}$$

If ρ represents the ratio $[MC^+]/[M^+]_T$, and since the formation constant is already known to be large ($>10^5$)(see Section 4.2) $[MC^+]_T \sim [C]_T$, the expression in equation 36 reduces to:

$$k_A + k_B = k_{-1}(1-\rho)^{-1} \qquad \text{equation 37}$$

The dissociation rates are accessible form the T_2^{-1} relaxation rates. When there is exchange, in the $0< \rho <1$ range, the observed transverse relaxation rate ($T_{2,obs}^{-1}$) contains a contribution from exchange. This contribution is not observed in the longitudinal relaxation rate (T_1^{-1}). In conditions of extreme narrowing and for moderately rapid exchange, one Lorentzian signal is observed for $0< \rho <1$, and the observed transverse relaxation rate

contains contributions from inhomogeneity and exchange. Under these conditions $T_{1,q}^{-1} = T_{2,q}^{-1}$ so, overall:

$$T_{2,obs}^{-1} = T_{1,q}^{-1} + T_{2,inh}^{-1} + T_{2,ex}^{-1} \qquad \text{equation 38}$$

The measured longitudinal relaxation rate is principally quadrupolar relaxation.[38] Contributions from other relaxation processes is negligible. The inhomogeneity is determined under conditions where there is no exchange ($\rho = 0$ or $\rho > 1$) and is the difference between the T_1^{-1} and the $T_{2,obs}^{-1}$ values. When k_A and k_B are much greater than T_2^{-1} at $\rho = 0$ and $\rho > 1$ and the difference (in Hz) between the chemical shifts for the solvated and complexed cations is related to the difference in transverse relaxation rates for the same two sites, as $4\pi(\nu_A - \nu_B)^2 >> (T_{2,A}^{-1} - T_{2,B}^{-1})^2$, the exchange contribution is related to $(k_A + k_B)$ according to this simple expression.[68,35b]

$$T_{2,ex}^{-1} = 4P_AP_B\pi^2(\nu_A - \nu_B)^2(k_A + k_B)^{-1} \qquad \text{equation 39}$$

The measured experimental values of chemical shifts and relaxation rates are used to determine the pseudo-first order rate constants $(k_A + k_B)$, which are then used to determine the rate of dissociation.

This approach applies to the formation of stable 1:1 complexes under extreme narrowing conditions, and is best used where the characteristics of the solvated and complexed cations can be identified. Lin and Popov, using ^{23}Na NMR showed that the chemical shift can vary as a function of ρ ($[ligand]/[cation]_T$) in three ways:[69]

1- The ^{23}Na chemical shift increases gradually with ρ, but does not attain a limiting value.
ex: (Na^+-15C5) in H_2O or DMF.
This indicates a <u>weak complex</u> and is only observed when the solvent is strongly solvating.

2- The ^{23}Na chemical shift varies linearly when $0< \rho <1$, and remains constant upon further addition of ligand.
ex: (Na^+-18C6) in AC or AN.
This indicates a stable 1:1 complex and occurs in solvents of low and medium donicity.

3- The ^{23}Na chemical shift varies linearly when $0< \rho <1$ and then changes direction.
ex: (Na^+-15C5) in NM.
This indicates the formation of a stable 1:1 complex, followed by the addition of a second ligand molecule to give a sandwich complex.

The first two phenomena are observed in the systems in this thesis. For the first case, the formation constant (K_f) is determined. For systems fitting the second case, kinetic calculations are made.

2.4 NMR Results

The approach of using three experimentally-determined parameters to access dissociation rate constants has been used successfully for many systems. The first ^{23}Na NMR spectra in solution were reported in 1960.[70] Jardetzky and Wertz looked at the Na^+ cation in aqueous solution in the presence of several anions. Grotens and Smid observed changes in the ^{23}Na signal linewidth as dimethyl-DB18C6 was added to $NaBPh_4$ solutions in THF.[71] Ion pairs were also observed in the early days of ^{23}Na NMR.[72] This information is what provides the starting point for subsequent, more sophisticated studies, which have been facilitated by more powerful FT NMR instruments. Lin and Popov's ^{23}Na study on 18C6, 15C5, B15C5 and several cryptands provided even more extensive information on chemical shifts as has been discussed earlier (see Section 2.3).[69]

Like ^{23}Na, ^{133}Cs is 100% abundant and is well-suited for NMR studies. Being larger than Na^+, the Cs^+ cation cannot be expected to form characteristically identical complexes. In fact, a sandwich complex, being a 2:1 Cs^+-18C6 complex, forms in PY[73] and several other solvents[74], including high dielectric amide solvents such as DMF and n-methylformamide.[75] With large crown ethers, such as DB24C8 and DB21C7, 1:1 complexes form in AC and MeOH.[76] Large cations are not the only ones which form sandwich complexes. When the

^{7}Li NMR study of the Li^{+}-12C4 system in NM and PC was made, 2:1 complexes were also observed to form.[77]

While alkali metal NMR provides information about these systems, useful data are also available from ^{1}H and ^{13}C NMR, the mainstays of synthetic organic chemists. Temperature-dependent changes in the ^{1}H spectra of K^{+}-C222 and other alkaline-earth and alkali -C222 complexes are indicative of exchange between the solvated cation and the complexed cation.[78] Structural information is accessible form both solution[79-81] and solid state[82] ^{13}C NMR. de Boer et al linked solution ^{1}H NMR results with solid state X-ray diffraction structures.[83] The 2:1 NM:18C6 forms in the solid state while in solution both the 1:1 and 2:1 complexes are observed. Solution studies in AN and 18C6 by ^{13}C NMR have shown 1:1 and 2:1 complexes also.[84]

Just as little mechanistic information is provided by the ^{1}H and ^{13}C NMR studies, ^{139}La NMR yields only the fact that exchange does occur between $LaCl_3.7H_2O$ and 18C6 in MeOH. The formation constant for La^{+++}-18C6 is accessible (log $K_f = 3.2 \pm 0.5$).[85]

There is a wealth of information on systems studied by ^{23}Na NMR. Competitive studies of $(Na\text{-}18C6)^{+}$ have involved the Cs^{+}:Na^{+}:BPh_4^{-}:18C6 system in DMF and AN.[86] Such work focuses less on mechanisms and more on the formation constants and the associated selectivity series.

Most of the ^{23}Na NMR results to be discussed are interpreted in light of a ^{39}K NMR study by Schmidt and Popov in 1983.[87] The ^{39}K NMR study of potassium salts in various solvents had preceded it by six years.[88] When Schmidt and Popov investigated the $(K\text{-}18C6)^{+}$ system in 1,3-dioxolane by ^{39}K NMR, they found that the model of dissociation (see equation 30) did not explain their results. The classical dissociation mechanism was not satisfactory. Another mechanism had been proposed by Shchori et al[66,67] but had not been needed previously. This mechanism was of an associative nature and would involve the participation of a second cation.

2.5 An Associative-type exchange mechanism

This second mechanism, which Shchori et al[66,67] had proposed but had not been shown to be operative previously, was needed to interpret Schmidt and Popov's data[87] and shortly thereafter was shown to be operative for Na^+-DB24C8 in NM[88]. We suggest the name of metal association interchange "M_{ai}" mechanism for this mechanism where there is participation from a second cation.

$$M^{+*} + (MC)^+ \underset{}{\overset{k_2}{\rightleftharpoons}} (M^*C)^+ + M^+ \qquad \text{equation 40}$$

As the complex dissociates, the second one forms in a concerted manner because, unlike the dissociative mechanism where the cation approaches afterwards, the second cation is already in position. The rates of appearance of the solvated and complexed cations are now expressed as:

$$d[M^+]/dt = k_2[M^+][MC^+] = k_B[MC^+] \qquad \text{equation 41}$$

$$d[MC^+]/dt = k_2[M^+][MC^+] = k_A[M^+] \qquad \text{equation 42}$$

The $(k_A + k_B)$ expression for this mechanism is therefore:

$$k_A + k_B = k_2[M^+] + k_2[MC^+] = k_2[M^+]_T \qquad \text{equation 43}$$

Now that two possible mechanisms are being considered the total expression for $(k_A + k_B)$ is:

$$(k_A + k_B) = k_{-1}(1-\rho)^{-1} + k_2[M^+]_T \qquad \text{equation 44}$$

In contrast, Shchori et al[66,67] determine the rates for the two decomplexation rates (k_{-1} and k_2) from an equation involving the lifetime of only the solvated species (τ_A).

$$(\tau_A[M^+C])^{-1} = k_{-1}[M^+] + k_2 \qquad \text{equation 45}$$

The classical k_{-1} is accessible, using either equation 44 or 45, but a second exchange mechanism, the M_{si} mechanism, is detectable by NMR. This mechanism is not detectable by other methods.

The Cs^+-DB24C8 and Cs^+-DB21C7 systems in AC and MeOH, which were mentioned earlier, are just two of the systems which do not follow the dissociative mechanism but rather the M_{si} mechanism.[76] The Na^+-DB24C8 system in NM, which has been studied quite closely,[89-92] will be discussed in further detail in Chapter 3. There are cases where both mechanisms are present. For Na^+-DB18C6 in AN the mechanism is purely dissociative, but in NM there is competition between the two.[90] The choice of anion influences the mechanism for ^{23}Na in THF solutions. When the counter anion is BPh_4^- the predominant mechanism is the dissociative one, but a change to SCN^- results in a change to the M_{si} mechanism.[93] Solvent plays a part too. In neat MeOH, the dissociative process predominates, but in neat PC the M_{si} mechanism predominates. Different solvent mixtures also influence the mechanism. In a 80-20 mol% THF-PC mixture, the dissociative mechanism is operative but if the ratio is changed to 40-60 mol% THF-PC the mechanism also changes.[94] The influence of these two factors (solvent and counter anion) will be examined in greater detail in Chapters 4 and 5 respectively.

The M_{si} mechanism is not restricted to larger crowns. In NM the predominant mechanism for both $(Na\text{-}B15C5)^+$ and $(Na\text{-}15C5)^+$ is the M_{si} mechanism at higher $[Na^+]_T$.[95,96] At lower concentrations, the dissociative mechanism becomes competitive. This is also seen with $(Na\text{-}DB24C8)^+$ in NM.[89,90] the $(Na\text{-}B15C5)^+$ follows the dissociative mechanism in AN.[96]

NMR has shown itself to be a useful tool in the study of decomplexation. The classical dissociation rate constant (k_{-1}) is accessible but a second mechanism, the M_{si}

mechanism, has been detected and under certain conditionsis the only operative mechanism. This mechanism has not been observed by other methods.

Chapter 3
Possible Anion Role in the M_{ai} Mechanism

3.1 Introduction

Ever since M_{ai} mechanism was first shown to be operative for $(K\text{-}18C6)^+$ in 1,3-dioxolane by Schmidt and Popov[87] it has been found in other systems. (see Section 2.5) Despite these examples of the M_{ai} mechanism, it has been suggested that the anion may assist in the decomplexation, and that a mechanism which includes a role for the counter-anion be proposed.[97] This idea was already tested, less directly, on the (Na^+-DB24C8) system in NM[91,92] but an experiment on the same system was designed to demonstrate clearly any participation of the counter anion. Two series were run: one with the concentration of counter anion maintained at 50mM while the concentration of Na^+ was varied, and a second where both concentrations varied yet were the same for any given sample. The similarities and/or differences in the resulting spectra and kinetic data should show any involvement of the counter anion.

3.2 $NaBPh_4$ and DB24C8 in NM

The $NaBPh_4$:DB24C8 system in NM has been studied quite closely. Chemical shifts show that there are two major Na^+ species present: the complexed and solvated sodium ions. There is some evidence for aggregate formation where (Na^+_{i+1},C_i) species are formed. Only 2% of the total Na^+ concentration is involved in this, with the largest contribution being from i=1. Overall, the contributions of the aggregates to the chemical shifts are non-observable, and those to the transverse relaxation rates are masked by the chemical exchange contribution. The longitudinal relaxation rates are the ones affected.[92]

When the kinetics of this system were investigated, the contribution from the aggregates was neglected due to two factors: their small population (≤2%) and the expected similarity between the chemical shifts of the 1:1 complex and the aggregates. This allowed the system to be treated as one of only two sites. ($k_A + k_B$) values were calculated and at

high $[Na^+]_T$ the relationship between $\log(k_A + k_B)$ and $\log[Na^+]_T$ is linear. k_2= $(2.8\pm0.3)\times10^5 s^{-1}mol^{-1}L$ (295K). The residual dissociative decomplexation mechanism becomes operative at lower $[Na^+]_T$, $\Delta G^{\ddagger}_{uni}$ ~65 kJ mol^{-1} (300K) as determined by subtraction of the M_{ai} contribution from the $(k_A + k_B)$. The activation parameters may be determined for the M_{ai} mechanism:[89]

$$\Delta H^{\ddagger} = 31\pm3 \text{ kJ mol}^{-1} \qquad \Delta S^{\ddagger} = -32\pm10 \text{ J K}^{-1}\text{mol}^{-1}$$

The role of the counter anion has been investigated for this system.[91] If the extraction of Na^+ from the (Na^+,C) complex were aided by the counter-anion, and ion-pairing were present, two equilibria should be considered. (see equations 45 and 46)

$$Na^+ + A^- \overset{K_{IP}}{\rightleftharpoons} (Na^+,A^-) \qquad \text{equation 45}$$

$$C + (Na^+,A^-) \underset{k_-}{\overset{k_+}{\rightleftharpoons}} (Na^+,C) + A^- \qquad \text{equation 46}$$

With PF_6^-, aggregation is not promoted, and it can be assumed that K_{IP} would be small. Under such circumstances, and after the related approximations, the measured rate constant would depend both on $[Na^+]_T$ and on ρ, if the counter anion were to participate.

$$(k_A + k_B) = k_+[C] + k_-[A^-] \equiv k_- [Na^+]_T \frac{\rho}{(1-\rho) K_{IP}} \qquad \text{equation 47}$$

The graph of $T_{2,ex}^{-1}$ vs ρ is parabolic. This is not consistent with counter anion participation. Within error limits and interpreting the data according to the M_{ai} mechanism, the $\Delta H^{\ddagger}$ and $\Delta S^{\ddagger}$ values are identical for BPh_4^- and PF_6^-.[90]

The role of the counter anion was further investigated through the use of SCN^- and I^-. Ion-pairing is more prevalent with these counter anions. K_{IP}(NaI,294K) = 80, K_{IP}(NaSCN, 294K) = 10^3. Aggregates may also form for NaSCN and DB24C8 in NM where there is <3% 2:1 Na^+:DB24C8. The presence of both thiocyanate and the aggregates yields a chemical shift vs ρ graph which is not linear for 0< ρ <1, but the $\delta(Na\text{-}DB24C8)^+$ is identical for all four anions (BPh_4^-, PF_6^-, SCN^-, I^-), which shows that the anion is not involved in the coordination sphere of the complexed sodium.

The rate for the M_{ai} mechanism (k_2) increases in the order: $BPh_4^- < PF_6^- < I^- < SCN^-$, which parallels the increase in coordinating strength of these anions. These results are summarized in Table IV.[87,88] The counter anion competes with the cation to coordinate with the Na^+ cation, but is not involved in the coordination sphere of the complex. The k_2 values depend upon the ion-paired cation to assist in the opening of the complex. Ion-pairing reduces the cation-cation repulsion in the transition state of the M_{ai} mechanism but the additional stability which this provides is offset by similar ion-pairing in the ground state.[88]

Table IV: $(Na\text{-}DB24C8)^+$ in NM: Activation parameters and the rate constant for the M_{ai} mechanism.

anion	k_2 (294K)	$\Delta H^{\ddagger}$	$\Delta S^{\ddagger}$	$\Delta G^{\ddagger}_{294}$
-	10^5 $M^{-1}s^{-1}$	kJ mol^{-1}	J $mol^{-1}K^{-1}$	kJ mol^{-1}
BPh_4^-	2.8±0.2	31±3	-32±10	41.9
PF_6^-	3.5±1.0	30±2	-37±10	41.4
I^-	4.5±1.0	n.d.	n.d.	40.7
SCN^-	13±2	n.d.	n.d.	38.5

n.d. = not determined

The entropies and enthalpies of activation were not reported since concentrations at or below the millimolar range would be required and these were not run. The useful temperature range

is effectively reduced because higher concentrations result in very rapid exchange rates at higher temperatures and limited solubility at lower temperatures.[91]

3.3 Results and Discussion

Despite the evidence supporting the M_{ai} mechanism for the $(Na\text{-}DB24C8)^+$ system in NM, further tests on the hypothesis of an associative M_{ai} mechanism were made. Through the use of *tert*-butylammonium tetraphenylborate and the analogous hexafluorophosphate salt, the BPh_4^- concentration could be maintained at 50mM while the $[Na^+]_T$ could be reduced.

Parallel series were prepared where $[Na^+]_T = [BPh_4^-]_T$ and $[Bu_4NBPh_4]_T + [NaBPh_4]_T = 50$ mM. $[Na^+]_T$ varied from 0.5mM to 20mM at 300K. $(k_A + k_B)$ values were determined by lineshape analysis. Figures 11 and 12 show the ^{23}Na NMR spectra observed. There is no appreciable difference whether or not the concentration of the counter anion is maintained constant or not. Very visible and significant changes in the rate of exchange occur when $[Na^+]_T$ is varied. In both cases, as the concentration of sodium ion decreases, the rate of exchange decreases, and the once-Lorentzian peak passes through coalescence and separates into two peaks.

In Figure 13, the spectra in Figure 11 are quantified. Within experimental errors the slopes are parallel with a difference in the y-intercept. However, both y-intercepts are close to the origin, suggesting no participation from the dissociative mechanism nor from any others. When $[NaBPh_4]_T + [Bu_4NBPh_4] = 50$mM there may be some interactions between the ions in solution. With an excess of $NaBPh_4$, and an equal amount of Bu_4N^+, especially at low $[Na^+]_T$, there is a possibility for interactions such as aggregation and ion-pairing, which might otherwise not occur. The amount of interaction is not significant however.

When the values of $(k_A + k_B)$ for several values of ρ are averaged Figure 14 is obtained. (see Table V) Through averaging, the systematic errors of any particular series of samples contribute to the size of the error rather than to the k_2 value determined from the

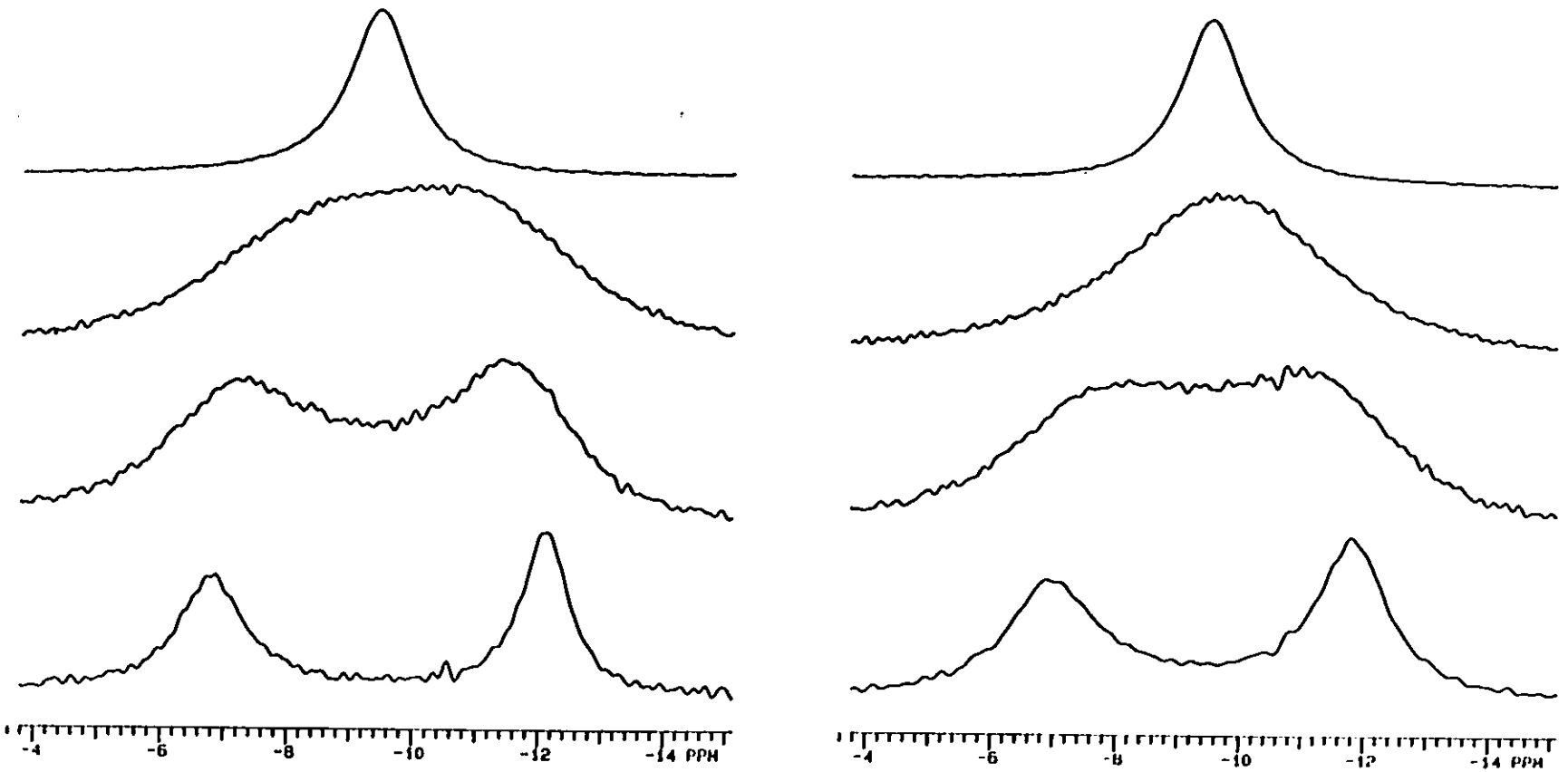

Figure 11: ^{23}Na NMR spectra of $NaBPh_4$ solutions in NM in the presence of DB24C8 ($[DB24C8]_T/[NaBPh_4]_T = 0.52$) at different sodium concentrations (300K).
(a) $[Na^+]_T = [BPh_4^-]_T$.
(b) $[NaBPh_4]_T + [Bu_4NBPh_4]_T = 50.0$ mM.

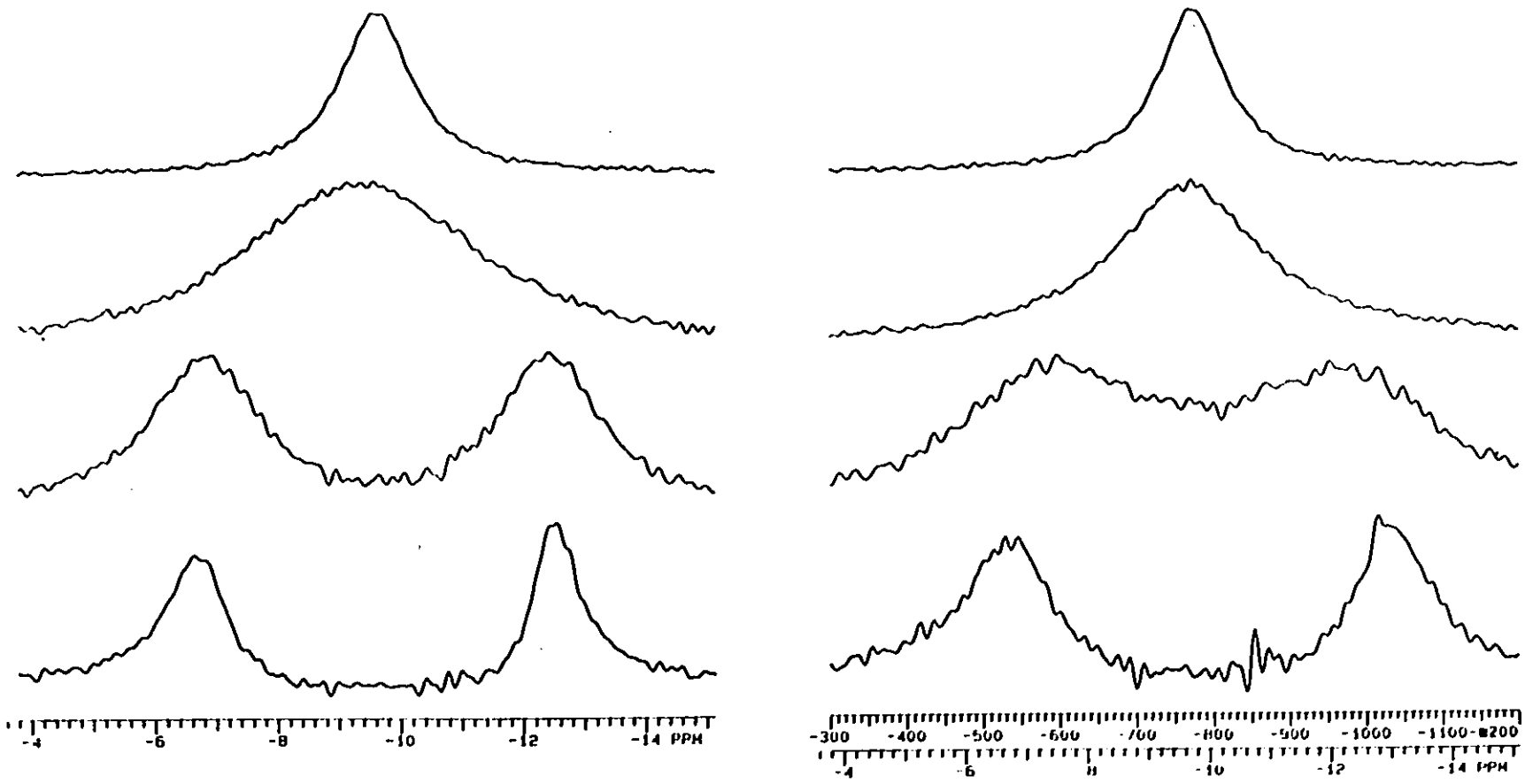

Figure 12: ^{23}Na NMR spectra of $NaPF_6$ solutions in NM in the presence of DB24C8 ($[DB24C8]_T/[NaPF_6]_T = 0.56$) at different sodium concentrations (300K).
(a) $[Na^+]_T = [PF_6^-]_T$.
(b) $[NaPF_6]_T + [Bu_4NPF_6]_T = 50.0$ mM.

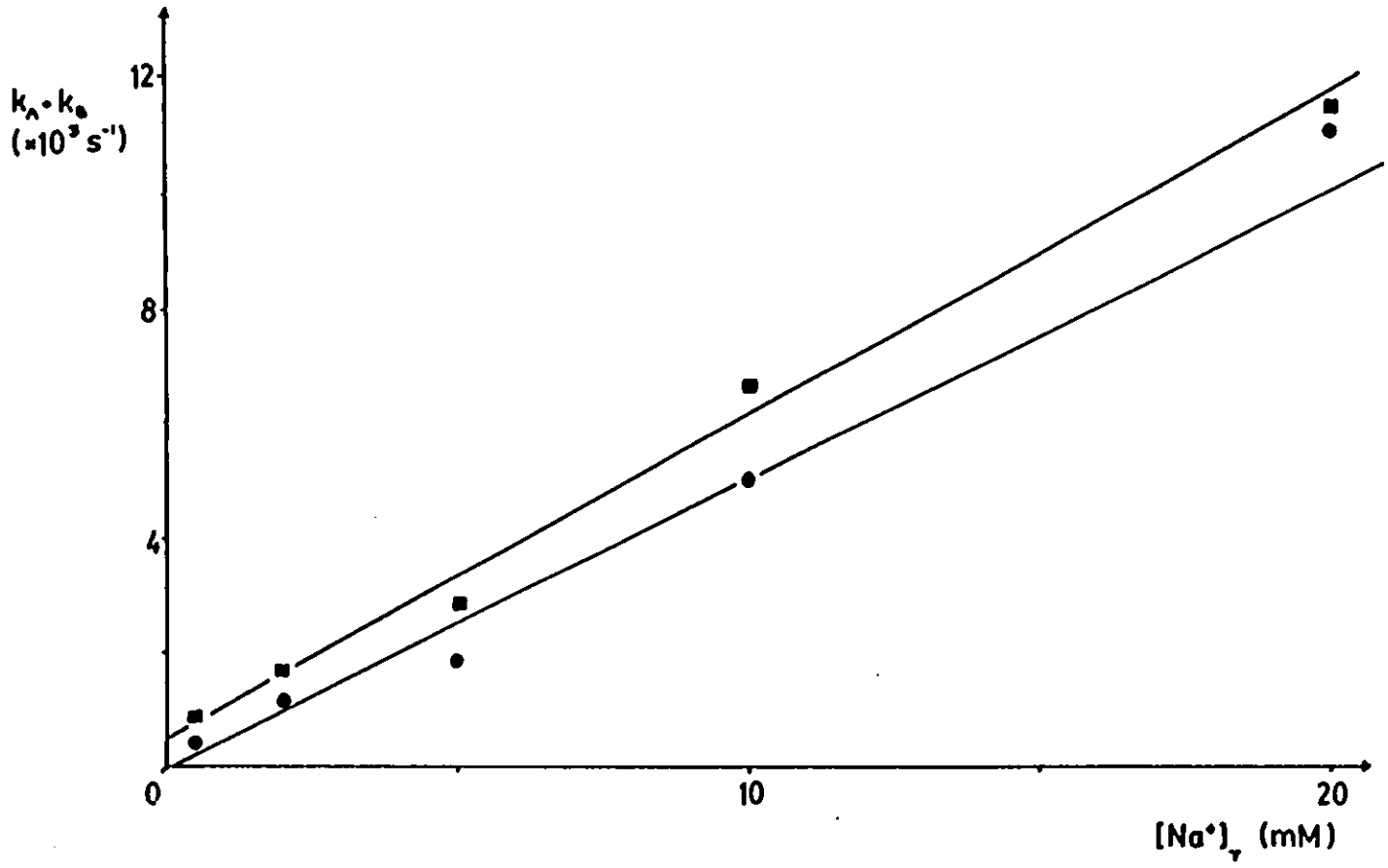

Figure 13: $NaBPh_4$ solutions in NM: $(k_A + k_B)$ vs $[Na^+]_T$ at (300.0±0.5) K.
$\rho = [DB24C8]_T/[Na^+]_T = 0.51$.
●: $[Na^+]_T = [BPh_4^-]_T$; $(k_A + k_B) = (5.0\pm0.5)\times10^5\ [Na^+]_T + (0\pm3)\times10^2$;
■: $[NaBPh_4]_T + [Bu_4NBPh_4]_T = 50.0$ mM; $(k_A + k_B) = (5.7\pm0.4)\times10^5\ [Na^+]_T + (4\pm3)\times10^2$.

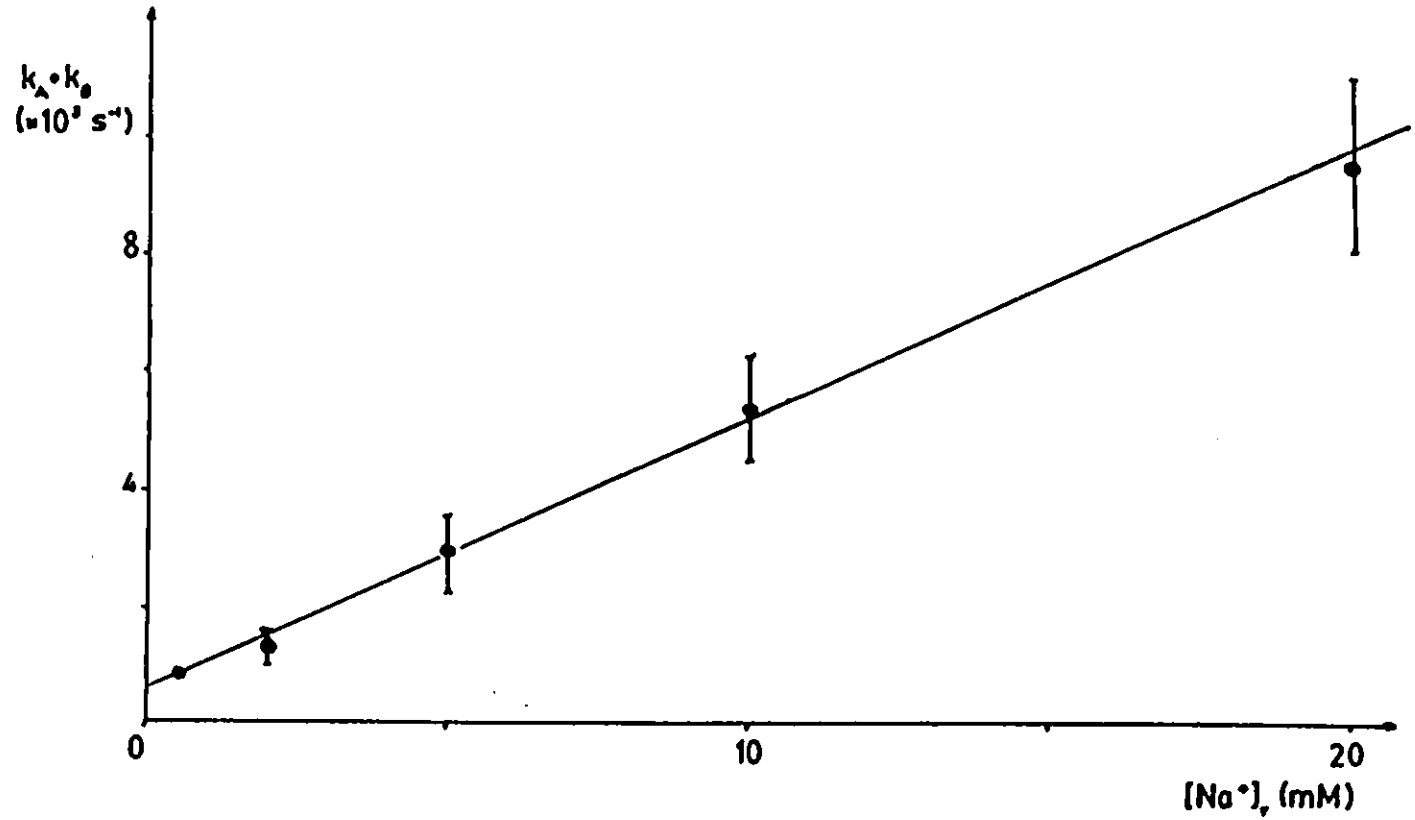

Figure 14: $NaBPh_4$ solutions in NM: average $(k_A + k_B)$ vs $[Na^+]_T$. Each data point is the result of the averaging (error bar = σ) over 4 independent determinations of $(k_A + k_B)$ for $\rho = [DB24C8]_T/[Na^+]_T = 0.30; 0.52; 0.62;$ and 0.70.
$(k_A + k_B) = (4.5\pm0.2)\times10^5\ [Na^+]_T + (6.6\pm0.8)\times10^2$.

Table V: Rate constants for the $NaBPh_4$-Bu_4NBPh_4 system

$[NaBPh_4]_T + [BuNBPh_4]_T = 50$ mM. T = 300K. $\pm\sigma$= error on $(k_A + k_B)$.

rho	$[Na^+]_T$ (M)	$(k_A + k_B)$ ($\times 10^3$ s^{-1})	equation: $k_A + k_B =$
0.300	0.0005	0.99±0.05	$(3.8\pm0.6)\times10^5[Na^+]_T + (9\pm5)\times10^2$
	0.002	1.09 ±0.03	
	0.005	3.94±0.05	
	0.010	4.86±0.04	
	0.020	7.92±0.09	
0.525	0.0005	0.84±0.04	$(5.7\pm0.4)\times10^5[Na^+]_T + (4\pm3)\times10^2$
	0.002	1.66±0.02	
	0.005	2.86±0.03	
	0.010	6.65±0.04	
	0.020	11.6±0.2	
0.620	0.0005	0.96±0.02	$(4.3\pm0.2)\times10^5[Na^+]_T + (6\pm1)\times10^2$
	0.002	1.46±0.02	
	0.005	2.49±0.03	
	0.010	4.57±0.07	
	0.020	9.6±0.1	
0.705	0.002	1.14±0.02	$(4.6\pm0.4)\times10^5[Na^+]_T + (4\pm4)\times10^2$
	0.005	2.63±0.07	
	0.010	5.51±0.05	
	0.020	9.07±0.08	

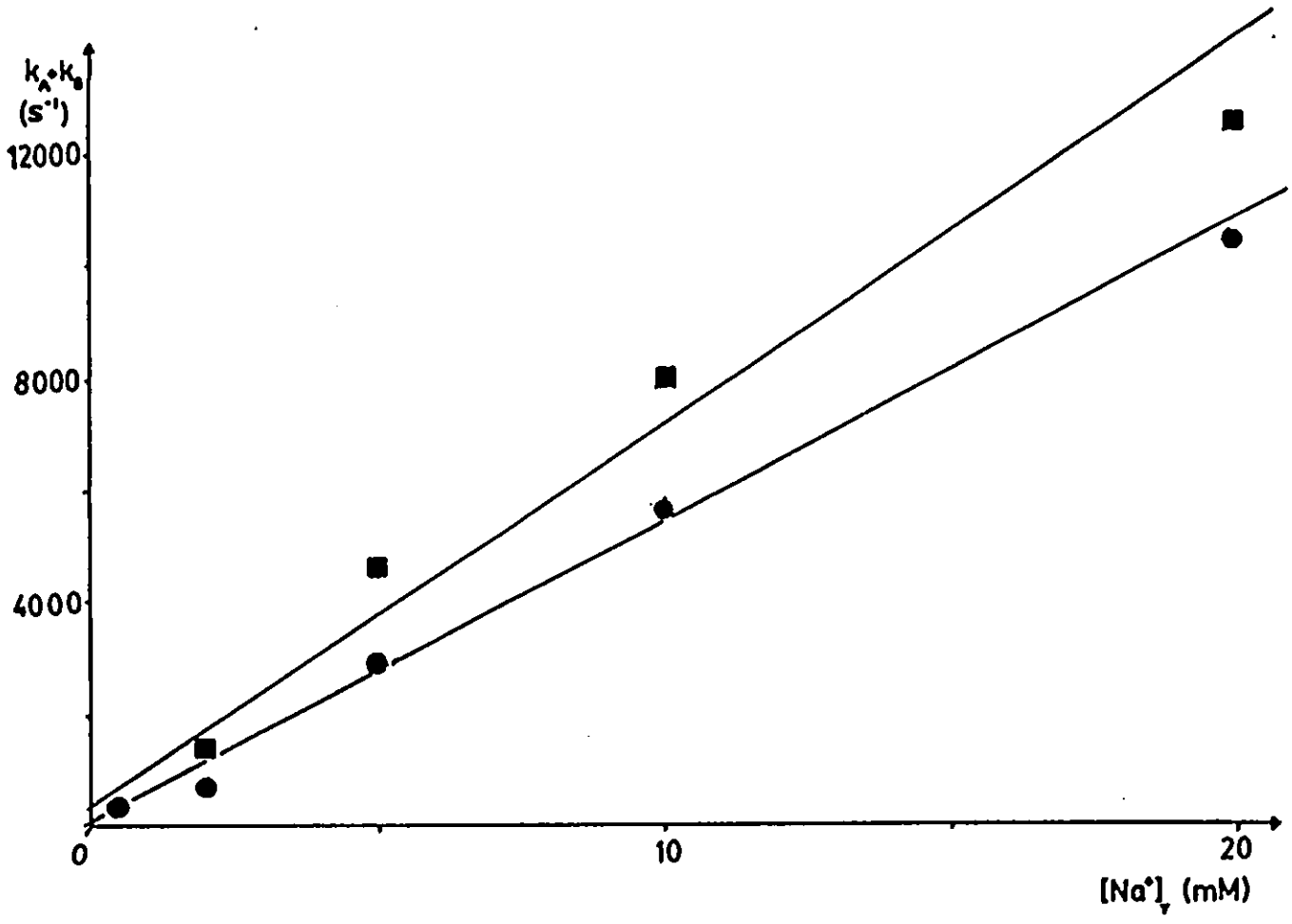

Figure 15: $NaPF_6$ solutions in NM: $(k_A + k_B)$ vs $[Na^+]_T$ at (300.0±0.5) K.
$\rho = [DB24C8]_T/[Na^+]_T = 0.56$.
●: $[Na^+]_T = [PF_6^-]_T$; $(k_A + k_B) = (5.4\pm0.4)\times10^5\ [Na^+]_T + (0\pm2)\times10^2$;
■: $[NaPF_6]_T + [Bu_4NPF_6]_T = 50.0$ mM; $(k_A + k_B) = (6.9\pm0.7)\times10^5\ [Na^+]_T + (3\pm4)\times10^2$.

slope. Here the evidence for other interactions is confirmed but once again this contribution is small.

With PF_6^- as the counter anion similar results are observed. The quantification of the spectra in Figure 12 yields the graph in Figure 15. Once again, though the slopes are similar, k_2 is slightly larger when the $[PF_6^-]_T$ is maintained rather than when it is varied. When $[PF_6^-]_T$ varies the y-intercept is the origin and when it is constant there is a small contribution from other interactions. Despite this contribution, the y-intercept is close to the origin within error limits.

3.4 Conclusions

These results show that the effect of maintaining the concentration of the counter anion constant is the introduction of effects associated with and expected for a large concentration of ions. These ions do not participate in the M_{ai} mechanism nor is there the introduction of a competitive alternate mechanism. The species which will complex, the Na^+ and the DB24C8, are quite swamped by the presence of so many other ions. It may be suggested that the M_{ai} mechanism is slightly accelerated by the excess of bulky non-coordinating ions in solution. These experiments definitely show that the M_{ai} mechanism is the mechanism which is operative for the decomplexation of $(Na\text{-}DB24C8)^+$ in NM.

Chapter 4
The $(Na\text{-}18C6)^+$ System in different Solvents

4.1 Background

The $(Na\text{-}DB24C8)^+$ system in NM decomplexes principally by the M_{ai} mechanism and under several sets of conditions other complexes do as well. Schmidt and Popov's 1983 study of the $(K\text{-}18C6)^+$ system in 1,3-dioxolane was the first report of the associative mechanism which we call the M_{ai} mechanism.[87] Strasser et al showed how solvent properties and choice of counter anion can influence the exchange mechanism.[93,94] In THF the $NaBPh_4$-18C6 system exchanges slowly at room temperature and two distinct ^{23}Na NMR signals are observed. The mechanism is shown to be the dissociative one. Changing the counter anion to SCN^- increases the rate of exchange and the mechanism changes to the M_{ai} mechanism.[93] The NaSCN-18C6 system was studied in MeOH where the dissociative mechanism is operative. When the $NaBPh_4$-18C6 system is studied in THF-MeOH (60-40 mol%) and in THF-PC (80-20 mol%) the dissociative mechanism is also functional but in neat PC and in THF-PC (40-60 mol%) the M_{ai} mechanism is followed once again.[94]

Lincoln et al examined the NaSCN-18C6 system in AC, MeOH and PY.[97] They observed the dissociative mechanism for all solvents. They were not successful in all of the solvents which they tried since in H_2O, DMSO, PC, AN, DMF and HMPA the exchange was in the fast exchange limit of the NMR timescale down to the solution freezing points. The aforementioned study will be discussed further with respect to this study's findings.

In this chapter the $(Na\text{-}18C6)^+$ complex will be examined in different solvents and at different temperatures. In Chapter 5 the influence of different counter anions will be investigated, all in an attempt to understand the nature of this complex more fully. As has been shown for the $(Na\text{-}DB24C8)^+$ system in NM, the tetraphenylborate anion is non-coordinating and it is not involved in ion-pairing. When studying the influence of solvent it is desirable to minimize other interactions and through the use of BPh_4^- this is achieved. For the $NaBPh_4$-18C6 system in AC, other mechanisms and interactions are absent and the dissociative process predominates.[98]

4.2 Results

$(Na\text{-}18C6)^+$ was studied in five solvents: acetone (AC), acetonitrile (AN), nitromethane (NM), propylene carbonate (PC), and pyridine (PY). In NM the difference in chemical shifts for the free and complexed sodium ion was too small for the transverse relaxation rate to be affected by the exchange. For the other four solvents the exchange contribution to the transverse relaxation rate is observable. At 301.5K the peaks are Lorentzian for AC, AN, and PC. In PY the rate of exchange is slow enough that two peaks are visible. When a Lorentzian signal is observed its chemical shift is the shifts of the two exchanging species.

$$\delta_{obs} = P_A\delta_A + P_B\delta_B \qquad \text{equation 48}$$

Figure 16 is typical of the relationship observed between the chemical shift and ρ. The linear increase in chemical shift for $0< \rho <1$, followed by a plateau at $\rho >1$ shows the formation of a strong 1:1 complex ($K_f>10^5$) with no further increase in stoichiometry. Figure 17 is very similar to Figure 16 in form, but it is different in one major way. The difference in chemical shift values for the solvated and complexed Na^+ in NM is small so the tranverse relaxation rate is unaffected by the exchange. Kinetic parameters are not accessible but it is possible to calculate an upper limit for the detectable $(k_A + k_B)$. A limit to the $T_{2,ex}^{-1}$ value, $T_{2,ex,lim}^{-1}$, is calculated from the $T_{1,obs}^{-1}$ and the inhomogeneity.

$$T_{2,ex,lim}^{-1} = 0.2 \times T_{1,obs}^{-1} + T_{2,inh}^{-1} \qquad \text{equation 49}$$

This takes into account the limitations on the experimental measurement of $T_{2,ex}^{-1}$ and the difference in chemical shifts, both of which are needed for $(k_A + k_B)$ determination. (see equation 39) The ^{23}Na NMR spectra for the AN series (see Figure 18) show clearly how the narrow peak of $(Na^+)_s$ broadens as 18C6 is added and the chemical shift moves until $\rho >1$

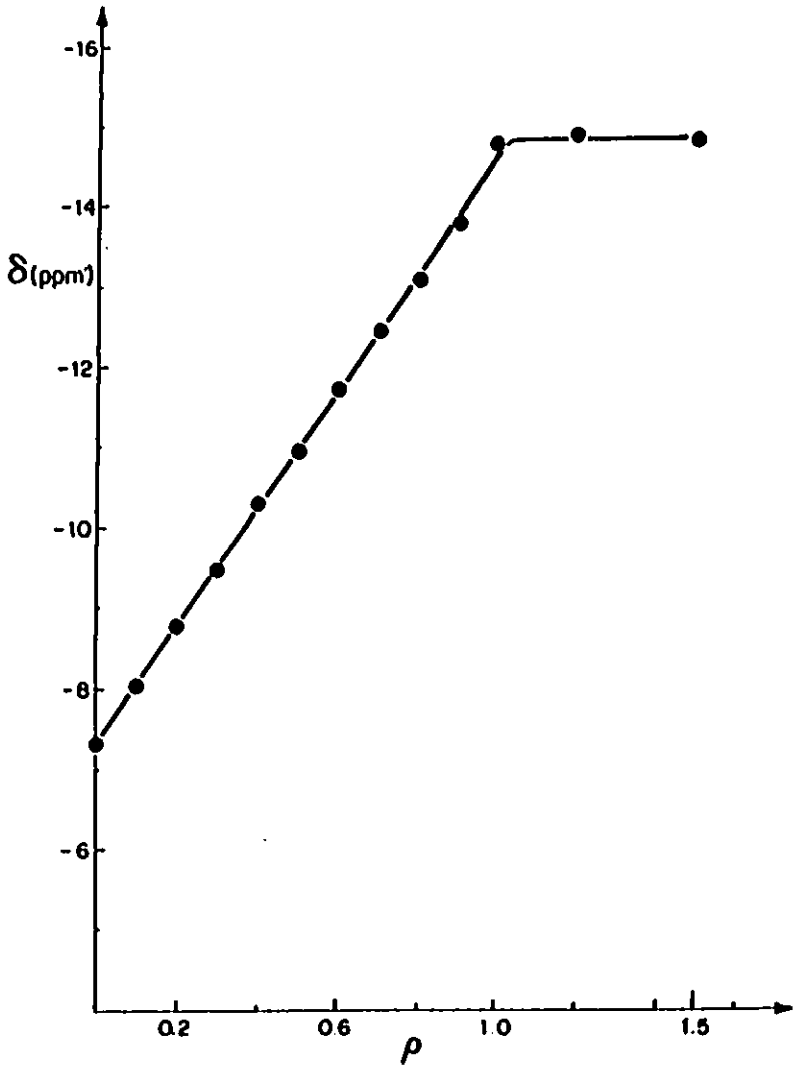

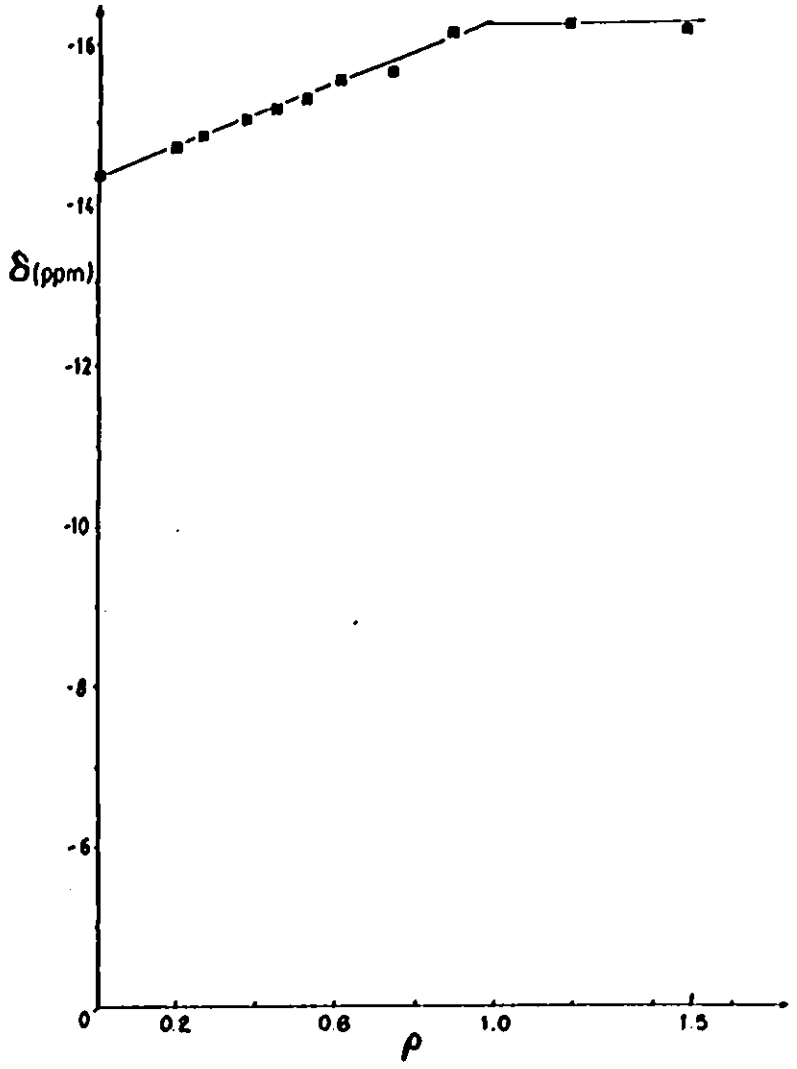

Figure 16: Chemical shift (δ) as a function of ρ for $NaBPh_4$-18C6 in AN. $[Na^+]_T$=20mM. T=295K.

Figure 17: Chemical shift (δ) as a function of ρ for $NaBPh_4$-18C6 in NM. $[Na^+]_T$=20mM. T=295K

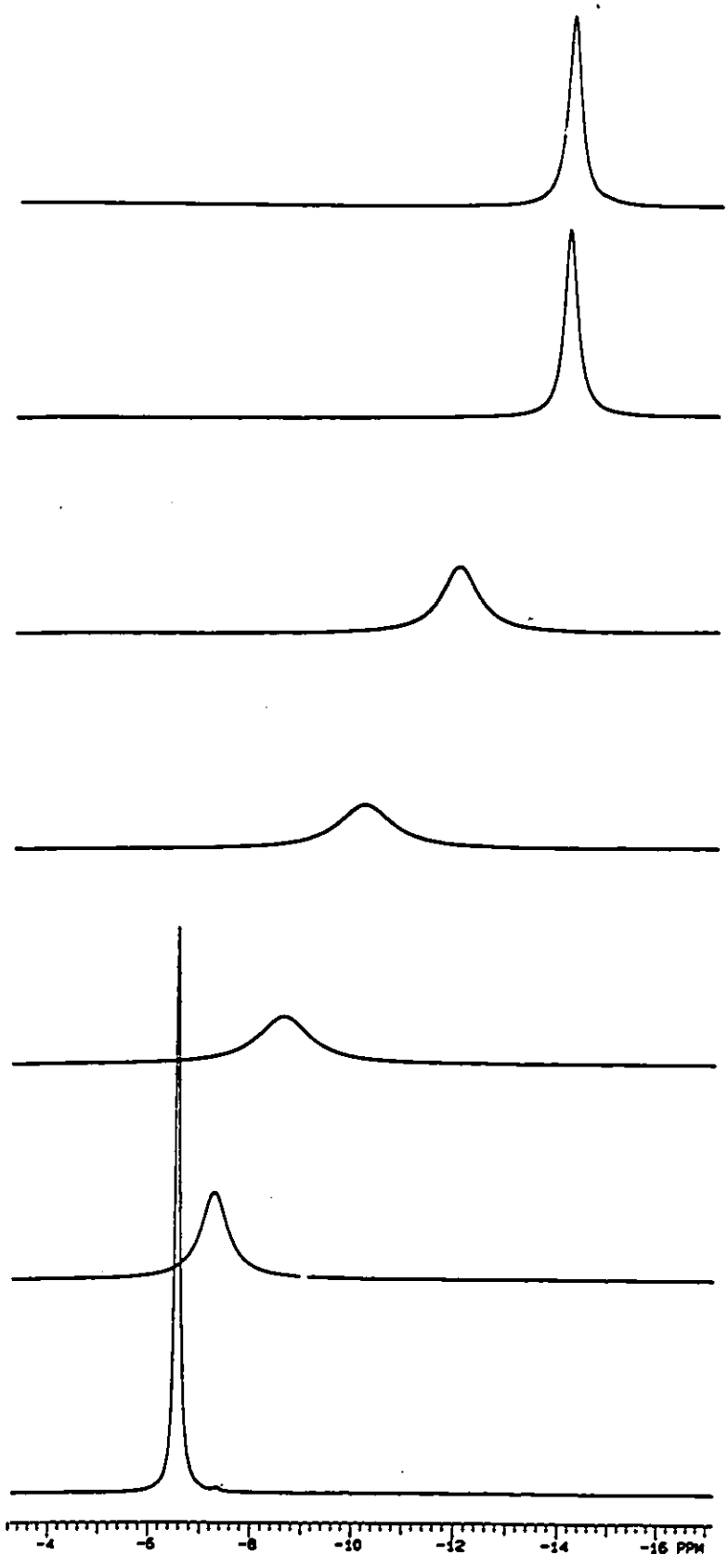

Figure 18: ^{23}Na NMR spectra of $NaBPh_4$-18C6 in AN with varying ρ values. $[Na^+]_T$=20mM. T=295K. Top to bottom: ρ= 1.5, 1.2, 0.7, 0.5, 0.3, 0.1, 0.0.

where a narrow peak, though not as narrow as $(Na^+)_s$, forms for $(Na\text{-}18C6)^+$. Even though ρ is increased from 1.2 to 1.5 the peak remains the same, uninfluenced by the excess 18C6. This confirms the 1:1 complex formation. In PY exchange is slower so the peak for solvated Na^+ broadens without changing in chemical shift but a second peak for the complex is observed and grows as that site becomes more populated. (see Figure 19)

There are differences in the T_1 and T_2 values for samples where $0< \rho <1$ because, as has been shown earlier, $T_{2,obs}^{-1}$ may contain a contribution from exchange while T_1^{-1} is not altered. T_1^{-1} does not vary as $[Na^+]_T$ is varied but $T_{2,obs}^{-1}$ does. (see Figure 20) As the concentration of Na^+ is increased from 5.0mM to 50mM the contribution from exchange at ρ =0.4 reduces from 400Hz to 160Hz. At ρ =0 and ρ >1 the small difference between $T_{2,obs}^{-1}$ and T_1^{-1} is due to inhomogeneity. Changes also occur when the temperature is varied. (see Figures 21 and 22) As the temperature is raised, the Lorentzian peaks in AN and AC narrow because the rate of exchange increases. As the temperature is lowered, and the rate of exchange decreases, the peaks are no longer Lorentzian and eventually two peaks are observed in AC and would be if it were lowered far enough in AN. When PY is the solvent, exchange is slow at room temperature so two peaks continue to be observed as the temperature is lowered. (see Figure 23)

If the mechanism of dissociation is only dissociative, the rate of exchange is linearly related to $(1-\rho)^{-1}$ with the origin being the y-intercept and the slope giving k_{-1}. Any contribution from the M_{ai} mechanism would be seen as a y-intercept >0, and being equal to $k_2[Na^+]_T$. (see Figure 24) Here $[Na^+]_T$ varies but the three lines have identical slopes, which means that the k_{-1} rate is constant. From the three y-intercept values, the k_2 rate can be determined.

When the series with identical $[Na^+]_T$ is run at different temperatures, and the rate of exchange is graphed vs $(1-\rho)^{-1}$ (see Figure 25) the slopes increase with temperature. The k_2 rates can be determined from each y-intercept. For AN there is no convergence at the origin, but with AC there is.

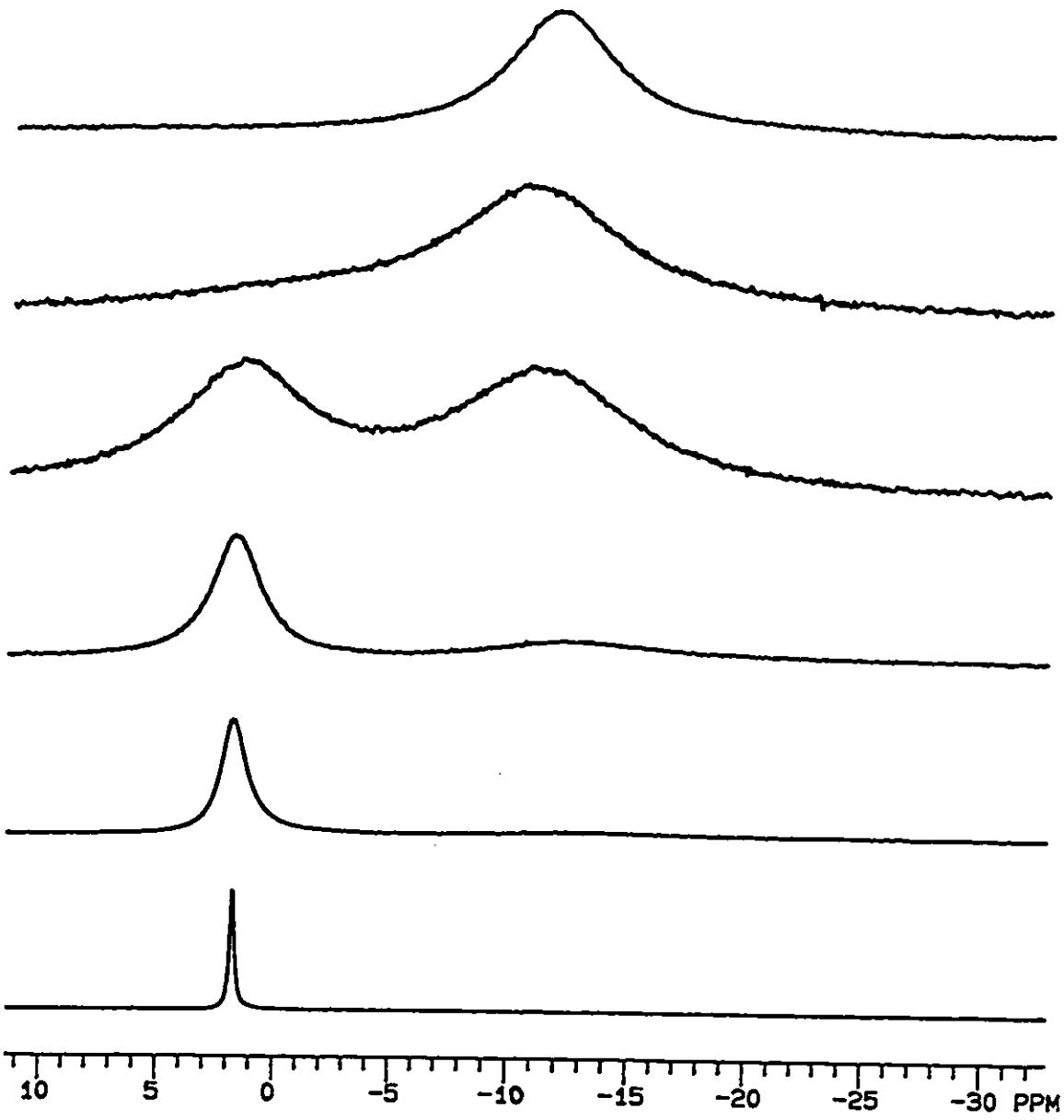

Figure 19: ^{23}Na NMR spectra of $NaBPh_4$-18C6 in PY with varying ρ values. $[Na^+]_T$=20mM. T=295K. Top to bottom: ρ= 1.2, 0.8, 0.6, 0.4, 0.2, 0.0.

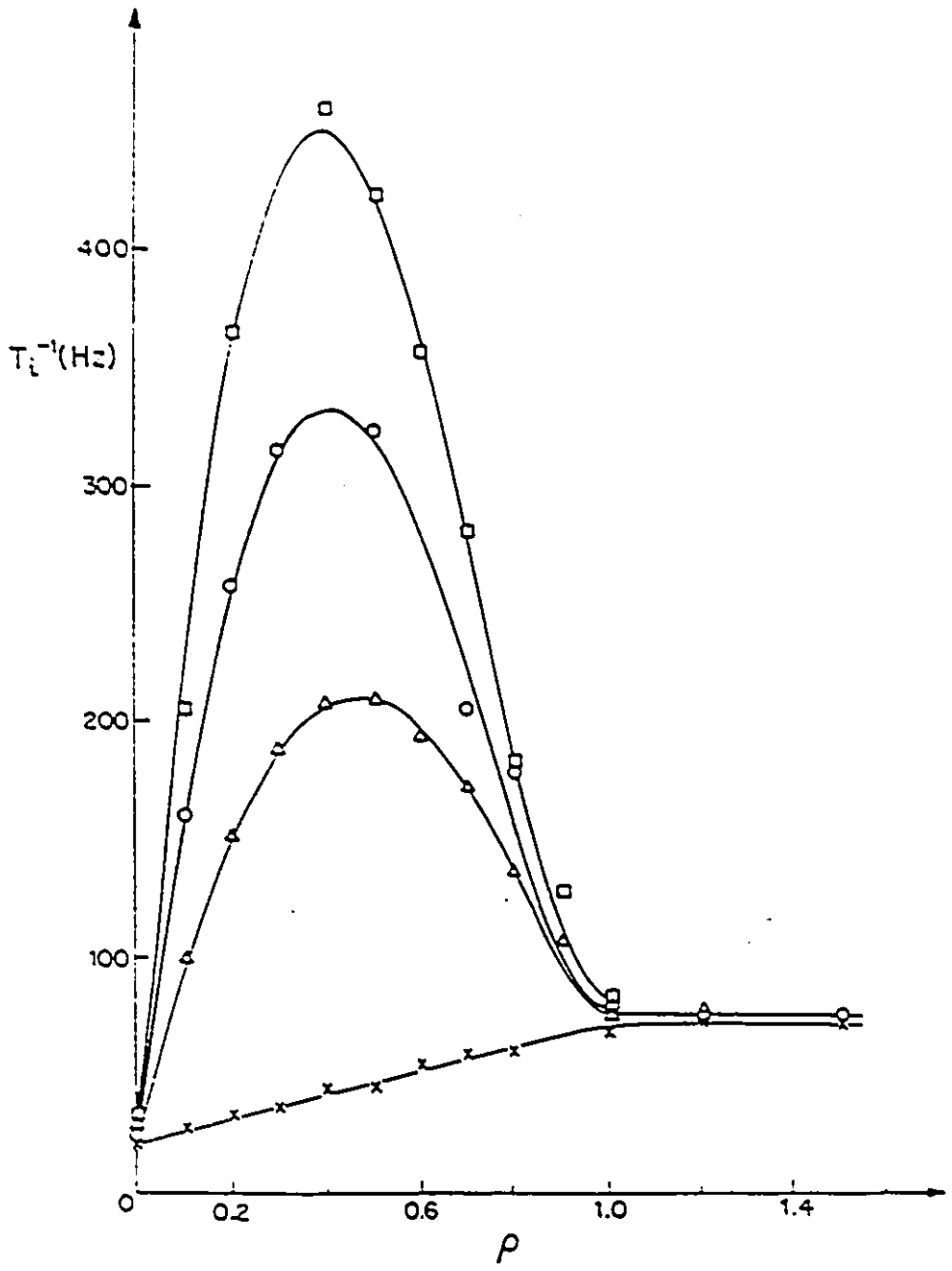

Figure 20: ^{23}Na relaxation rates as a function of ρ for $NaBPh_4$-18C6 in A.N. ^{23}Na transverse (Δ,○,□)(i=2) and longitudinal (×)(i=1) relaxation rates. $[NaBPh_4]_T$ = 5.0mM (□), 20.0mM (○,×), and 50mM (Δ). T=295K. The data points are experimental and the curves are calculated from the values of k_{-1} and k_2 given in Table VII, using equation 44.

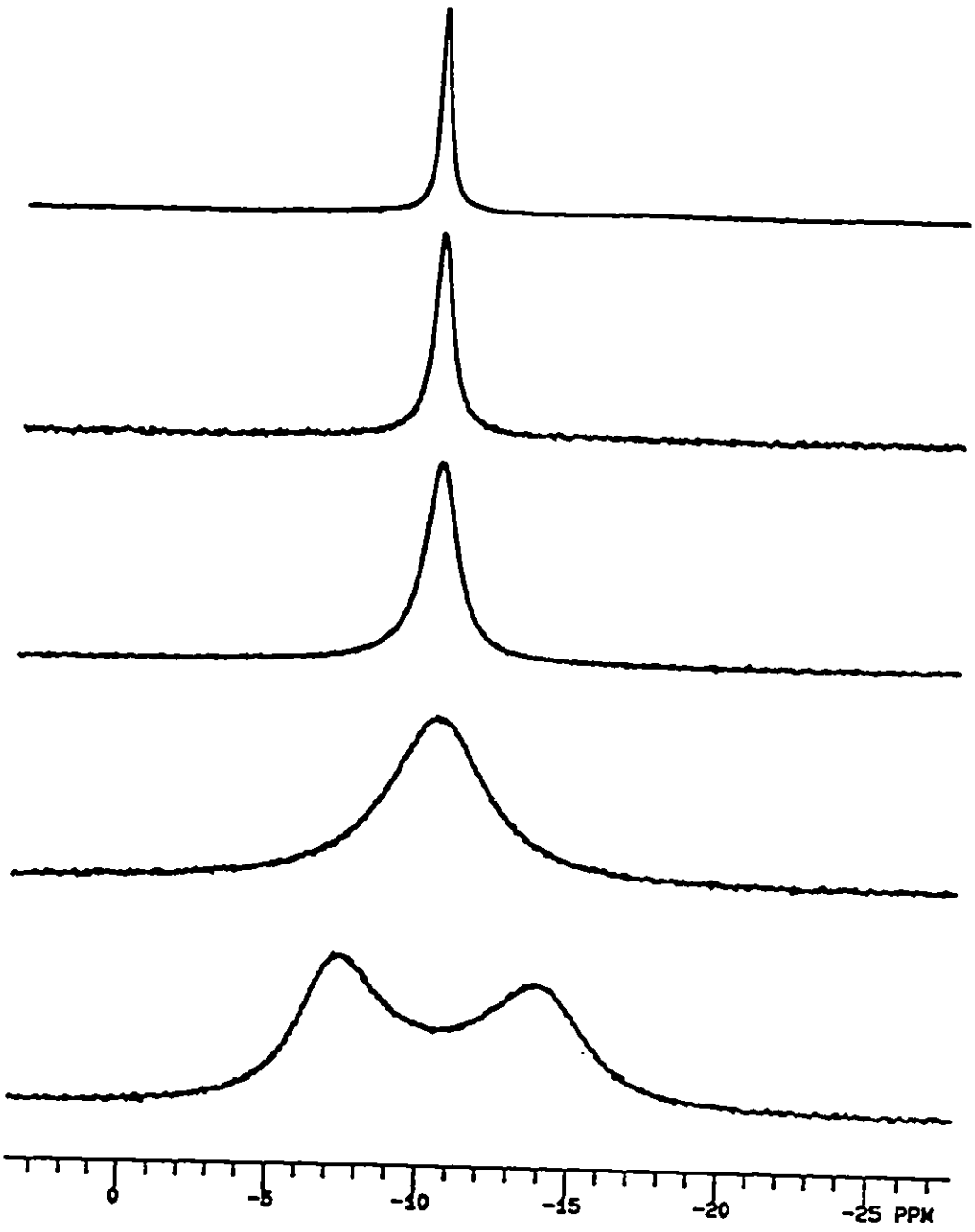

Figure 21: ^{23}Na NMR spectra of $NaBPh_4$-18C6 in AN of ρ=0.5 at varying temperatures. $[Na^+]_T$= 20mM. Top to bottom: T= 324.4K, 307.6K, 295.2K, 273.6K and 252.6K.

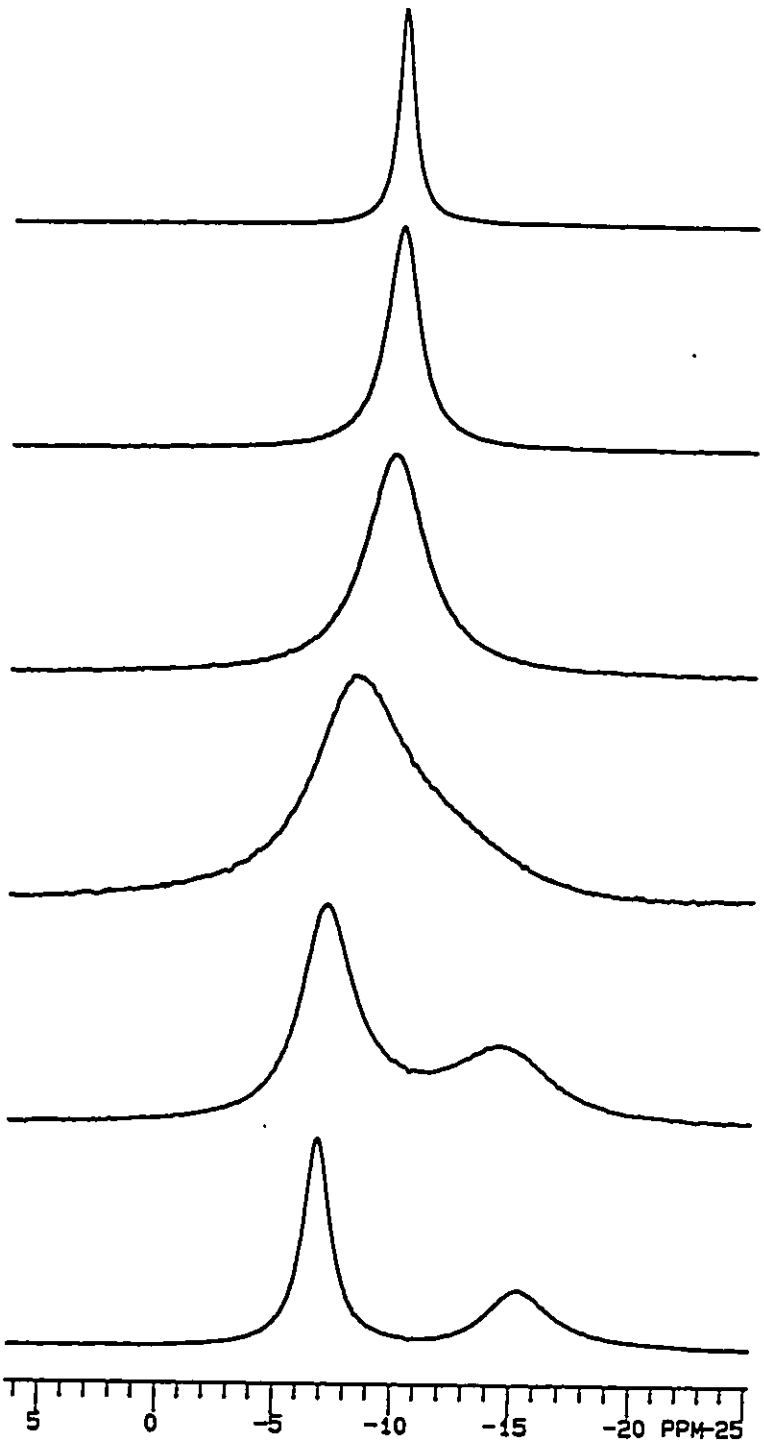

Figure 22: ^{23}Na NMR spectra of $NaBPh_4$-18C6 in AC of ρ=0.4 at varying temperatures. $[Na^+]_T$= 20mM. Top to bottom: T= 301.5K, 288.2K, 279.2K, 268.8K, 258.8K and 249.4K.

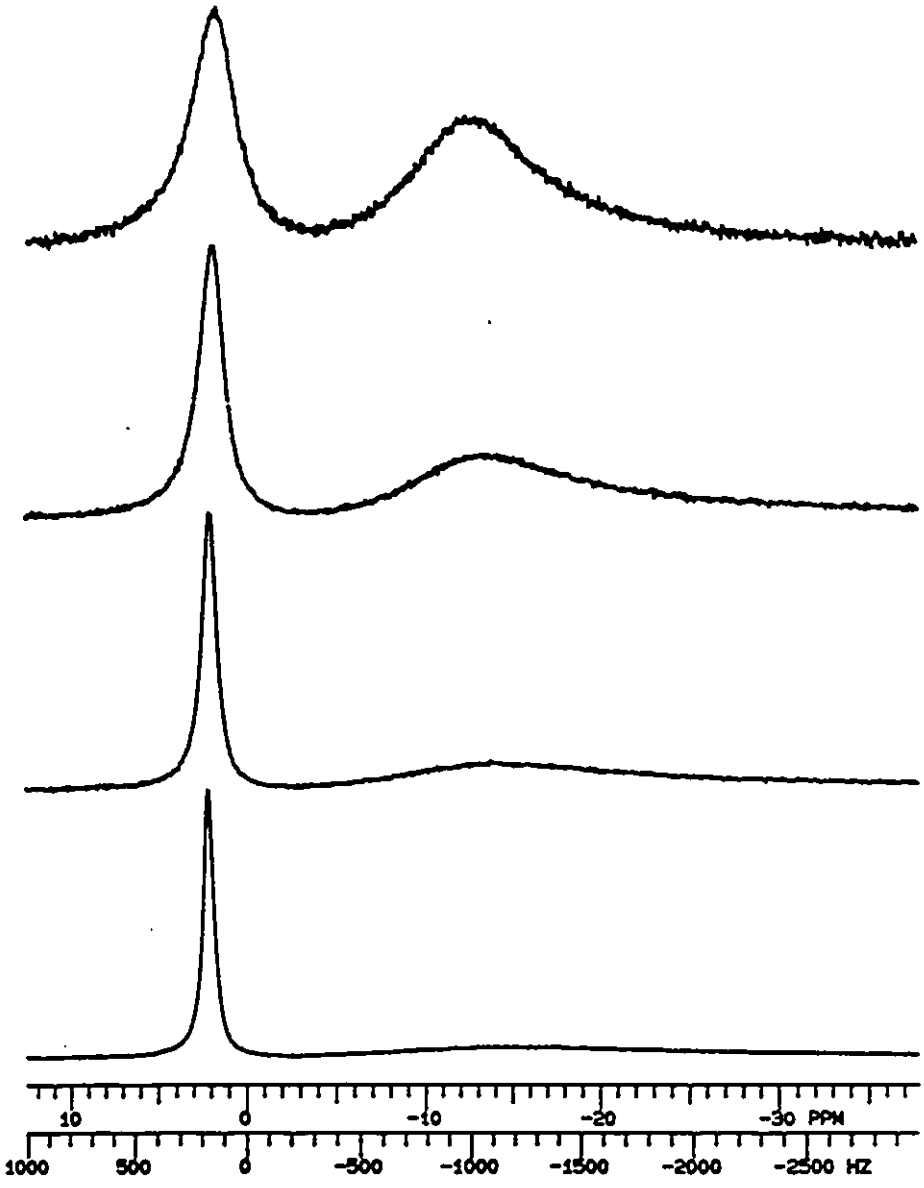

Figure 23: ^{23}Na NMR spectra of $NaBPh_4$-18C6 in PY of ρ=0.68 at varying temperatures. $[Na^+]_T$= 20mM. Top to bottom: T= 288.2K, 279.2K, 268.8K and 258.8K.

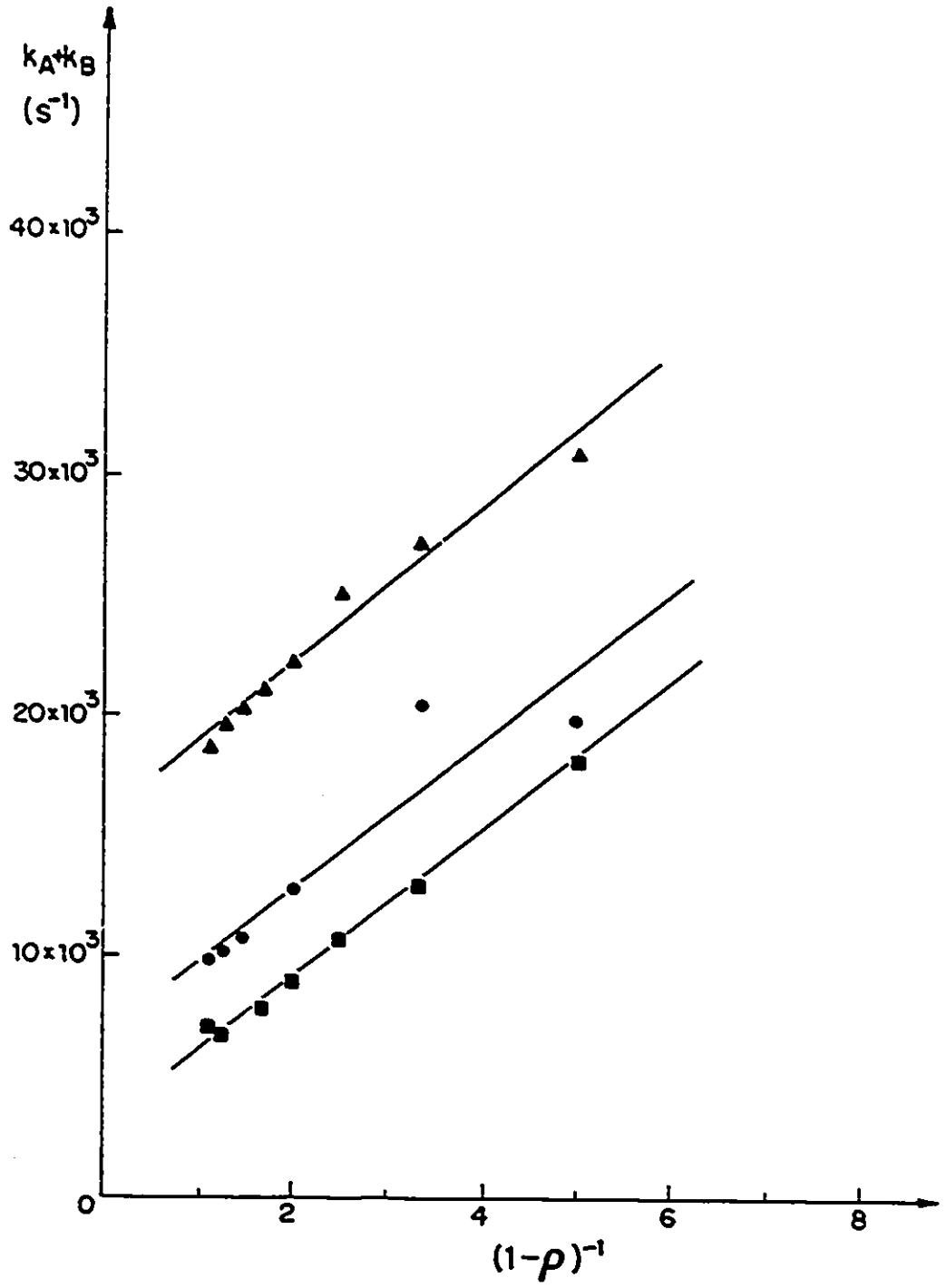

Figure 24: $(k_A + k_B)$ as a function of $(1-\rho)^{-1}$ for $NaBPh_4$-18C6 in AN for three $[Na^+]_T$. $[NaBPh_4]_T$ = 5.0mM (■), 20.0mM (●), and 50mM (▲). T=295K.

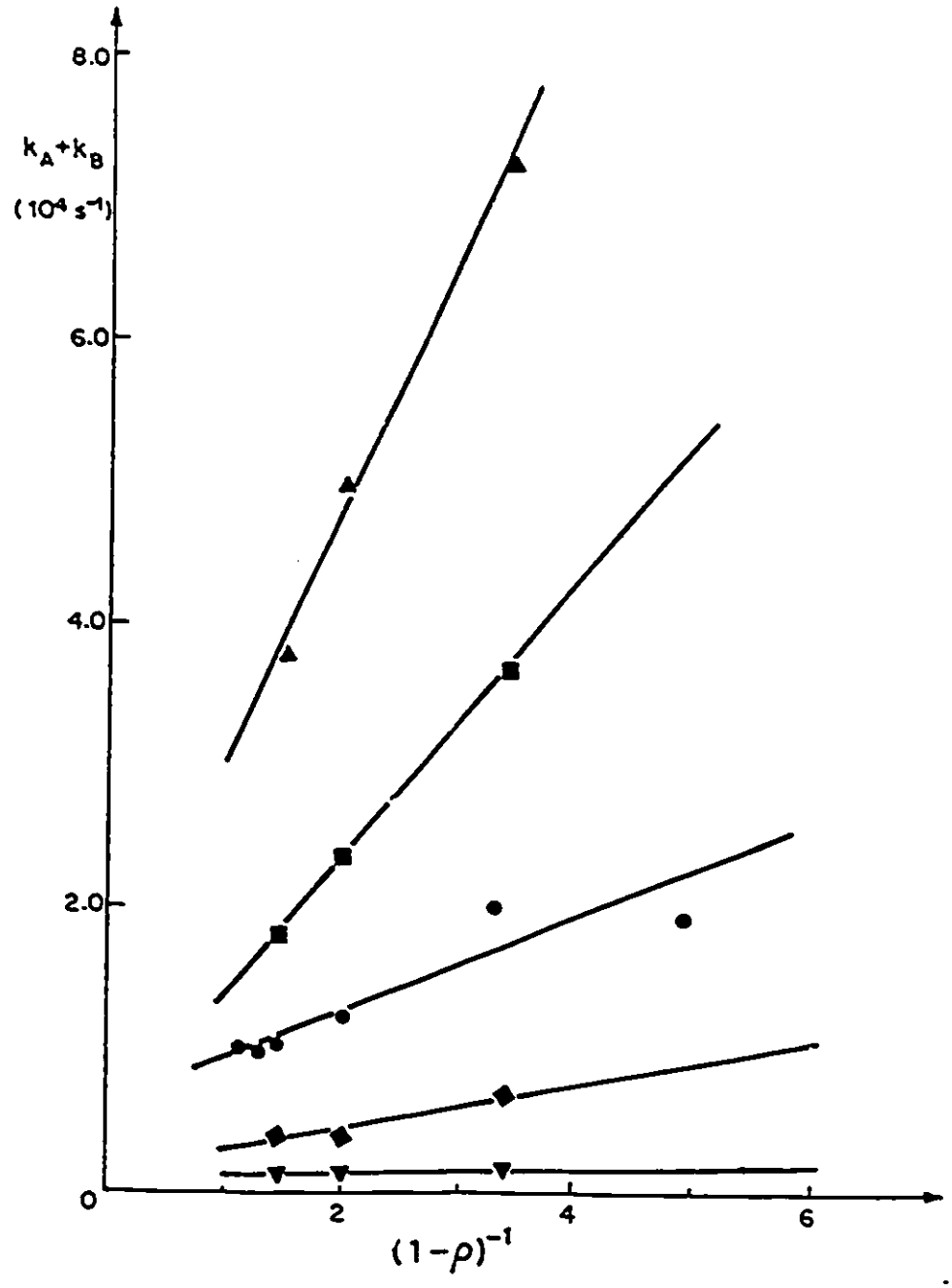

Figure 25: ($k_A + k_B$) as a function of $(1-\rho)^{-1}$ for $NaBPh_4$-18C6 in AN at five temperatures: 252.6K (▼), 273.6K (♦), 295.2K (●), 307.6K (■), and 324.4K (▲). $[NaBPh_4]_T$= 20mM.

The plots of $T_i^{-1}(i=1,2)$ vs ρ for AC and PC are different in appearance (see Figure 26) and these solvents are quite different in terms of viscosity. (3.03 and 25.3mP respectively) This is responsible for order of magnitude differences between the relaxation rates, which are from 30-200Hz for AC, and 200-400Hz for PC. The T_1^{-1} increases from 30Hz to 80Hz in AC and from 200Hz to 300Hz in PC in the transition from solvated Na^+ to complexed Na^+ because the complex is the more dissymmetric of the two. This is reflected in the quadrupolar coupling constant (χ). The mechanism of exchange is the factor responsible for the differences in shape. Further evaluation of the data supports this. The pseudo-first order rate constants do not vary with $(1-\rho)^{-1}$ in identical manners. (see Figures 27 and 28) In the case with AC, the straight lines extrapolate to and converge at the origin. There is no evidence for the M_{ai} mechanism here. In contrast, when the solvent is PC, the lines do not extrapolate to the origin, nor do they converge. The predominant mechanism is the M_{ai} mechanism while there is also a contribution from the dissociative mechanism. Here the contributions from each mechanism can be evaluated separately.

The principal difference between the series in PY and the others is that the pseudo-first order rate constant for every sample was determined by full lineshape analysis since none of the peaks were Lorentzian. The graph of $(k_A + k_B)$ vs $(1-\rho)^{-1}$ is virtually identical in appearance to the one for AN. (see Figure 29) The dissociative mechanism is operative but there are contributions from the M_{ai} mechanism.

Using an Eyring plot, the activation parameters for the dissociative mechanism for each solvent can be determined and, in the case of PC, the values for the M_{ai} mechanism may also be determined. The errors on the k_2 values are such that it would be unwise to calculate activation parameters for the M_{ai} mechanism in any of the other solvents. (see Figure 30) For NM, as explained earlier, only the limiting value for $(k_A + k_B)$ may be determined. It appears, along with other characteristics of $(Na\text{-}18C6)^+$ in Table VI. Table VII summarizes the kinetic parameters of $(Na\text{-}18C6)^+$ in various solvents.

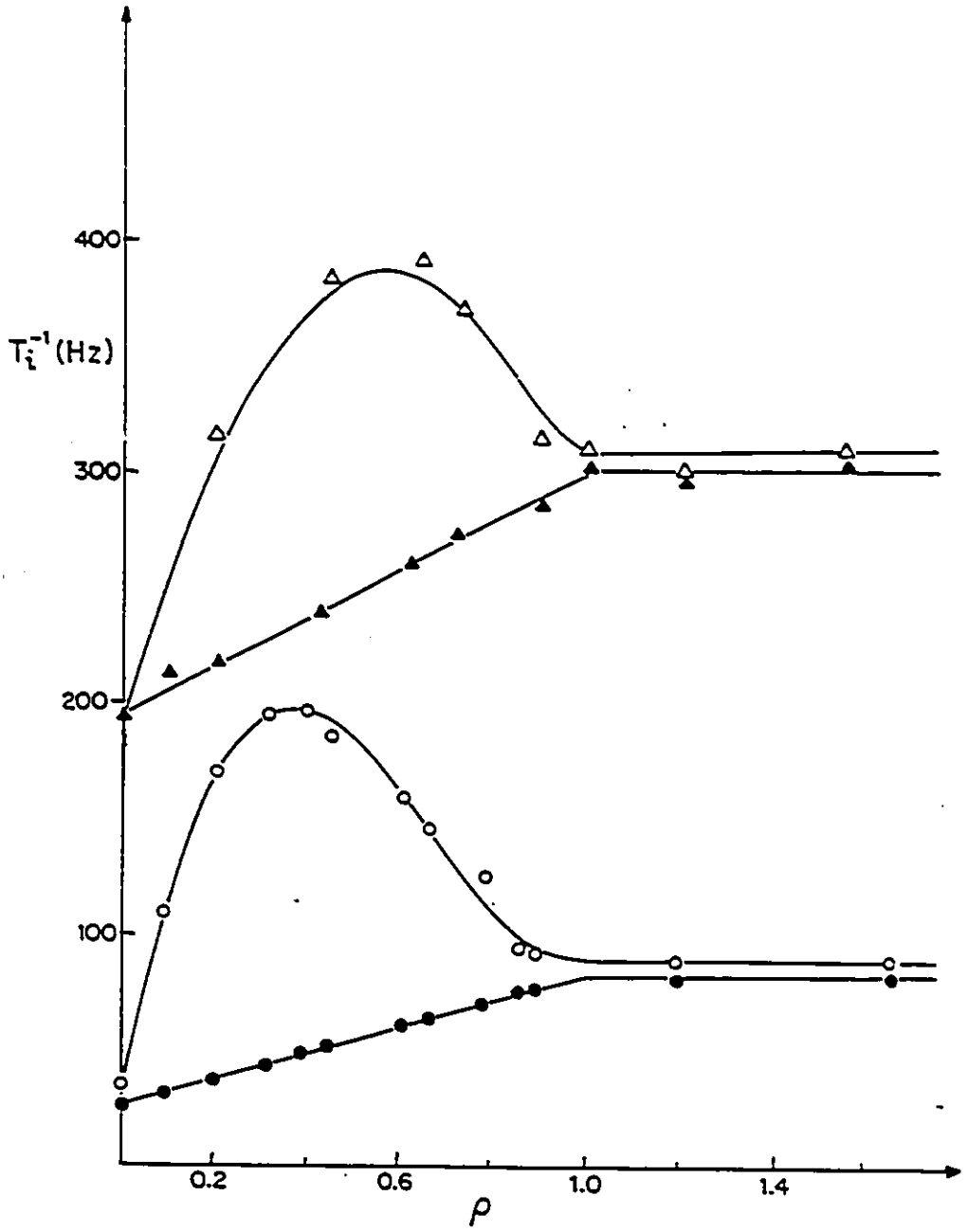

Figure 26: ^{23}Na relaxation rates as a function of ρ for $NaBPh_4$-18C6 in AC (○,●) and PC (△,▲). ^{23}Na transverse (△,○)(i=2) and longitudinal (▲,●)(i=1) relaxation rates. $[NaBPh_4]_T$ = 20.0mM. T=295K. The data points are experimental and the curves are calculated from the values of k_{-1} and k_2 given in Table VII, using equation 44.

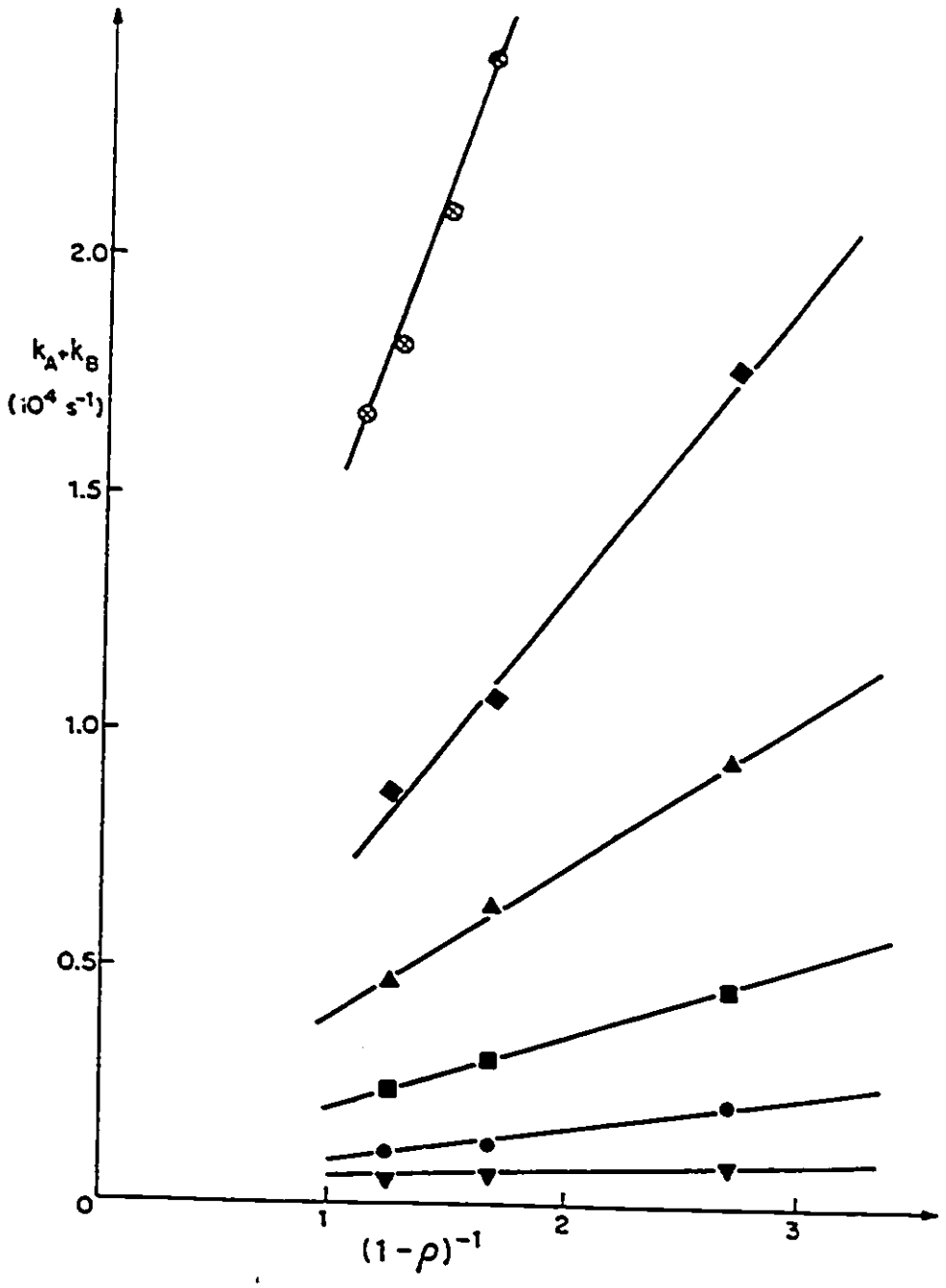

Figure 27: $(k_A + k_B)$ as a function of $(1-\rho)^{-1}$ for $NaBPh_4$-18C6 in AC at six temperatures: 249.4K (▼), 258.8K (●), 268.8K (■), 279.2K (▲), 288.2K (♦), and 301.5K (⊗). $[NaBPh_4]_T$= 20mM.

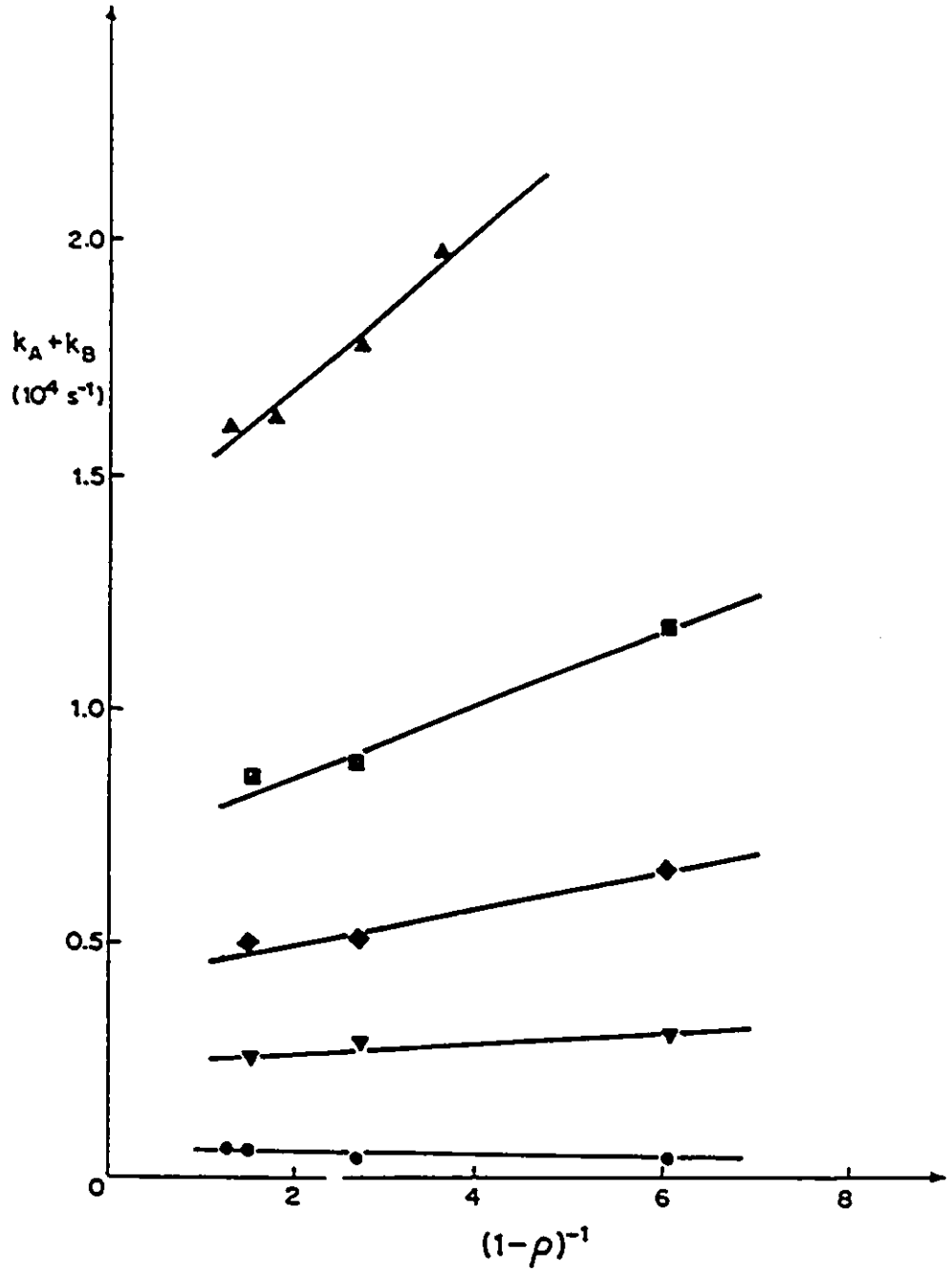

Figure 28: $(k_A + k_R)$ as a function of $(1-\rho)^{-1}$ for $NaBPh_4$-18C6 in PC at five temperatures: 249.4K (●), 268.8K (▼), 279.2K (♦), 288.2K (■), and 301.5K (▲). $[NaBPh_4]_T$= 20mM.

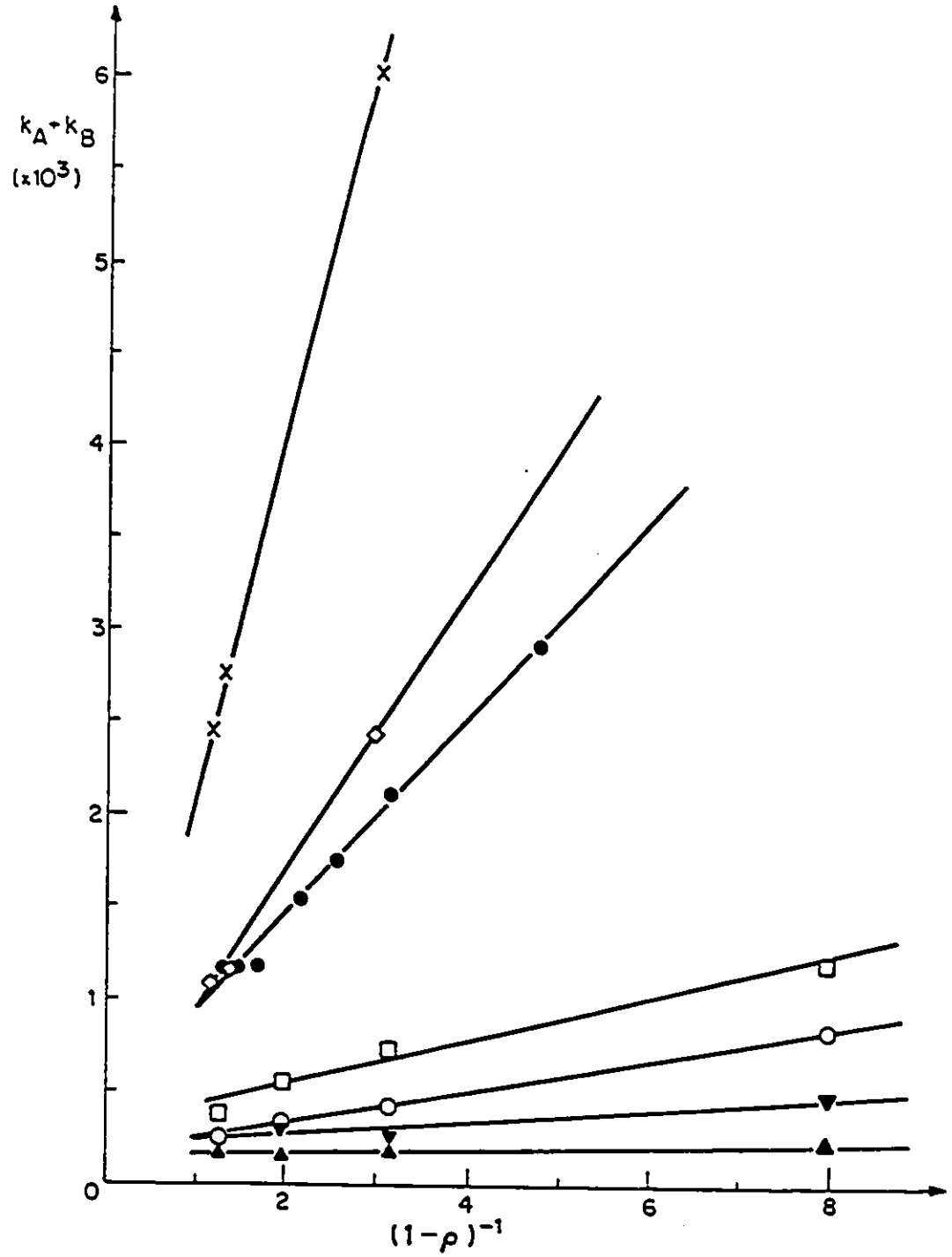

Figure 29: $(k_A + k_B)$ as a function of $(1-\rho)^{-1}$ for $NaBPh_4$-18C6 in PY at seven temperatures: 258.9K (▲), 268.8K (▼), 279.2K (○), 288.2K (□), 301.5K (●), 310.7K (◊) and 324.4K (×). $[NaBPh_4]_T$= 20mM.

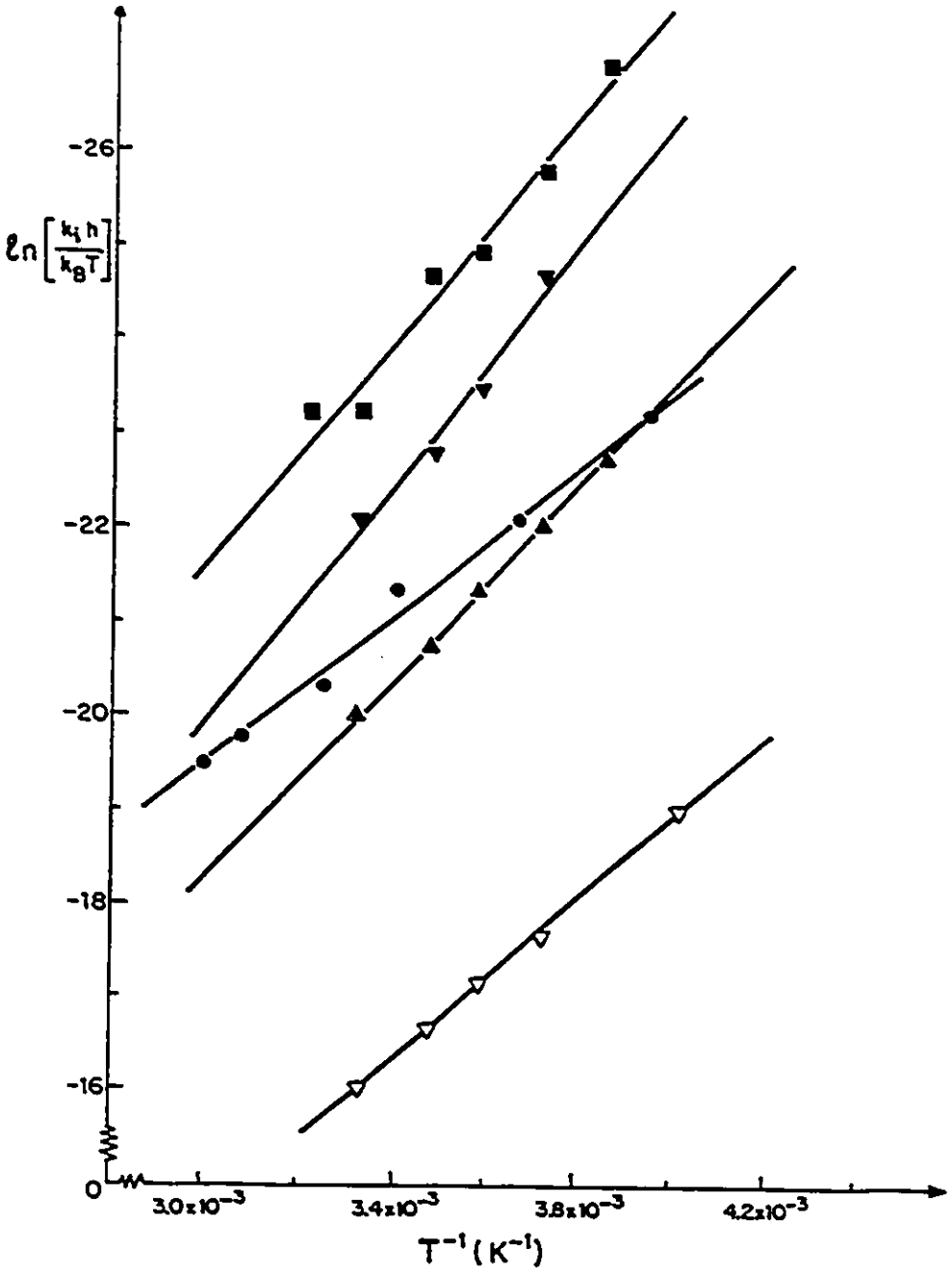

Figure 30: ($\ln k_i - \ln[k_B T/h]$) as a function of T^{-1} for $NaBPh_4$-18C6 in PY (■), PC (▼,▽), AC (▲), and AN (●). i=2 (▽), otherwise i=-1.

Table VI: ^{23}Na NMR Characteristics of $(Na\text{-}18C6)^+$ in Various Solvents.

solvent	DN	ϵ (298K)	η(mP) (298K)	$\delta(Na\text{-}C)^+$ (ppm)	$\Delta\delta$(Hz)	$T_1^{-1}(Na\text{-}C)^+$ (Hz)	$(k_A+k_B)_{lim}$ (s^{-1})
NM	2.7	35.9[A]	6.14	-16.3	121	332	3.4×10^3
AN	14.1	36.0	3.41	-14.9	590	73.0	2.6×10^5
PC	15.1	64.9	25.3	-16.2	475	297	3.7×10^4
AC	17.0	20.6	3.03	-15.8	600	82.0	2.1×10^5
PY	33.1	12.9	8.84	-12.4	1080	1280	8.2×10^4

A) 303K

Table VII: Kinetics Parameters of $(Na\text{-}18C6)^+$ in Various Solvents.

solvent	$(k_A + k_B)$	k_{-1} (s^{-1})	k_2 ($M^{-1}s^{-1}$)	$\Delta H^{\ddagger}$ ($kJ.mol^{-1}$)	$\Delta S^{\ddagger}$ ($J.mol^{-1}.K^{-1}$)	$\Delta G^{\ddagger}_{301.5}{}^{A}$ ($kJ.mol^{-1}$)	$\Delta G^{\ddagger}_{301.5}{}^{B}$ ($kJ.mol^{-1}$)
AN	$(1.28\pm0.04)\times10^4$	$(3.8\pm0.5)\times10^3$	$(2.6\pm0.4)\times10^5$	32±2	-65±8	53.2±0.4	42.6±0.4
PC	$(1.70\pm0.05)\times10^4$	$(1.6\pm0.2)\times10^3$	$(6.9\pm0.3)\times10^5$	54±6	-5±20	55.4±0.3	-
PC	-	-	-	35±1[C]	-16±3[C]	-	40.2±0.1
AC	$(2.91\pm0.08)\times10^4$	$(1.48\pm0.02)\times10^4$	-	44±1	-21±2	49.8±0.1	-
PY	$(1.47\pm0.05)\times10^3$	$(5.3\pm0.2)\times10^2$	$(2.0\pm0.3)\times10^4$	49±4	-30±10	58.1±0.1	49.0±0.4

A) dissociative mechanism

B) M_{si} mechanism

C) M_{si} mechanism. All others are for the dissociative mechanism.

4.3 Discussion

The mechanistic contributions have been separated from the observed rate constant of dissociation for $(Na\text{-}18C6)^+$. In AC this is straight forward because the contribution from the M_{ai} mechanism is negligible, so the measured rate can be directly related to k_{-1}. Lincoln et al have published activation parameters for the NaSCN-18C6 system in AC.[97] In their study $[Na^+]_T$=100mM. The choice of counter anion and $[Na^+]_T$ would probably cause the differences which are observed between the two sets of activation parameters. As will be seen in Chapter 5, SCN^- forms ion pairs with Na^+, so Lincoln's system would contain ion-paired species whose rates of dissociation could not be expected to be identical to those where none is present. The same interpretation can be applied when comparing the results in PY.[97] The Australian study did not obtain kinetic data with AN and PC but, at lower concentrations, and with a salt known not to ion-pair, success would have been more probable.

In PY and AN there are contributions from both mechanisms. Separation of the two components shows that the contribution of the dissociative mechanism is the major one. B15C5 has been studied in AN too.[96] The dissociative rate constant (k_{-1}) at 301.5K is the same, within experimental error, for B15C5 and 18C6 being $(3.5\pm0.1)\times10^3$ s^{-1} and $(3.8\pm0.5)\times10^3$ s^{-1} though the contribution to the M_{ai} mechanism is more than an order of magnitude larger for B15C5 than for 18C6.

Strasser and Popov have reported that the M_{ai} mechanism is operative for $(Na\text{-}18C6)^+$ in PC.[94] Buschmann has reported thermodynamic parameters for $(Na\text{-}18C6)^+$ complex formation in PC, as determined by potentiometric and calorimetric titrations.[99] Strasser and Popov did not identify and extract the small contribution of the dissociative mechanism from the observed rate of decomplexation so it is difficult, and not very wise, to directly compare the values obtained for the M_{ai} mechanism by both parties. What is important is that this study also identifies the M_{ai} mechanism to be operative in PC. Overall this system in PC is particularly interesting because the determination of the activation parameters for both

mechanisms was possible. This had not been previously achieved and showed that certain systems can be cleanly separated into individual contributions. Lin and Popov reported ^{23}Na chemical shifts as a function of ρ for the addition of Na^+ to 18C6 in several solvents, including AN, NM, PC and AC.[69] Their results agree with the ones found in this study.

If the model for dissociative decomplexation were simply one where a sodium-ether oxygen bond is replaced by a sodium-solvent bond one would expect the $\Delta H^{\ddagger}$ to follow the trend where an increase in DN would lower the activation enthalpy. This is not the case since the values for $\Delta H^{\ddagger}$ follow the trend: AN < AC < PY ≅ PC. The electron-donating ability of the solvent, which is reflected by its DN, is clearly not directly related to the energetics of dissociation. Since the relaxation rate of the complex is not linearly related to the solvent viscosity, it is evident that at least one solvent molecule coordinates with the complex. The range of chemical shifts within the different solvents is smaller for $(Na\text{-}18C6)^+$ (3.9 ppm) than it is for $(Na\text{-}DB18C6)^+$ (8.2 ppm) which indicates that there are fewer coordinating solvent molecules for $(Na\text{-}18C6)^+$ than for $(Na\text{-}DB18C6)^+$. Plausible conformational rearrangements leading to the transition state are accompanied by partial desolvation of $(Na\text{-}18C6)^+$ and reorganization of the partially decomplexed crown ether.[90] Others have also inferred this from work involving the complexing of 18C6 with acetonitrile and nitromethane.[84]

The enthalpy-entropy compensation effect is operative here, and is reminiscent of what occurs in the thermodynamic process of the complexation of cations with other crown ethers, cryptands, podands and antibiotics.[100] The plots of $T\Delta S$ vs ΔH for 1:1 complexation of cations with crown ethers gives a "fair-to-good" positive correlation. The origin of the compensation effect in the thermodynamic parameters is not entirely clear because they are governed by several factors. It would be oversimplistic to attribute the effect viewed for the activation parameters of the decomplexation process to any one cause. Okoroafor and Popov conclude that since the overall enthalpies and entropies of complexation are the sums of the

contributions from each step or process, these steps must be better known before the nature of the macrocyclic effect can be elucidated.[101]

The $\Delta G^{\ddagger}_{300K}$ for the dissociative process for $(Na\text{-}18C6)^{+}$ in AN is 53 $kJ.mol^{-1}$. (See Table VIII) This is identical for $(Na\text{-}DB18C6)^{+}$ in AN.[90] The compensation effect for the enthalpy and entropy of activation is the reason why they are the same. The lower activation enthalpy for $(Na\text{-}18C6)^{+}$ is because the 18C6 is more flexible than DB18C6. For the M_{ai} mechanism $\Delta G^{\ddagger}$ varies as PC < AN < PY. This suggests that the desolvation of the incoming cation is the major contribution to the exchange barrier. Actually there are several differences between the two systems: the rigidity of the ligand, the basicity of the ether oxygens and the structures in solution; but the values of the activation parameters remain remarkably similar.

Table VIII: The Kinetic Parameters for $(Na\text{-}18C6)^{+}$ and $(Na\text{-}DB18C6)^{+}$.

	$NaBPh_4$-DB18C6 in AN	$NaBPh_4$-18C6 in AN
$\Delta H^{\ddagger}$ ($kJ.mol^{-1}$)	40±2	32±2
$\Delta S^{\ddagger}$ ($J.mol^{-1}.K^{-1}$)	-44±8	-65±8
$\Delta G^{\ddagger}_{300K}$ ($kJ.\ mol^{-1}$)	53±2	53.2±0.4

4.4 Summary and Conclusions

In the four non-aqueous solvents used, the sodium cation forms a 1:1 complex with 18C6 and exchanges between a solvated site and a complexed site. Determination of the pseudo-first order rate constants for the exchange for different concentrations and temperatures permits the separation of the contributions from the two competitive mechanisms: the dissociative and the M_{ai} mechanisms. In PC, the activation enthalpy and

entropy for each process may be determined. In AC, $(Na\text{-}18C6)^+$ decomplexes exclusively by the dissociative mechanism. Having found such a system, it can be used to further probe the roles of other system components such as the counter anion. This will be the focus of Chapter 5. In these systems there is a compensation effect for the enthalpy and entropy of activation, which leads to identical free energies of activation for $(Na\text{-}18C6)^+$ and $(Na\text{-}DB18C6)^+$ in AN.

Chapter 5
The $(Na\text{-}18C6)^+$ System: the role of the counter anion in the dissociative mechanism

5.1 Background

The contribution from the anion is negligible when tetraphenylborate ion is used, but when thiocyanate is the counter anion, ion-pairing between the sodium cation and the thiocyanate anion must be considered. The dissociative mechanism has been shown to be predominant for several systems using this counter anion. As was shown in Chapter 4, Lincoln et al observed the dissociative mechanism with the NaSCN-18C6 system in AC, MeOH and PY.[97] Others had observed the M_{ai} mechanism when SCN^- was the counter anion.[93] In THF, with $NaBPh_4$, the dissociative mechanism is operative, but when SCN^- is used, the M_{ai} mechanism is operative. Rate parameters were calculated for the M_{ai} mechanism. The change in mechanism was attributed to the degree of ion-pairing. The M_{ai} mechanism involves a transition state where two sodium cations must be in close proximity. The strong ion-pairing reduces the charge-charge repulsion, which BPh_4^- does not offset.[93] The fact that the presence of SCN^- does not always result in the predomination of the M_{ai} mechanism leaves its exact influence in question.

Phillips et al needed to take ion-pairing into consideration when they studied sodium-crown ether systems in methylamine with bromide as the counter anion.[102] Their model of two-site exchange involved solvated and complexed sodium cations which were completely ion-paired. No unpaired species were considered. The dissociative mechanism was observed for the NaBr-18C6 system. The exchange rate for the NaBr-15C5 system was too fast to be measured on the NMR timescale.

Ion-pairing has been studied by ^{23}Na NMR for several decades. Erlich and Popov examined changes in ^{23}Na chemical shifts for several salts in non-aqueous solvents.[103] Among the eleven solvents used were AC, AN, PY and MeOH. Sodium tetraphenylborate and sodium perchlorate have chemical shifts which are independent of salt concentration.

Sodium iodide and sodium thiocyanate chemical shifts do depend upon salt concentration but the iodide more so than the thiocyanate.[103] Greenberg et al extended the previous study by adding five solvents and using NaBr in addition to the other four salts.[104]

Cox et al have examined the effect of anions in the dissociation of metal cryptates in MeOH by spectrophotometry.[105] The choice of counter anion does have an influence on the rate of dissociation by forming ion-pairs with the central metal ion and catalyzing the reaction. The choice of ligand may suppress this action by making it difficult for the anion to approach.

Stöver and Detellier have studied the role of the counter anion for the dissociation of $(Na\text{-}DB24C8)^+$ in NM.[91] This was discussed in some detail in Section 3.2. A change in counter anion led to a change in reaction rate rather than a change in reaction mechanism.

This chapter will examine how the use of SCN^-, rather than BPh_4^-, influences the dissociation of $(Na\text{-}18C6)^+$. From the literature the possible effects are not evident. Strasser et al's work[93] would suggest that a change in mechanism will be observed while Cox et al's work[105] would suggest a catalytic effect. Finally an acceleration of the existing mechanism is a possibility. The changes in ^{23}Na chemical shifts which Erlich and Popov observed[103] will be confirmed and the changes in relaxation rates will be investigated in AC and AN. The rates of dissociation of $(Na\text{-}18C6)^+$ in AC and the energetics of ion-pairing when SCN^- is present will be examined in detail.

5.2 Results

Changing the counter anion from tetraphenylborate to thiocyanate has a rather dramatic effect. The graph of relaxation rates vs $(1-\rho)^{-1}$ for the two sets of samples in AC (see Figure 31) is a clear illustration of the changes. At this temperature (301.5K) only one peak is observed because there is moderately rapid exchange under extreme narrowing conditions and a 1:1 complex forms for both systems. At $\rho = 0$, where there is only solvated Na^+ in solution, both relaxation rates have increased. The contribution from exchange for

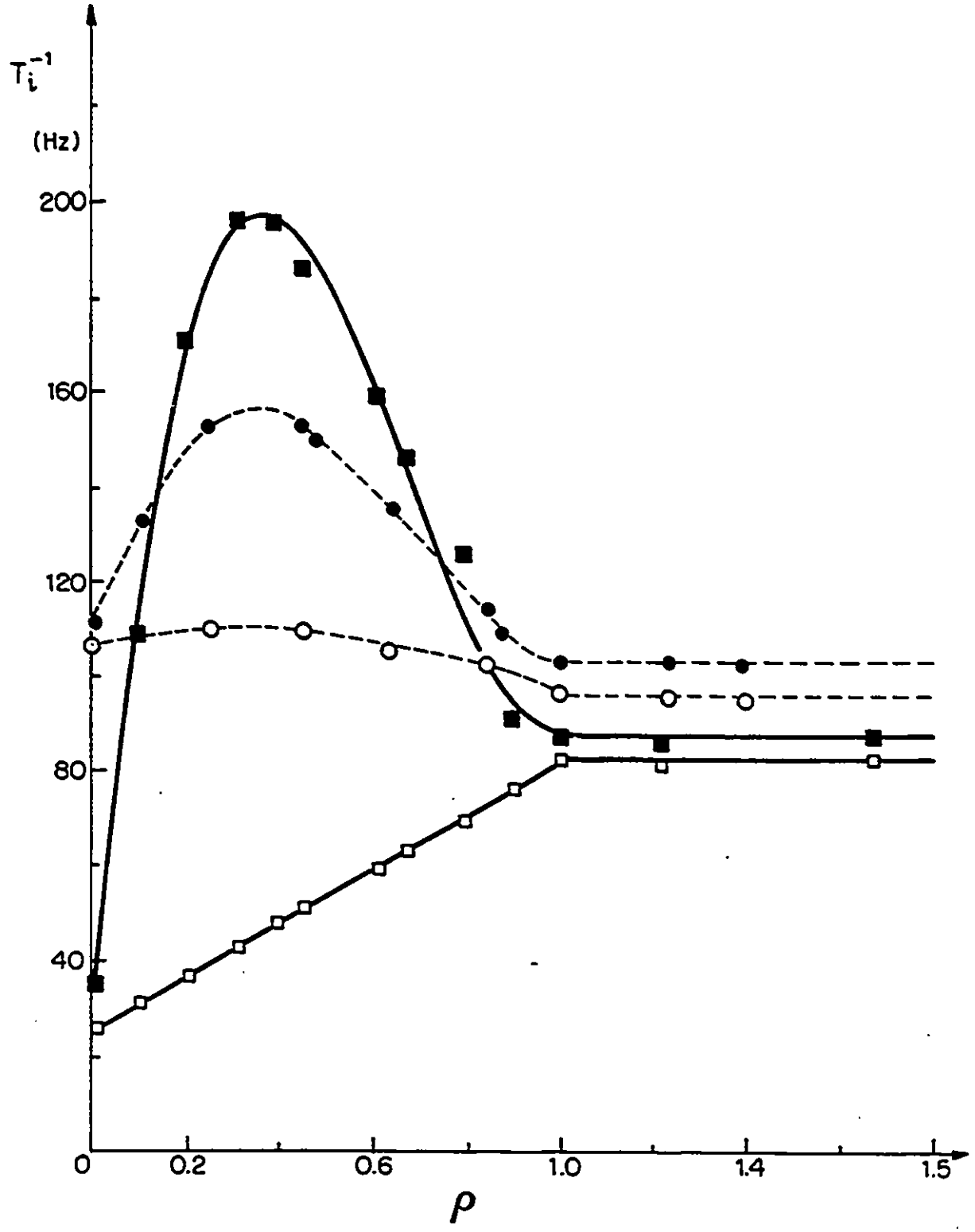

Figure 31: ^{23}Na transverse (i=2; ■,●) and longitudinal (i=1; □,○) relaxation rates of $NaBPh_4$ (■,□) and NaSCN (●,○) in acetone as a function of $\rho = [18C6]/[Na^+]_T$. $[Na^+]_T = 2.00 \times 10^{-3}$ M. T = 301.5±0.5 K. The data points are experimental, and the curves are calculated from the values obtained from equation 44 and given in Table XI.

$0< \rho <1$ is much less for the system involving SCN^-. Finally at $\rho >1$, while both relaxation rates are higher for the SCN^- system than for the one using BPh_4^-, the differences are much smaller relative to the others. The slight curvature in the line representing the longitudinal relaxation rate of NaSCN is due to ion-pairing. The same graph in AN shows a very similar result. (see Figure 32) When a temperature study is done on the NaSCN-18C6 system in AN, the observed pseudo-first order rate constants show that the dissociative mechanism and the M_{ai} mechanism are both operative. (see Figure 33) If the contribution from ion-pairing is ignored, activation parameters for the dissociative mechanism may be determined from the $k_{-1,obs}$. The results are surprisingly similar for the $NaBPh_4$-18C6 system in the same solvent, yet the initial assumption was probably not valid. (see Table IX)

Erlich and Popov[103] showed how the presence of thiocyanate ions affected ^{23}Na chemical shifts, but separating both the operative mechanisms and the contributions from ion-pairing in AN is quite complex. In AC, where there is exclusively the dissociative mechanism when BPh_4^- is the counter anion, one of the complications has been eliminated. Rather than tackling the region with two species in exchange immediately, the regions where there is only one form of Na^+ were investigated. This was due to the belief that the insights gained on the variations for $\rho =0$ and $\rho >1$ would greatly facilitate the interpretation of the $0< \rho <1$ region, which was bound to be more complex. Figure 34 shows how the chemical shift varied with the concentration of sodium salt. When the salt is $NaBPh_4$, as expected, the chemical shift of $(Na^+)_s$ is constant. In AC and AN the chemical shift of $(Na^+)_s$ decreases as the concentration increases. The transverse relaxation rates vary in a similar manner. (see Figure 35) Similar determinations were made for the complexed species. (see Figure 36) Computer regressions were then run on a model which included contributions to the relaxation rates from only the solvated and 1:1 ion-paired species. The success of these regressions meant that ion-paired aggregates were not considered to be present in significant concentrations. The species which ion-pair at $\rho =0$ are given in equation 50.

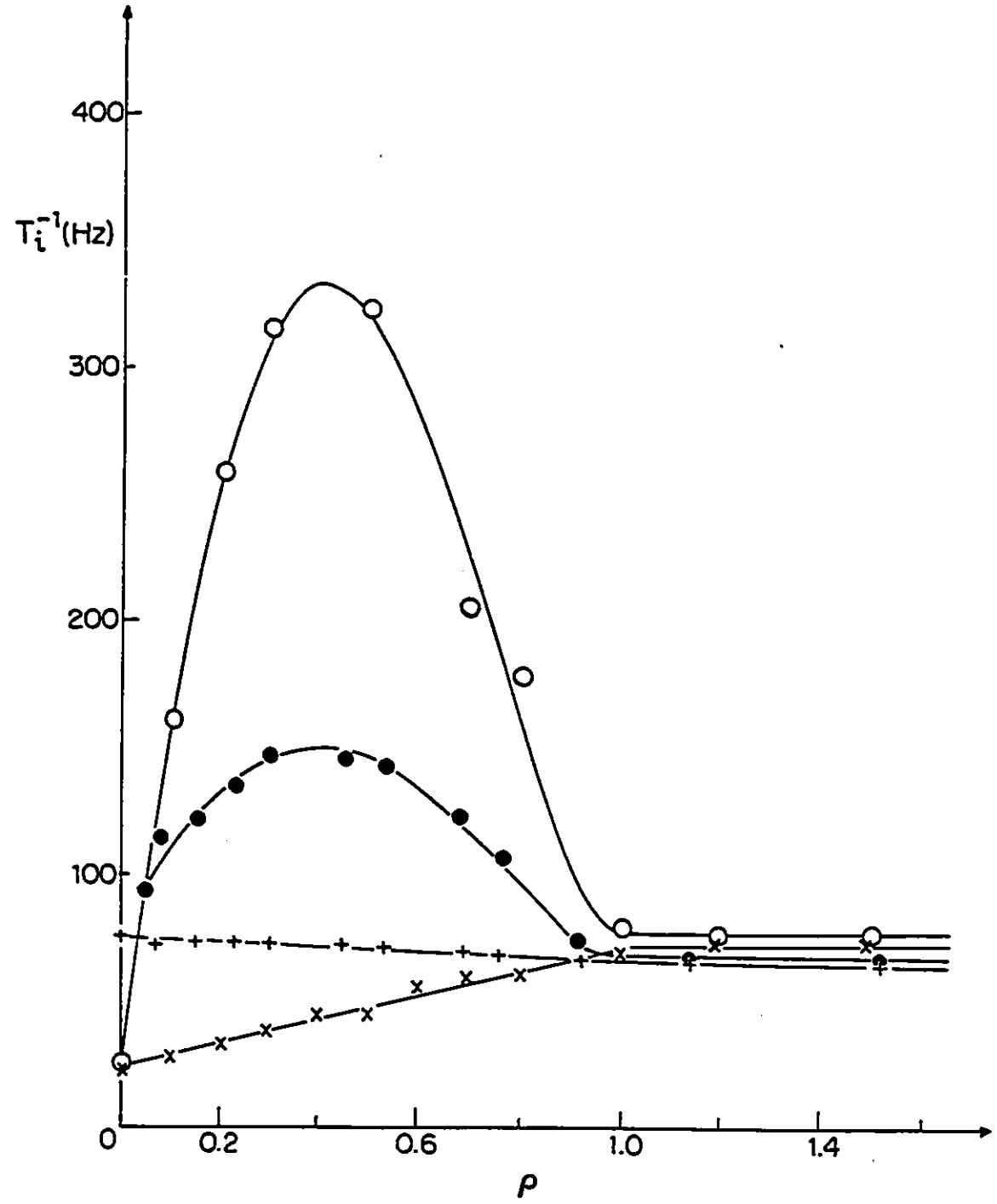

Figure 32: ^{23}Na transverse (i=2; ○,●) and longitudinal (i=1; ×,+) relaxation rates of $NaBPh_4$ (○,×) and NaSCN (●,+) in acetonitrile as a function of $\rho = [18C6]/[Na^+]_T$. $[Na^+]_T = 2.00 \times 10^{-3}$ M. T = 301.5±0.5 K. The data points are experimental, and the curves are calculated from the values obtained from equation 44.

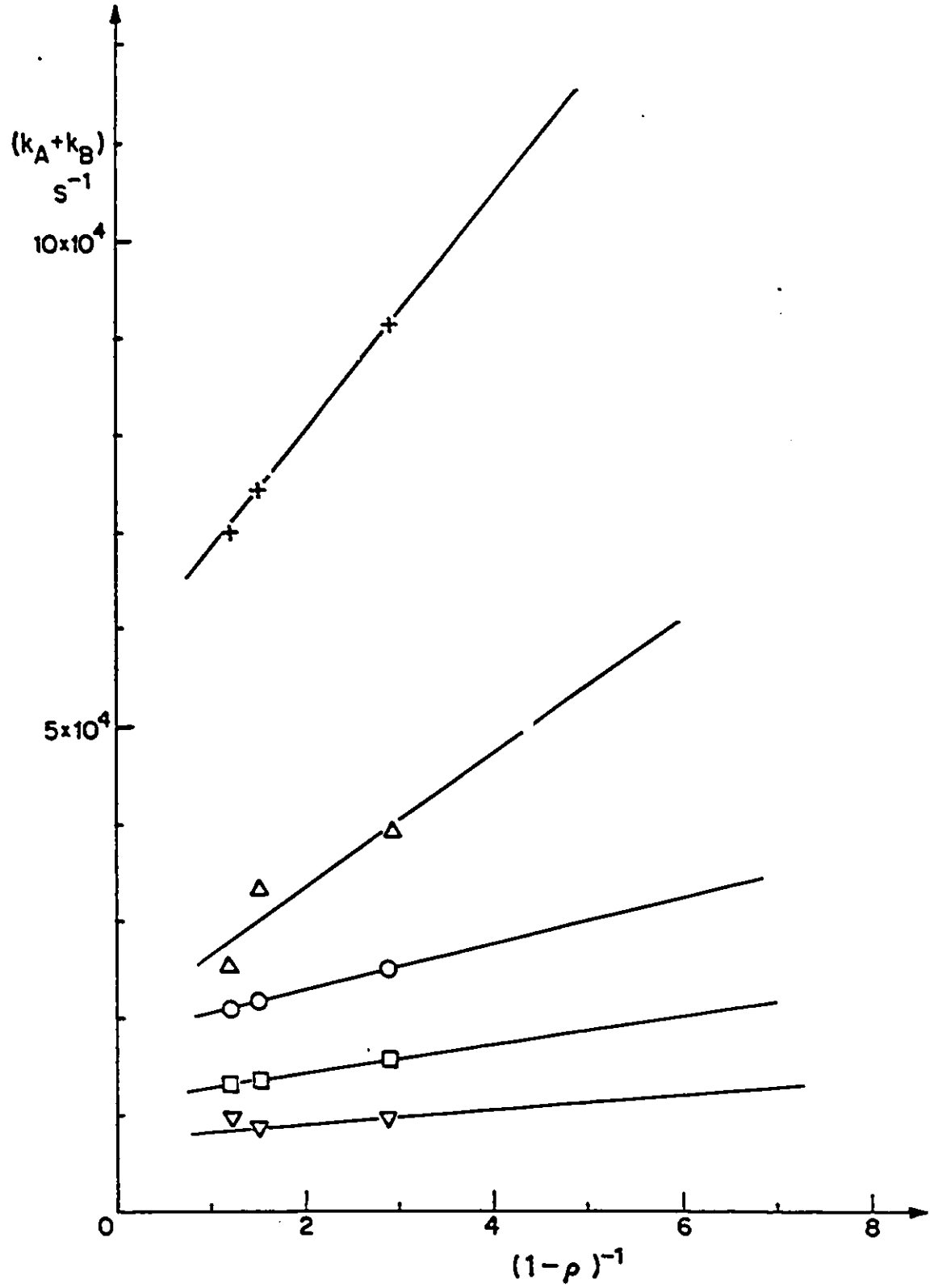

Figure 33: Pseudo-first-order rate constants ($k_A + k_B$) as a function of $(1 - \rho)^{-1}$ for NaSCN-18C6 in AN at five temperatures: 249.5K (∇), 259.0K (□), 269.2K (○), 279.2K (Δ), 301.5K (+). $[Na^+]_T = 2.00\times10^{-2}$M.

Table IX: Pseudo-first order rate constants and activation parameters for NaX-18C6 systems in AN. X= BPh_4^- and SCN^-.

$(k_A + k_B)$ (ρ =0.5) NaSCN-18C6-AN	T (K)	$(k_A + k_B)$ (ρ =0.5) $NaBPh_4$-18C6-AN
-	324.4	4.79×10^4
-	307.6	2.36×10^4
7.92×10^4	301.5	1.28×10^4
4.36×10^4	288.2	-
3.30×10^4	279.2	-
-	273.6	3.91×10^3
2.23×10^4	269.2	-
1.40×10^4	259.0	-
-	252.6	1.40×10^3
$\Delta H^{\neq}$= 25 kJ.mol^{-1}		32±2 kJ.mol^{-1}
$\Delta S^{\neq}$= -64 J.mol^{-1}.K^{-1}		-65±8 J.mol^{-1}.K^{-1}

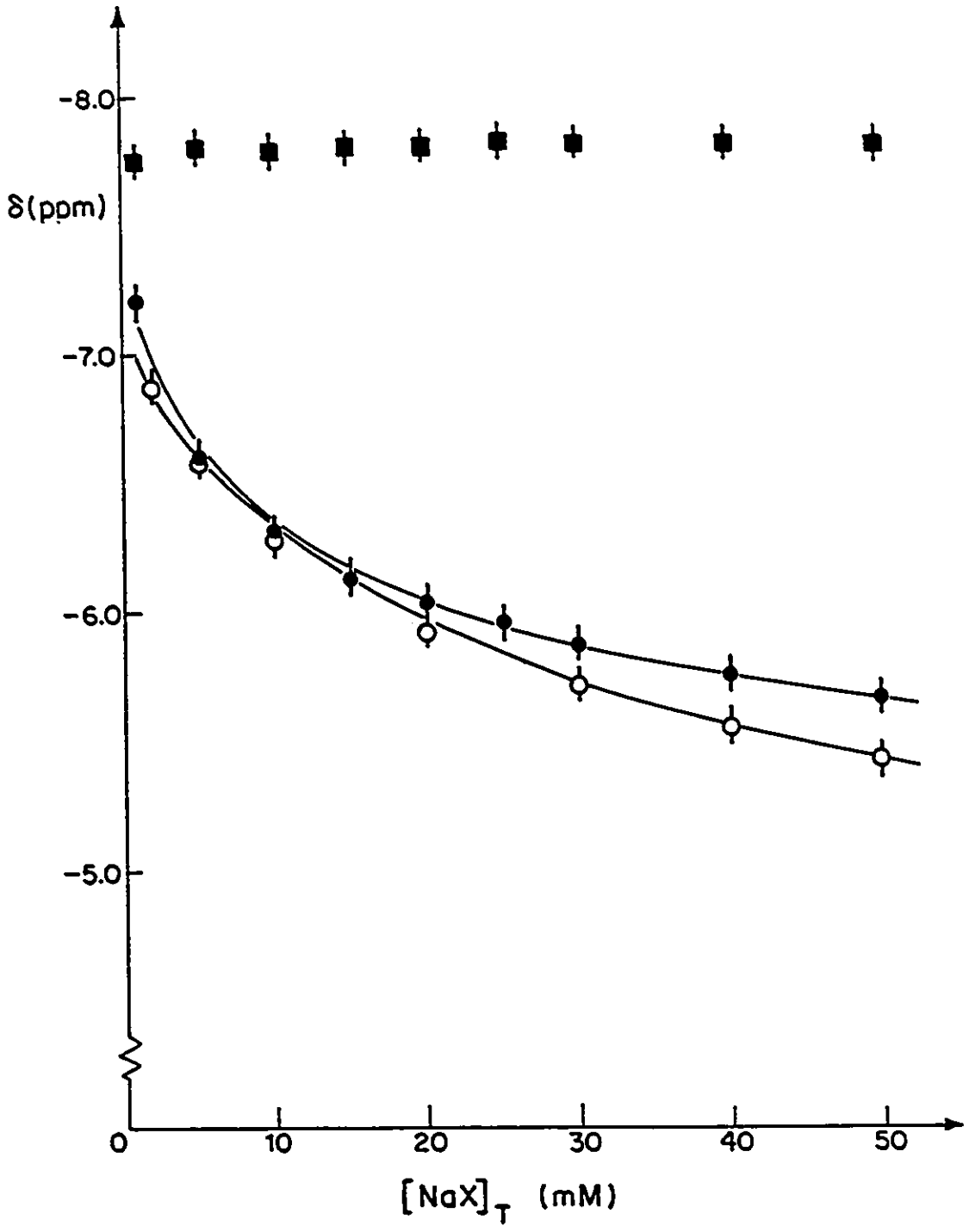

Figure 34: ^{23}Na chemical shifts of $NaBPh_4$ (■) and NaSCN (●,○) in acetone (■,●) and in acetonitrile (○) as a function of sodium ion concentration. T = 301.5±0.5 K. The data points are experimental, and the curves are calculated from the values given in Table X.

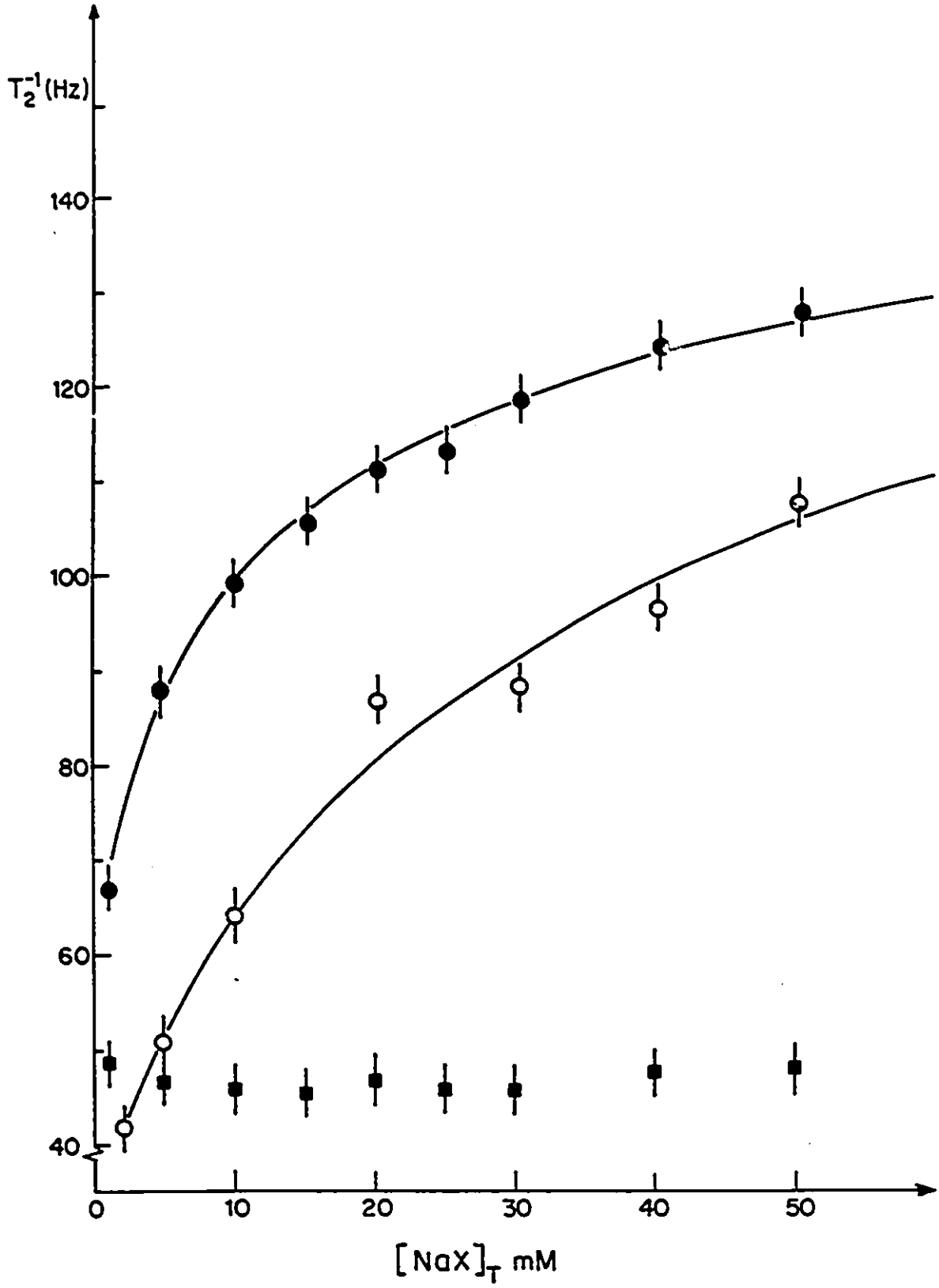

Figure 35: ^{23}Na transverse relaxation rates of $NaBPh_4$ (■) and NaSCN (●,○) in acetone (■,●) and acetonitrile (○) as a function of sodium ion concentration. T = 301.5±0.5 K. The data points are experimental, and the curves are calculated from the values given in Table X.

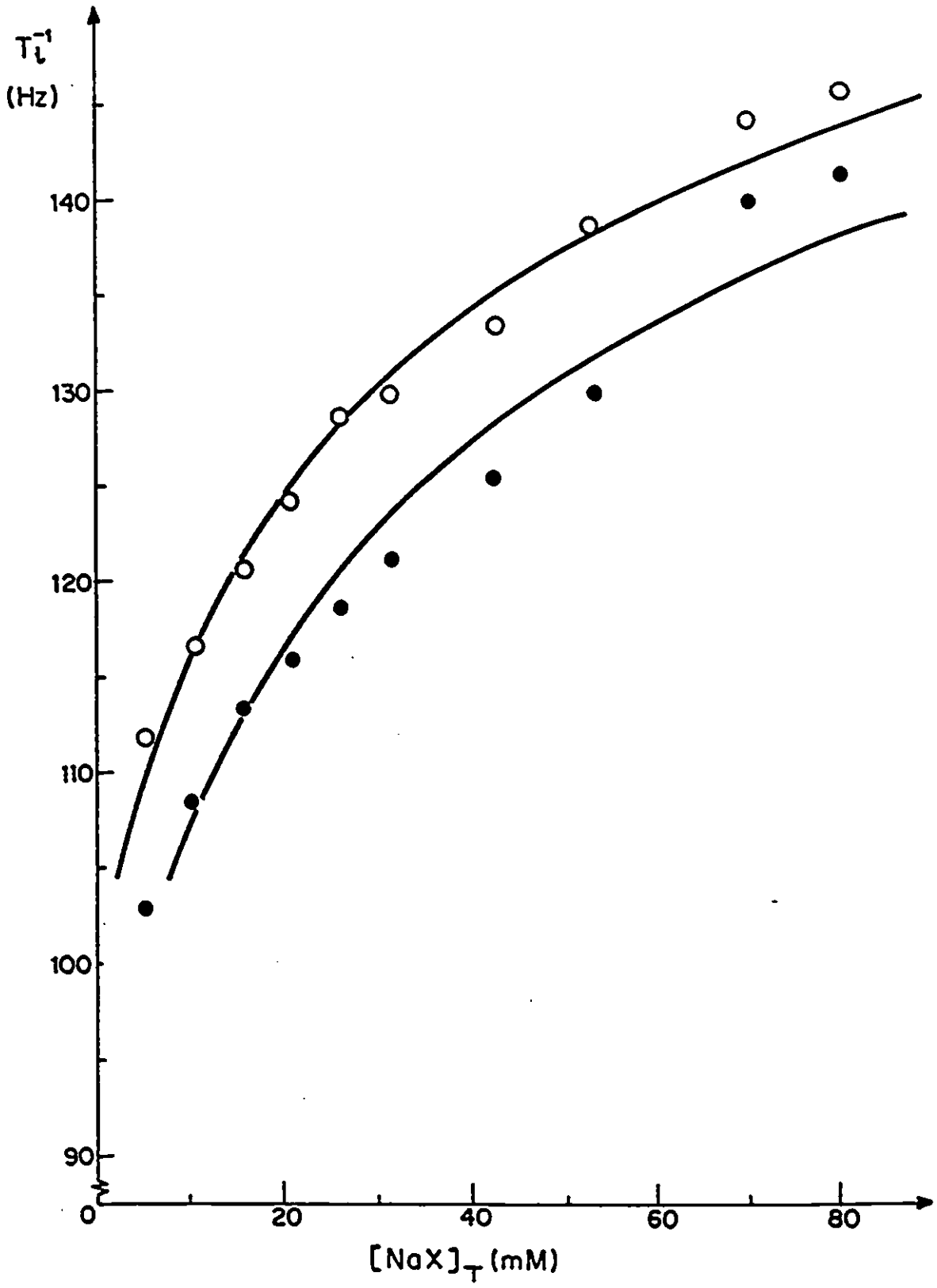

Figure 36: ^{23}Na transverse (○) and longitudinal (●) relaxation rates of $(Na\text{-}18C6)^+$ in AC as a function of sodium ion concentration. T = 301.5±0.5 K. The data points are experimental, and the curves are calculated from the values given in Table X.

$$Na^+ + SCN^- \overset{K_{IP}}{\rightleftharpoons} (Na^+,SCN^-) \qquad \text{equation 50}$$

When SCN^- is present there are fewer solvated sodium ions in solution. The SCN^- affects the ability of Na^+ to complex 18C6 in that there is now competition between the crown ether and SCN^-. (see equation 51)

$$(Na^+,SCN^-) + 18C6 \overset{K_{CIP}}{\rightleftharpoons} ((Na\text{-}18C6)^+,SCN^-) \qquad \text{equation 51}$$

When $[SCN^-]_T$ = 100mM, and no crown ether is present, only 28% of the SCN^- ions are unpaired but solvated. When tetraphenylborate is present, as has been shown, ion-pairing is not detected. Table X describes the different species which involve sodium. All of the species involving SCN^- in both AC and AN are fully characterized. The ion-pairing constants (K_{IP} and K_{CIP}) were determined in both solvents and will prove useful in determining how each species participates.

The graph of T_2^{-1} as a function of ^{23}Na chemical shift for NaSCN in AC gives a good linear relationship (RMS=0.987)(see Figure 37). This confirms complex formation and is a check on the quality of the data.

Once the characteristics of the species at $\rho = 0$ and $\rho > 1$ were determined, the influence of SCN^- upon the mechanism and the rate of exchange were explored more fully. Figure 31 shows that there is a difference when the counter anion is varied but this is strictly a qualitative observation. In order to quantify the influence of the counter anion, the amount of each was varied. Figure 38 shows how the contributions from exchange vary as the concentration of each counter anion is varied while maintaining the total concentration of sodium cation constant. The $T_{2,ex}^{-1}$ does not vary linearly with the increase in $[SCN^-]_T$. The curves are not parabolic with maxima at $\rho = 0.5$, which suggests that the mechanism of

Table X: Characteristics of Na^+ in Acetonitrile and Acetone

solvent	X^-	$\delta(Na^+)_s$(ppm)	δ(NaX)(ppm)	$T_2^{-1}(Na^+)_s$(Hz)	T_2^{-1}(NaX)(Hz)	K_{IP}	T_1^{-1}(Na-18C6)$^+$(Hz)	δ(Na-18C6)$^+$(ppm)	K_{CIP}
AN	BPh_4^-	-7.4 ± 0.1	-	28 ± 1	-	-	56.1 ± 0.2	-14.9 ± 0.1	0.003
	SCN^-	-7.42 ± 0.07	-4.30 ± 0.07	15 ± 5	153 ± 4	0.104	58.0 ± 0.6	-14.6 ± 0.1	0.005
AC	BPh_4^-	-7.8 ± 0.1	-	47 ± 1	-	-	88 ± 1	-15.8 ± 0.1	0.035
	SCN^-	-7.37 ± 0.03	-4.68 ± 0.03	59 ± 1	164 ± 1	0.100	89 ± 3	-14.7 ± 0.1	0.030

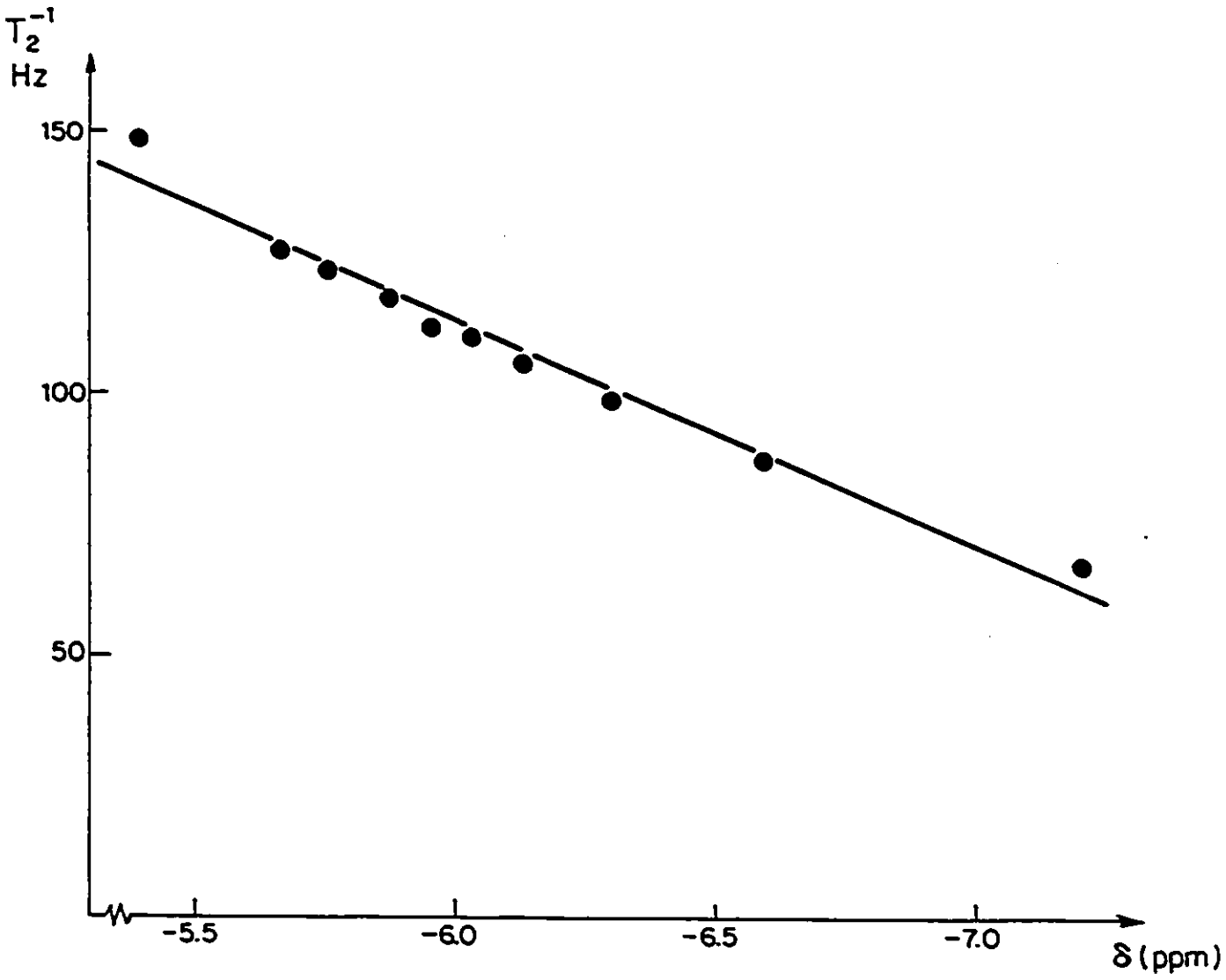

Figure 37: ^{23}Na transverse relaxation rate for solvated Na^+ in AC as a function of ^{23}Na chemical shift. T = 301.5±0.5 K.

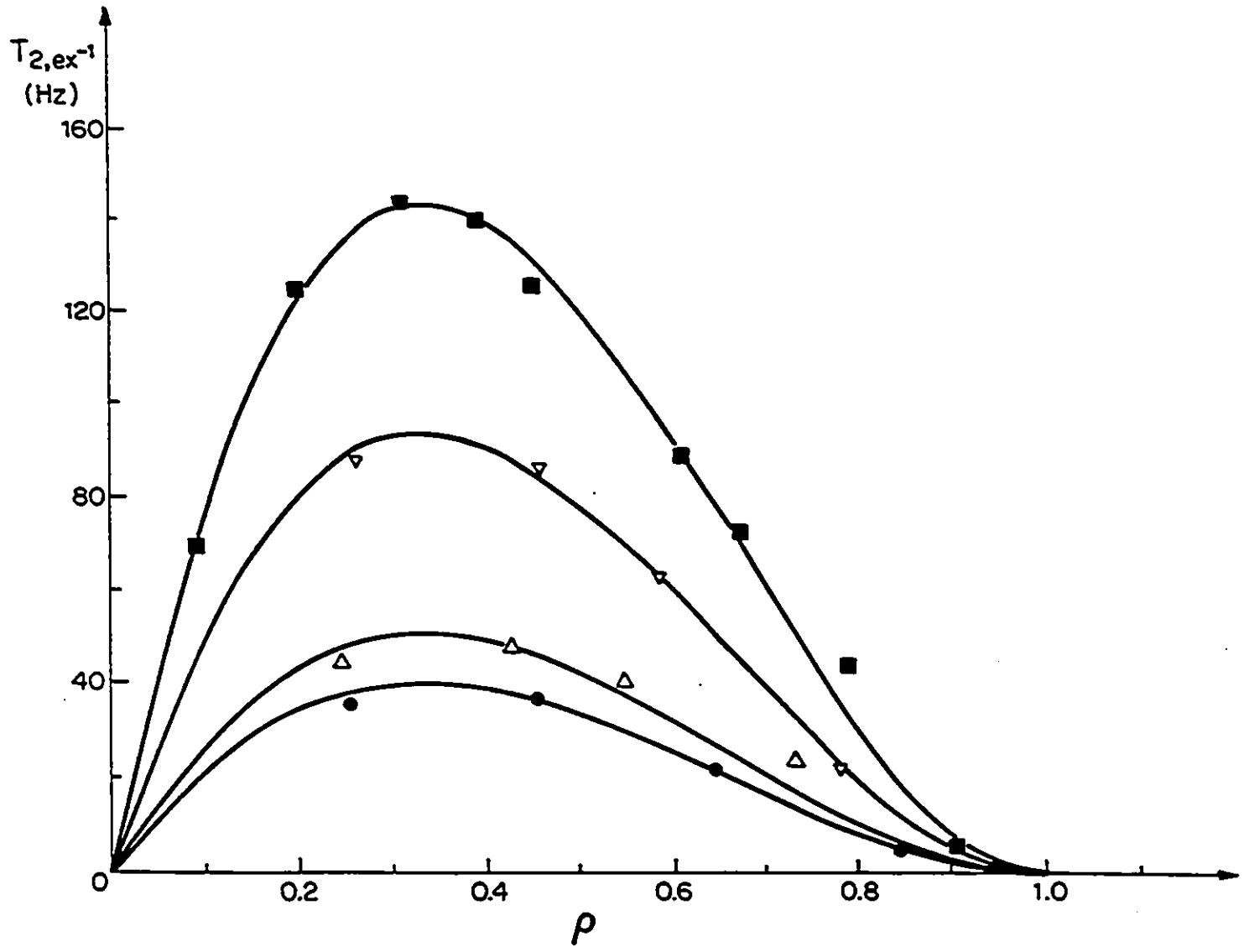

Figure 38: Exchange contributions to the ^{23}Na transverse relaxation rate for the sodium cation in the presence of 18crown6 in AC. The counter-anions were BPh_4^- and SCN^- in various proportions. The proportion of BPh_4^- varies from 100% (■), 87.7% (▽), 49.7% (△), to 0% (●), with the remainder as SCN^-. The data points are experimental, the curves are calculated from equations 39 and 44 and the values of k_{-1} given in Table XI. $[Na^+]_T = 5.00 \times 10^{-2}$M.

exchange is not the M_{ai} mechanism. For these systems the maxima are at $\rho = 0.33 \pm 0.02$ instead. When BPh_4^- is the counter anion, it has already been shown that the dissociative mechanism is operative but others[93] have reported the M_{ai} mechanism to be operational when SCN^- is the counter anion. When the pseudo-first order rate constants are determined for the systems in Figure 38 the absence of the M_{ai} mechanism is more apparent. (see Figure 39 and Table XI) The change of counter anion does not signal a change in mechanism but rather a change in rate.

Table XI: Dissociative Exchange Rates for $NaBPh_4$:NaSCN systems

BPh_4^-:SCN^- (%)	$k_{-1,obs}(\times 10^4)(s^{-1})$
100:0	1.48±0.02
88:12	2.38±0.02
50:50	5.2±0.2
0:100	7.7±0.1

5.3 Discussion

The scheme of equilibria which may serve as the model for how the rate of dissociation may be increased when the thiocyanate ions are present is given in Figure 40. The ion-pairing constants for both the solvated and complexed Na^+, as given in equations 50 and 51, are incorporated. The dissociative rate constant (k_{-1}) is present but a second dissociative rate constant (k_{-1}'), that of the ion-paired complex, is introduced. This "alternate" route would be the path which is available for systems with ion-pairing but not for those like $NaBPh_4$-18C6. The presence of SCN^- accelerates the dissociative mechanism rather than introducing another mechanism, and this equilibria scheme incorporates that characteristic. The next step was to separate the $k_{-1,obs}$ into its two component parts: k_{-1} and k_{-1}'.

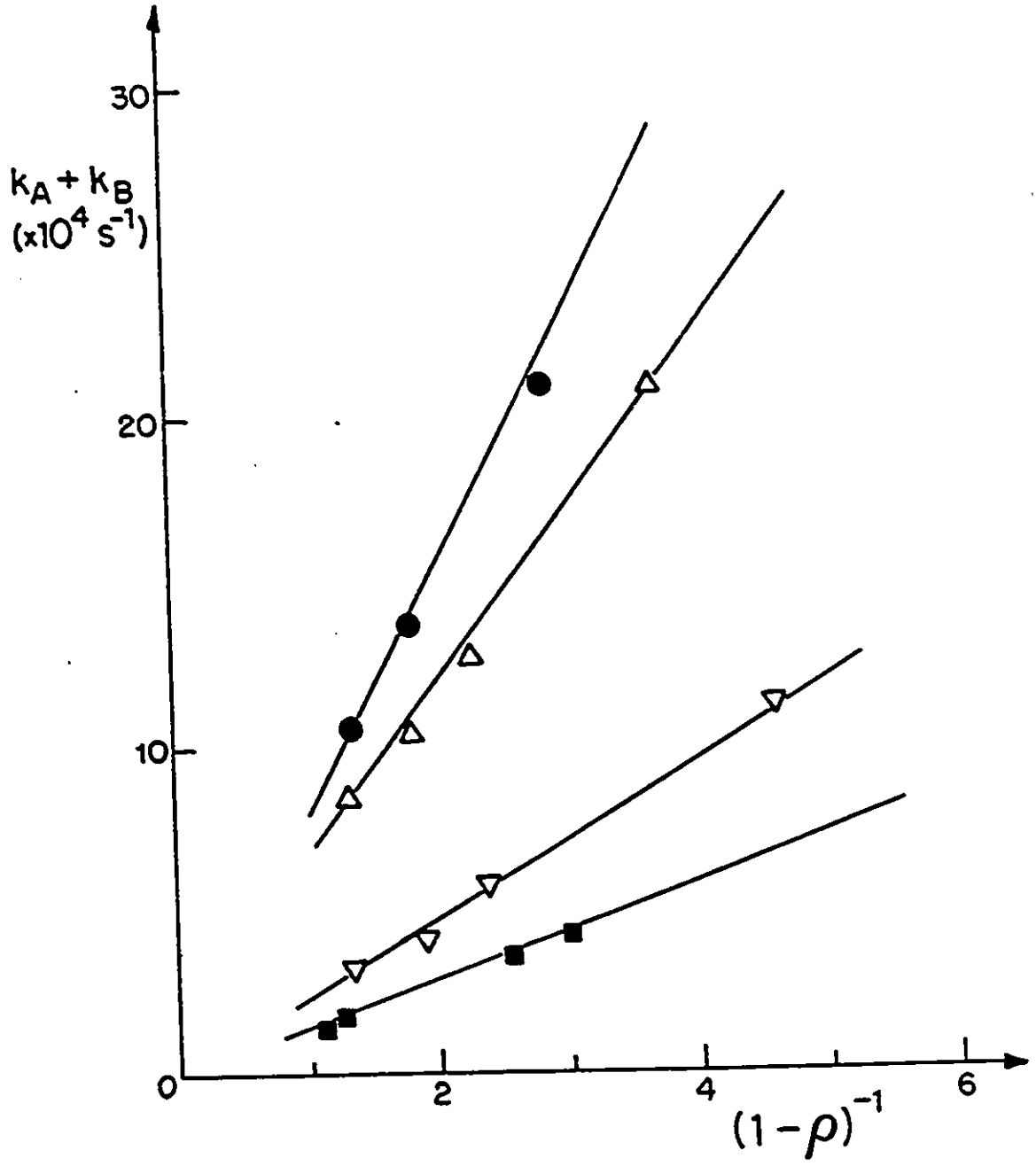

Figure 39: Pseudo-first-order rate constants ($k_A + k_B$) for the exchange of Na^+ between two sites (solvated and complexed sodium) in AC, as a function of $(1 - \rho)^{-1}$ at different ratios of BPh_4^- and SCN^-. The proportion of BPh_4^- varies from 100% (■), 87.7% (▽), 49.7% (△), to 0% (●), with the remainder as SCN^-. T = 301.5 ±0.5 K. The curves are calculated from k_{-1} values. $[Na^+]_T = 5.00x10^{-2}M$.

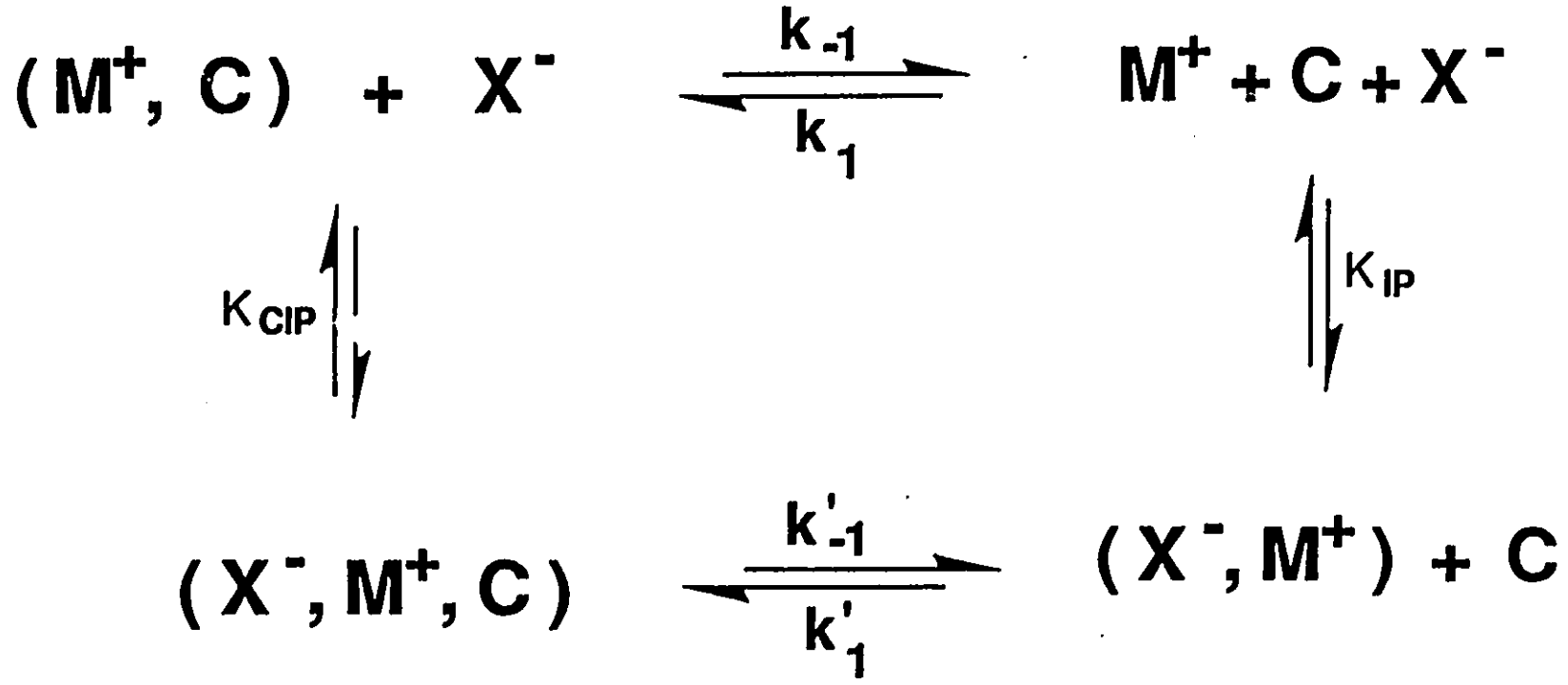

Figure 40: The scheme of equilibria which incorporates the ion-pairing of the solvated cation and the complex, and the dissociation of the complex, both ion-paired and solvated.

5.3.1 Derivation of the all-inclusive Rate Relationship

Separating the contributions to the observed rate of dissociation can be made using a relationship which relates the pseudo-first order rate constant ($k_A + k_B$), both dissociative rates (k_{-1} and k_{-1}'), the ion-pairing constant for the complex (K_{CIP}) and the total concentration of SCN^- ($[SCN^-]_T$).[106] Equation 44 was adequate as the expression for the overall ($k_A + k_B$) until ion-pairing has to be considered. As has been shown earlier in this chapter, in this system the solvated sodium cations, $[Na^+]_{S,T}$, site "A" in two-site exchange are in two forms $(Na^+)_s$ and $(Na^+,SCN^-)_s$. The complexed sodium cations, $[Na\text{-}18C6^+]_T$ or site "B", are also in two forms: $(Na\text{-}18C6)^+$ and $(Na\text{-}18C6^+,SCN^-)$. The total amount of sodium, $[Na^+]_T$ is the sum of $[Na^+]_{S,T}$ and $[Na\text{-}18C6^+]_T$. The rates of appearance for the free and complexed sodium cation, for equation 51, may be expressed as:

$$d([Na^+]_T)/dt = k_B[(Na\text{-}18C6)^+]_T = k_{-1}'[Na\text{-}18C6^+,SCN^-] \qquad \text{equation 52}$$

$$d[Na\text{-}18C6^+]_T/dt = k_A([Na^+]_T) = k_1'[Na^+,SCN^-][18C6] \qquad \text{equation 53}$$

Based on the relationship given in equation 33, and remembering that $(P_A + P_B)=1$, $(k_A + k_B)$ may be expressed as:

$$(k_A + k_B) = \frac{k_B}{P_A} \times \frac{P_B}{P_B} \times (P_A + P_B) \qquad \text{equation 54}$$

Substitutions lead to:

$$(k_A + k_B) = k_{-1}'[Na\text{-}18C6^+,SCN^-]\,([Na^+]_T/[Na^+]_{S,T}[Na\text{-}18C6^+]_T) \qquad \text{equation 55}$$

A linear relationship is observed between $(k_A + k_B)$ and $[SCN^-]_T$. In Figure 41 this is shown for $\rho = 0.5$. Since at $\rho = 0.5$, $[Na^+]_{S,T} \equiv [Na\text{-}18C6^+]_T = 0.5[Na^+]_T$, equation 55 reduces to:

$$(k_A + k_B) = k_{-1}'[Na\text{-}18C6^+,SCN^-]\ (4/[Na^+]_T) \qquad \text{equation 56}$$

$[Na\text{-}18C6^+,SCN^-]$ can be related to K_{CIP}, see Figure 40, so the relationship is further simplified:

$$(k_A + k_B) = k_{-1}'(K_{CIP}[Na\text{-}18C6^+][SCN^-]_F/(4/[Na^+]_T) \qquad \text{equation 57}$$

$[SCN^-]_F$ is the concentration of free, un-ionpaired thiocyanate ions. At the concentrations used here, and since K_{CIP} is quite small, the approximation that this is equal to $[SCN^-]_T$ may be made. The amount of ion-paired complex $(Na\text{-}18C6^+,SCN^-)$ is also very small, allowing for the assumption that $[Na\text{-}18C6^+]_T \equiv [Na\text{-}18C6^+]$. Once again the relationship is reduced.

$$(k_A + k_B) = 2k_{-1}'\,K_{CIP}[SCN^-]_T \qquad \text{equation 58}$$

When this contribution is combined with that from the dissociative mechanism the total expression for $(k_A + k_B)$ becomes:

$$(k_A + k_B) = 2k_{-1} + 2k_{-1}'\,K_{CIP}[SCN^-]_T \qquad \text{equation 59}$$

The slope of the linear relationship observed in Figure 41 provides access to k_{-1}' $((4.2\pm0.3)\times10^4 s^{-1})$, while the intercept provides access to k_{-1} $((1.6\pm0.2)\times10^4 s^{-1})$.

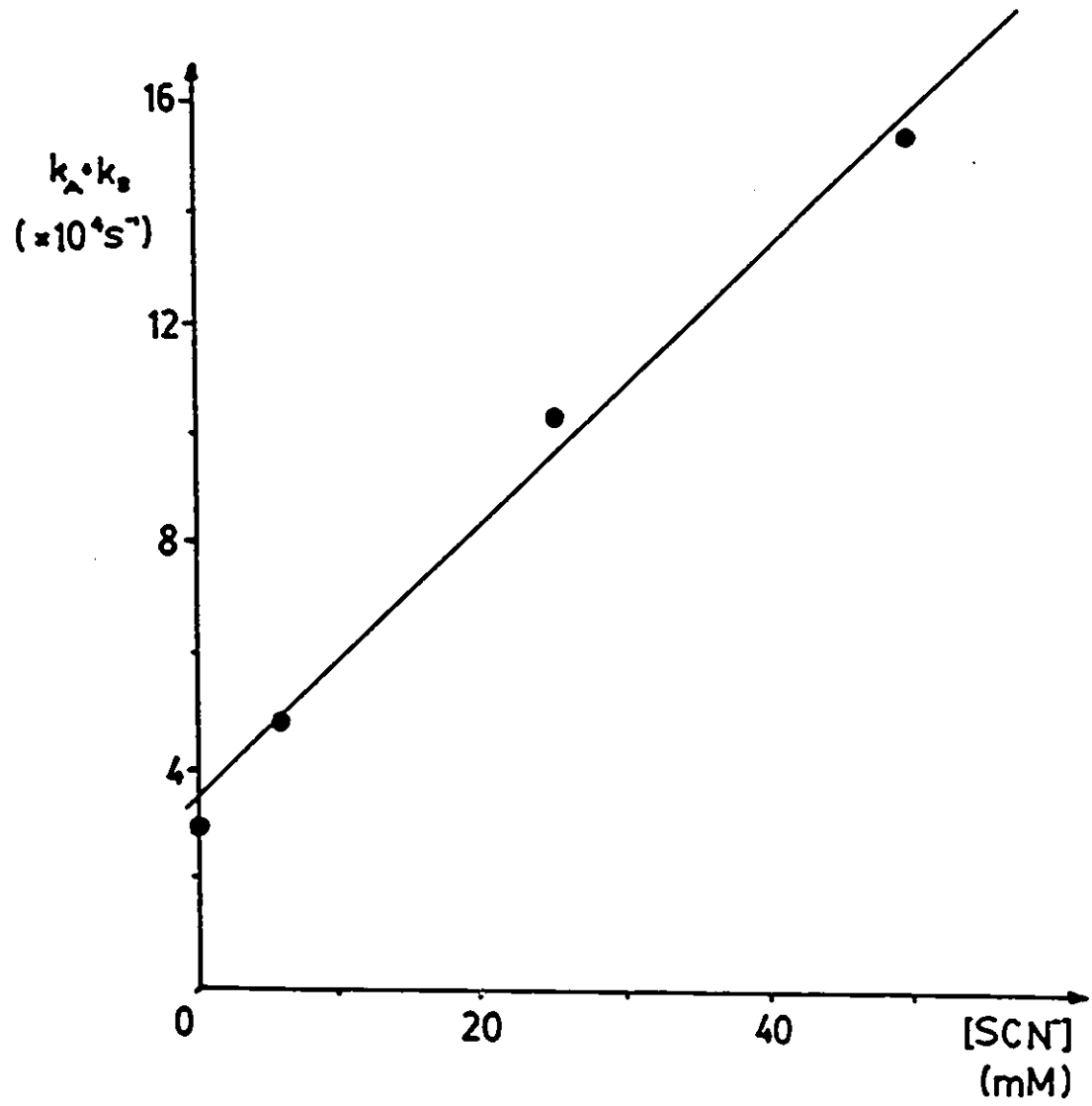

Figure 41: Pseudo-first-order rate constants ($k_A + k_B$) for the exchange of Na^+ between two sites (solvated and complexed sodium) in AC, as a function of $[SCN^-]_T$ at different ratios of BPh_4^- and SCN^-. T = 301.5±0.5 K. $[Na^+]_T = 5.00 \times 10^{-2}$M.

5.3.2 Determination of Free energies of Activation

From the dissociative rate constants the $\Delta G^{\ddagger}$ for each species, $(Na\text{-}18C6)^{+}$ and $(Na\text{-}18C6^{+},SCN^{-})$, may be calculated. (see equation 60) They are 49.5±0.2 $kJ.mol^{-1}$ and 47.2±0.2 $kJ.mol^{-1}$ respectively, therefore differing by 2.3±0.4 $kJ.mol^{-1}$.

$$k = \frac{k_B T}{h} e^{-\Delta G^{\ddagger}/RT} \qquad \text{equation 60}$$

The energetics for the SCN^{-} ion-pairing may be calculated. (see Figure 42) Using the equilibrium constants K_{IP} and K_{CIP} in equation 61, it can be determined that the ion-paired complex is 8.8 $kJ.mol^{-1}$ less stable than $(Na\text{-}18C6)^{+}$, while the ion-paired sodium ion is 5.8 $kJ.mol^{-1}$ less stable than the solvated sodium.

$$\ln K = -\Delta G / (RT) \qquad \text{equation 61}$$

The formation constants for these complexes have been shown to be $>10^4$ (see Sections 4.2 and 5.2) so, from this value the minimum free energy differences between the solvated and complexed sodium cations and the ion-paired and complexed-ionpaired sodium cations can be calculated. The assumption that the rate of complexation is close to diffusion control limits can therefore be verified and is confirmed. So, the barrier for the decomplexation is lower for the ion-paired species but the solvated complex is more stable. This means that the small portion of ion-paired complexes which do form are more likely to dissociate. This is the faster "alternate" route which is not available in the presence of BPh_4^{-}.

5.4 Conclusions

The characterization of the four species present in the NaSCN-18C6 system in AC has lead to the determination of the ion-pairing constants for both the sodium cation and the

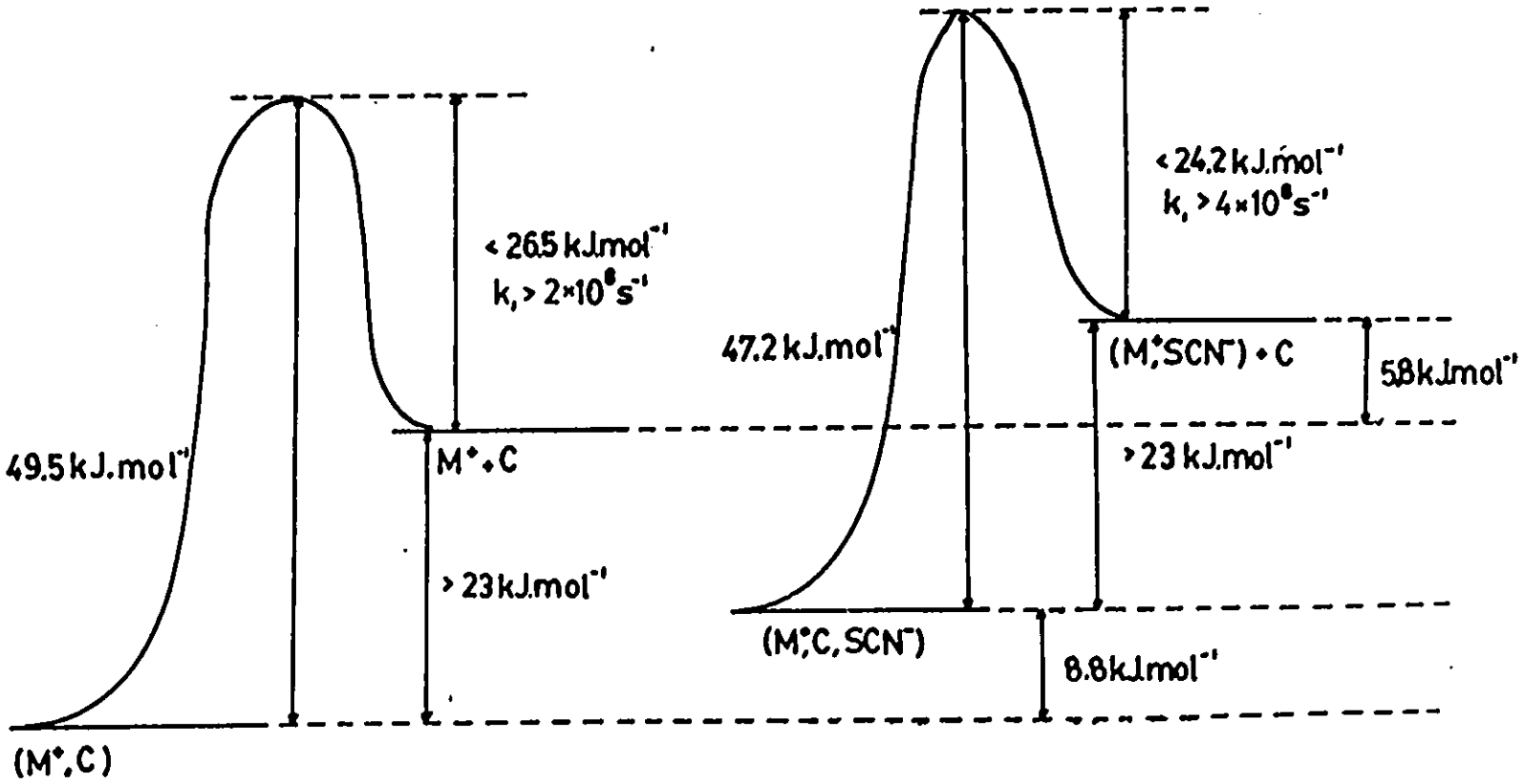

Figure 42: The energetics for the ion-pairing of SCN^- in AC. The values are for the system where $M^+ = Na^+$ and C= 18C6. T = 301.5±0.5 K.

complex. The rates of decomplexation (k_{-1} and k_{-1}') were accessed after a few, reasonable assumptions were made. Finally, the energetics of SCN^- ion-pairing were described completely. All of this information has contributed to the understanding of how the introduction of SCN^-, to replace BPh_4^-, accelerates the reaction while not changing the mechanism.

Chapter 6
Microdynamics of the $(Na\text{-}18C6)^+$ System

6.1 Background

Using the ^{23}Na NMR probe the chemical shifts and relaxation rates are accessible. Another characteristic which is available from NMR data is correlation time (τ_c). Since ^{23}Na is a quadrupolar nucleus the T_{2q}^{-1} is related to the correlation time by:

$$\frac{1}{T_{2q}} = \frac{2\pi^2}{5}\chi^2\tau_c \qquad \text{equation 62}$$

It is clear that the ^{23}Na quadrupolar relaxation rate cannot be used to determine both the quadrupolar coupling constant (χ) and the correlation time (τ_c). One way to access the correlation time is to make the approximation that it is the same as the reorientational correlation time of another nucleus in the complex. In this case the ^{13}C of the 18C6 is used.

One of the teams to have used this approach previously is Kintzinger and Lehn in their study of sodium cryptates.[107] Assuming that these complexes are quite rigid, the ^{13}C correlation time would also represent the reorientational motions of the $^{23}Na^+$ encapsulated by the cryptand. C222 had the lowest χ value and it increased from C221 to C211. The χ value is lowest when the number of oxygen atoms is greatest. Theoretical calculations for τ_c using the Debye relation had been made but the values obtained were five times larger than the experimentally determined values for the cryptates. The microviscosity was one factor which had not been fully considered when the calculations were made.

Bisnaire et al examined the $(Na\text{-}DB24C8)^+$ complex.[108] In NM, PC, AC, AN and PY the χ is ~0.9 MHz. This is comparable to χ(C222) which equalled 1.0 MHz. The $(Na\text{-}DB24C8)^+$ complex would therefore be expected to be equally symmetrical and well-shielded from the solvent and counter anion. One would not expect either to be in the first coordination sphere of the complex. A second study by the Detellier group looks at the $(K\text{-}DB30C10)^+$ complex.[109] The first interesting observation about this complex is that its

^{39}K chemical shifts in PY, AC, AN and NM are identical. Solvated K^+ does not have the same chemical shift in each solvent but the complex does (-13.3 ppm). This shows that the complexed K^+ is completely isolated from solvent influences. The χ is 1.7 MHz. Using this value the ratio between the electric field gradients can be estimated.

$q(^{39}K) / q(^{23}Na)$	$\equiv 0.9$	KSCN complex	
	$\equiv 1.1$	KPF_6 complex	equation 63

The similarity in the two electric field gradients confirms the similarity in the two cation environments, which are ones where the oxygen atoms from the ligand coordinate exclusively.

Eliasson et al also studied quadrupolar coupling constants by a multinuclear method.[110] Their study was generally with perchlorate salts and in acetonitrile. There was little variation in the values obtained with different counter anions. This suggests that the counter anion has little influence. When K^+ complexes are studied much higher χ values are obtained which is less surprising considering the sizes of the cavities and the corresponding cation diameter.

Table XII: Eliasson et al's QCC values

complex	QCC (MHz)
$NaClO_4$-15C5-AN	1.2
$NaClO_4$-18C6-AN	1.2
$KClO_4$-18C6-AN	3.4
NaI-15C5-AN	1.2
NaI-18C6-AN	1.2
KI-18C6-AN	3.5

6.1.1 Complex Structure in the Solid State

A wide variety of crown ether - alkali metal cation and crown ether - neutral molecule complexes have been determined and reported. In 1974 X-ray crystal structures for 18C6[111,112], NaSCN-18C6[113], KSCN-18C6[114], RbSCN-18C6[115] and CsSCN-18C6[116] were all reported. Only the NaSCN-18C6 complex was hydrated. The structure for 18C6-2NM is just one of the complexes with neutral molecules which has been studied by X-ray crystallography.[83,117,118] The 18C6 in this structure has D_{3d} symmetry (see Figure 8) and the crown cavity is symmetrical. The NM molecules are centred above and below the cavity and the methyl hydrogens of the NM interact weakly with the oxygen atoms of the crown ether. The 18C6-2AN complex has also been investigated by Roger's group.[119,120] It is not overly different in form from the 18C6-2NM complex. Full D_{3d} symmetry is observed. These complexes are much stronger than those with DB18C6 because the 18C6 is much more flexible.[121] Despite these X-ray data, a structure of utmost interest is absent. No structure of non-hydrated 18C6 with sodium is reported.

Despite the best efforts of the crystallographer, the link between solid state and solution is often unclear. Solid state NMR may be one of the ways to bridge the gap since NMR is also used to study solutions. Magic angle spinning provides a high resolution spectrum. ^{13}C NMR of the KSCN-18C6 complex gives two peaks at 295K which indicate that the complex is more rigid than the free 18C6.[122] There are six unique ^{13}C atoms in free 18C6 which are visible at 210K and whose chemical shifts span 5.6ppm. The chemical shifts of the complex span only 1.5ppm and the stereochemistry is fixed.[122] Solid state NMR of alkali phenoxides in the presence of 18C6 in ethereal solvents do not form complexes which contain only metal salts. Rather, three component 1:1:2 (crown:salt:phenol) complexes form.[123] The NaSCN-18C6.H_2O was also examined and the results support Dobler et al's structure of a distorted pentagonal bipyramid[113] but once again no report of the non-hydrated complex is made.[82] A more recent study of 18C6 by ^{13}C solid state NMR investigates the

motion of the 18C6 further. It is believed that the O-CH_2-CH_2-O units exchange positions about the ring, thus maintaining the X-ray crystallographic structure but explaining the NMR data too.[124]

de Boer et al also provided a link between the crystal structure of a complex and its nature in solution.[83] They studied 18C6-2NM by ^{1}H solution NMR and determined its X-ray crystal structure. The thermodynamic constants of complexation were determined for the 18C6-NM and 18C6-2NM complexes and for 1:1 and 1:2 complexes with AN and malonitrile ($CH_2(CN)_2$) by ^{1}H NMR in benzene-d_6. For NM and AN the values obtained were $\Delta H°$= -32 kJ.mol^{-1} and -25 kJ.mol^{-1} respectively and $\Delta S°$= -105 J.mol^{-1}K^{-1} and -92 J.mol^{-1}K^{-1} respectively.

Section 2.1 has already given some description of the (Na-18C6)$^+$ complex focusing principally on computational methods. Damewood et al have developed protocols for the development of parameters necessary to describe the interactions between 18C6 and neutral molecules.[125] They studied the same systems as de Boer et al[83] because these systems are well known and documented. The 18C6 molecule changes conformation as it complexes with AN or NM, from C_i to D_{3d}. The D_{3d} conformation is maintained as the 1:2 guest/host complex is formed.[125]

Raman spectroscopy gives further information about the solution structure of (Na-18C6)$^+$ and 18C6.[51,60] The isomerization of the crown ether has been examined. If the C_2 conformation is the one which is suited for complexing Na^+, the $C_1 \rightarrow C_2$ process at 25°C proceeds at a rate of $10^7 s^{-1}$. Activation parameters have also been determined using ultrasonic absorption. The Raman data shows that the 18C6 and the SCN^- compete to complex the Na^+.[51]

Takeuchi et al's Raman spectroscopy study in MeOH[60] contained structural information of several alkali metal-18C6 complexes (refer also to Section 2.1). The stable D_{3d} conformation for (Na-18C6)$^+$ was observed as well as a second conformation which this study could not describe in great detail. They could say that it was metastable and that the

complexed 18C6 was probably in a form similar to one adopted by the free 18C6 in MeOH but the Raman data did not afford further details. The experimental Raman data suggests quite strongly that many 18C6 conformers, distorted from the D_{3d} structure, coexist and the C_i conformation is not the most stable one in solution. This is in distinct contradiction with the results of molecular mechanics calculations which found that the C_i conformer is at least as stable as the D_{3d} conformer.

As a final example of solution studies on 18C6 complexes with neutral molecules such as AN and NM as a guide to their nature is one using ^{13}C NMR and IR techniques.[84] Here the AN and NM are not the solvents but are present in specific small molar fractions. Interactions with the other portion of the solvent (CCl_4 or benzene) were also taken into consideration. In benzene solutions 1:1 and 1:2 complexes for 18C6-AN and 18C6-NM were observed. The strength of the 18C6-solvent interaction decreases as: NM > AN > $CHCl_3$ > AC >> benzene, CCl_4; but it must be remembered that this is quite a small interaction, usually four orders of magnitude smaller than the formation constants of the alkali metal-crown ether complexes.

6.1.2 This study of the ^{23}Na QCC

The ^{23}Na quadrupolar coupling constant (χ) for $(Na\text{-}18C6)^+$ will be determined in AC, AN, PC, PY and NM using the same approach as others[107-110]. This set of data should provide insight as to the symmetry about the Na^+ cation. Upon comparing the results with those obtained previously on other systems and using other techniques, further knowledge as to the character of the $(Na\text{-}18C6)^+$ complex should be gained.

6.2 Results

The ^{13}C NMR $T_{1,obs}$ values were determined for free 18C6 and complexed 18C6 in the five solvents. The NOE $^{13}C\text{-}\{^1H\}$ values were measured for both species. In AN and AC both SCN^- and BPh_4^- were used as counter anions, while in the other three solvents only the

BPh_4^- was used. These results are all summarized in Table XIII. Background on T_1 and NOE measurements has been given in Sections 1.5.2 and 1.5.4.

6.2.1 Determination of the Quadrupolar Coupling Constant (χ)

The first step in calculating the quadrupolar coupling constant (χ) is the determination of the quadrupolar contribution to the transverse relaxation rate ($T_{2,q}^{-1}$) from the observed transverse relaxation rate ($T_{2,obs}^{-1}$).

$$\frac{1}{T_{2,obs}} = \pi \nu_{\frac{1}{2}} = \frac{1}{T_{2,inh}} + \frac{1}{T_{2,q}} \qquad \text{equation 64}$$

Under extreme narrowing conditions, and neglecting the asymmetry parameter, $T_{2,q}^{-1}$ is given by equation 65, where τ_c is the correlation time characteristic of the quadrupolar relaxation. χ is further defined in equation 66.

$$\frac{1}{T_{2,q}} = \frac{3\pi^2}{10} \frac{2I+3}{I^2(2I-1)} \chi^2 \tau_c \qquad \text{equation 65}$$

$$\chi = \frac{e^2 q Q (1+\gamma_\infty)}{h} \qquad \text{equation 66}$$

where Q is the quadrupole moment, q is the electric field gradient at the quadrupolar nucleus site and $(1+\gamma_\infty)$ the Steinheimer antishielding factor. For ^{23}Na, a spin 3/2 nucleus, equation 65 is reduced to equation 62 where, as stated earlier, there are two unknowns for one known. In this study the approximation is made that the ^{23}Na correlation time is identical to the reorientational correlation time of the ^{13}C in the 18C6. Under extreme narrowing conditions the ^{13}C dipole-dipole relaxation rate ($T_{1,DD}^{-1}$) is related to the effective correlation time (τ_{eff}) by:

Table XIII: Summary of Results of ^{23}Na Linewidth and ^{13}C NMR Measurements

	AN	AC	PC	NM	PY
$\nu_{1/2}$ ^{23}Na (Hz)					
18C6-$NaBPh_4$	24.4±0.2	27.8±0.3	95±2	110±2	411±7
18C6-NaSCN	21.4±0.3	39.1±0.8			
$T_{1,obs}$ ^{13}C (s)					
18C6	1.746±0.025	3.429±0.097	0.881±0.027	1.104±0.088	2.074±0.023
18C6-$NaBPh_4$	2.105±0.045	2.006±0.044	0.423±0.007	1.430±0.024	0.395±0.012
18C6-NaSCN	1.860±0.013	2.008±0.032			
$T_{1,DD}$ ^{13}C (s)					
18C6	1.21±0.02	3.11±0.09	0.63±0.03	0.71±0.07	1.47±0.06
18C6-$NaBPh_4$	1.56±0.04	1.41±0.05	0.31±0.03	0.90±0.09	0.26±0.02
18C6-NaSCN	1.35±0.03	1.45±0.06			
NOE ^{13}C-{^1H}					
18C6	2.85±0.04	2.18±0.02	2.78±0.09	3.08±0.19	2.80±0.12
18C6-$NaBPh_4$	2.68±0.04	2.81±0.08	2.74±0.23	3.15±0.31	2.99±0.22
18C6-NaSCN	2.72±0.06	2.75±0.10			
τ_{eff} (ps)					
18C6	18.7±0.4	7.3±0.2	36.1±1.6	33.6±3.4	15.2±0.7
18C6-$NaBPh_4$	14.6±0.4	16.0±0.6	70.8±6.1	23.3±2.3	86.6±5.8
18C6-NaSCN	16.7±0.4	15.7±0.6			
χ (MHz)					
18C6-$NaBPh_4$	1.14±0.02	1.18±0.02	1.03±0.05	1.94±0.10	1.93±0.07
18C6-NaSCN	1.01±0.01	1.41±0.03			

$$\frac{1}{T_{1,DD}} = \left(\frac{\mu_0}{4\pi}\right)^2 N_H \gamma_H^2 \gamma_C^2 \hbar^2 r_{C\text{-}H}^{-6} \tau_{eff} \qquad \text{equation 67}$$

where $r_{C\text{-}H}$ is the C-H bond length and N_H the number of directly attached hydrogens. $r_{C\text{-}H}$ can be taken as 1.085×10^{-10}m. The dipole-dipole contribution to the measured ^{13}C $T_{1,obs}$ is determined from the NOE observed.

$$T_{1,DD} = T_{1,obs} \times \frac{1.98}{NOE_{obs}} \qquad \text{equation 68}$$

This shows how the three measured values: ^{13}C $T_{1,obs}$, ^{13}C-{^1H} NOE and ^{23}Na $\nu_{\frac{1}{2}}$; can be used to determine χ.

6.3 Discussion

In order to observe how 18C6 is changed by complexation, the solvated 18C6 and the $(Na\text{-}18C6)^+$ complex were both studied. In order to see if the choice of counter anion had a significant role in the symmetry of the complex SCN^- and BPh_4^- ions were used in AC and AN. These solvents are the same ones in which the role of the counter anion was investigated by ^{23}Na NMR (see Chapter 5). The choice of counter anion does influence the ^{23}Na $\nu_{\frac{1}{2}}$ but in AC the ^{13}C $T_{1,obs}$ values are the same within experimental error. This translates into τ_{eff} values which are the same. A small difference is observed in AN. The χ values for the $(Na\text{-}18C6)^+$ complex in AC and AN, in the presence of both BPh_4^- and SCN^-, show that all four complexes are quite symmetrical. The environment about the sodium cation is more similar when BPh_4^- is present than when SCN^- is present.

The NOE values show that near maximum enhancement (3.00) is observed in all cases. This is not surprising since other sources of relaxation, such as chemical shift anisotropy (CSA) or interactions with unpaired electrons were not expected. Degassing to

remove all traces of O_2 was done to ensure that relaxation would not be effected via paramagnetic impurities.

The effective correlation times (τ_{eff}) differ for the free and complexed 18C6. The lowest value is for the 18C6 in AC while the highest was in PY for the complex. This is a measure of how long a complex/molecule is in one position, or how long it takes for it to move away and "forget" where it was.[38] Short correlation times therefore indicate rapid molecular motion. Since there are several factors which may influence the correlation time, such as solvent viscosity and the DN of the solvent, the variations in correlation times do not fall in the same order as those trends. There is not even a consistency in how the correlation time changes as the complex is formed. In AN and NM there is a decrease while for the others an increase is observed as a consequence of complexation.

The χ values show that two types of $(Na\text{-}18C6)^+$ complexes are observed. Those in AC, AN and PC are all quite symmetrical. It would appear that the 18C6 oxygen atoms are able to effectively shield the Na^+ cation from influences from the solvent or the counter anion. The distorted pentagonal bipyramidal structure is supported. The crystal structure may indeed be very similar to the one seen in solution. As has been discussed in Chapter 3, the counter anion would not be expected to play a significant role either.

6.3.1 The $(Na\text{-}18C6)^+$ complex in NM and PY

The χ values in PY and NM are the same within experimental error, and the Na^+ environments are less symmetrical than in the other three solvents. PY is a strongly donating solvent (DN=33.1). The solvent molecules would predictably coordinate with the complex. This strong coordination could quite easily compete with 18C6 oxygen atoms, and if successful would displace the sixth crown ether oxygen. The 18C6 would therefore "wrap" around the Na^+ less effectively causing a less symmetrical environment about it. Using ^{23}Na NMR the exchange rates were slow enough that two peaks were often observed. At least one solvent molecule is believed to be coordinating during the partial desolvation of the

complexed cation and the reorganization of the solvent cage. These events accompany the conformational rearrangements which lead to the transition state. The presence of this solvent molecule(s) and its/their influence on the symmetry of the Na^+ environment is understandable.

The asymmetry about the Na^+ cation in NM cannot be attributed to high solvent donor :bility (DN=2.7). One plausible explanation is the higher internal pressure of NM. The Hildebrand solubility parameter (δ^2) describes the relationship between the physical properties of the solvent and its effectiveness in dissolving certain solutes. It is a measure of the energy required to overcome all of the intermolecular forces which hold the liquid together.[126,127] In AC the Hildebrand solubility parameter (δ^2) is only 410 $J.cm^{-3}$. It is higher in AN (615 $J.cm^{-3}$), higher again in NM (675 $J.cm^{-3}$) and 2317 $J.cm^{-3}$ for H_2O.[126,127] The solvent having a higher δ^2 value would be expected, other factors being equal, to form a solvent cage about the complex which exerts a large pressure. If large enough, the sixth oxygen would be hampered from bending around close enough to the Na^+ to encapsulate it effectively. The 18C6 would therefore maintain a more open conformation and the Na^+ environment would be less symmetrical.

6.3.2 Comparisons between this set of data and previous results

As outlined in Section 6.1, $(Na\text{-}DB24C8)^+$ and $(K\text{-}DB30C10)^+$ have both been studied using this approach. The $(Na\text{-}DB24C8)^+$ complex is more symmetrical than $(Na\text{-}18C6)^+$ in all of the studied solvents. The χ value for $(K\text{-}DB30C10)^+$ in acetone-d_6, when SCN^- is the counter anion, is 1.4±0.3MHz, which is identical to that for $(Na\text{-}18C6)^+$ under the same conditions. The ^{39}K NMR chemical shift for $(K\text{-}DB30C10)^+$ in NM, PY, AN and AC is -13.3ppm, which shows that $^{39}K^+$ is totally isolated from influence by the solvent. The counter anion and solvent molecules are expelled from the coordination sphere of the cation. The range in ^{23}Na NMR chemical shifts for $(Na\text{-}DB24C8)^+$ (~1ppm) also suggests the exclusion of other molecules from about the Na^+ when it is complexed. The ^{23}Na

chemical shift range for $(Na\text{-}18C6)^+$ with BPh_4^- is 4ppm for these five solvents, and only 1.4ppm if PY is excluded. Since PY and NM have already been shown to be different, the small chemical shift difference (1.3ppm) suggests once more that counter anions and solvent molecules are not in close proximity with the cation. Similar χ values for $(Na\text{-}DB24C8)^+$ (0.8-1.2 MHz) in a range of solvents as for $(Na\text{-}18C6)^+$ in AN, AC and PC also support this argument for a symmetrical environment for the Na^+ cation, as created by the crown ether oxygens. By extrapolation, the wrapping process of Na^+ in $(Na\text{-}18C6)^+$ complexes in AC, AN and PC with BPh_4^- and in AN with SCN^- is similar to that for K^+ and Na^+ in DB30C10 and DB24C8 respectively.

6.4 Conclusions

The Na^+ environments in AC, AN and PC are all quite symmetrical. In NM high internal pressure precludes the ether oxygens from surrounding the Na^+ as completely as in the previously mentioned solvents. In PY the highly donating solvent competes with the sixth ether oxygen and effectively distorts the complex, also rendering it asymmetric. The Na^+ quadrupolar coupling constant is accessed through the ^{23}Na $\nu_{\frac{1}{2}}$, the ^{13}C NMR $T_{1,obs}^{-1}$ and the $^{13}C\text{-}\{^1H\}$ NOE measurements, which allow the calculation of τ_{eff} of the complex which is assumed to be equivalent to the τ_c of the Na^+, because of its purely reorientational origin.

Chapter 7
The (Na^+-Lasalocid) System and the (Na^+-18C6A_4) System

7.1 Background

The past few chapters have dealt with $(Na\text{-}18C6)^+$ under several sets of conditions: various solvents, different counter anions and in view of determining the ^{23}Na quadupolar coupling constant. This chapter will attempt to link the approaches used on the synthetic 18C6 to the synthetic 18C6A_4 and the naturally-occurring lasalocid A. Monensin, an acyclic carboxylic ionophore, will be discussed though it was not used to obtain any of the experimental results.

7.1.1 Lasalocid A and Monensin structures

Lasalocid A (X-537 A) has been examined in the literature since 1951.[128] Its structure has been elucidated by both X-ray diffraction techniques[129-134] and by NMR studies[135-137]. The barium[129] and silver[130] salts of lasalocid are 1:2 cation:lasalocid A dimers with head-to-tail associations. The 1:2 water:lasalocid A complex is a head-to-head dimer.[131] These dimeric forms are seen in nonpolar solvents but the monomeric form has been shown to predominate in polar solvents.[135-137] The free acid is prefolded very similarly to (Na-Las) according to ^1H NMR.[137] Chiang and Paul report the X-ray structures of both the sodium salt of lasalocid A and the free acid, crystallized from MeOH as monomeric with the inclusion of one MeOH molecule.[132] Smith et al report the X-ray structure of the sodium salt of lasalocid crystallized from 95% EtOH as an intermediate in the monomer to dimer transition. Each complex includes two each of sodium, lasalocid A and water.[133] Friedman et al show, using IR, that both hydrogen bonding and metal complexation stabilize the cyclic form which is present when the complex is formed.[126]

Monensin has been the subject of structural papers[138] and kinetic studies[139] since 1967. NMR was an aid in the determination of its structure but X-ray techniques gave the crystal structure.[140] The biological properties of monensin were outlined in detail in that

same year, when particular emphasis was placed on its effectiveness in the treatment of coccidiosis in chickens, as well as describing its chemistry, derivatives and isolation.[141] Being linear like lasalocid, monensin must undergo rearrangement in order to coordinate with the cation in question. When sodium cations are complexed there are two head-to-tail hydrogen bonds. The Na^+ is six-fold coordinated.[142] The complex formed with K^+ is slightly different, mainly attributed to the fact that monensin complexes Na^+ selectively over K^+, and has a greater stability with Na^+ than K^+.[143] In order to accommodate the larger K^+, a distortion of a constrained portion of the molecule from its low-energy conformation must occur.

7.1.2 NMR studies of Lasalocid A and Monensin

Since ionophores complex alkali metal cations effectively, there are several nuclei which may be useful in their study: ^{23}Na, ^{39}K, ^{1}H and ^{13}C to name but four. If the ionophore is incorporated into a system where a biological membrane is present, as in transport studies, ^{31}P becomes another candidate.

^{1}H and ^{31}P NMR have been used to look at the interactions between lasalocid A and liposomes formed from synthetic lipids. The results suggest that the aromatic ring is close to the membrane interface while the remainder of the molecule is within the membrane interior.[144] ^{1}H NMR was the technique used, by the same researchers, to study the transport kinetics of three lanthanide cations across unilamellar vesicles.[145] A third transport study, this one across red-blood-cell membranes, as studied by ^{23}Na NMR, investigated Na^+ and K^+ fluxes mediated by lasalocid A.[146] ^{31}P, ^{35}Cl and ^{39}K NMR were also used to examine Cl^- and K^+ transport, with the ^{31}P NMR studies serving as controls. The diversity of nuclei permitted a complete study of the K^+, Na^+ and Cl^- fluxes induced by lasalocid A in erythrocytes.

Shen and Patel[135,136] used ^{1}H and ^{13}C NMR for their studies on lasalocid. Their principal focus was structure elucidation but they did do a kinetic study on the exchange

between the free molecule and its complex with Ba^{++} (BaX_2) using lineshape anlaysis of the ^1H spectra at various temperatures.[135] The rate constants for the BaX^+ complex in MeOH at 25°C were found to be 5.2×10^3 s^{-1} for the dissociation and 1.5×10^{10} $M.s^{-1}$ for the formation.

Amat et al determined the spin-lattice relaxation rates (T_1^{-1}) for several ^{23}Na complexes including monensin and lasalocid. In AN the T_1^{-1}(NaMon) is 602 s^{-1} while T_1^{-1}(NaLas) is 549 s^{-1}. In comparison, $T_1^{-1}(Na^+)$ was found to be 190 s^{-1}. The majority of their study focussed on sodium-cryptate complexes, and they went on to compare stopped-flow kinetic results with ^{23}Na NMR results. The dissociation of (Na^+,C211) in 25% MeOH-H_2O was the chosen system. Table XIV summarizes their findings.[147]

Table XIV: The (Na^+,C211) system in 25% MeOH-H_2O. T= 298K.

	stopped-flow	NMR
k_d (s^{-1})	37.6	36.4
ΔH^* ($kJ.mol^{-1}$)	63.8±0.9	66.0±1.1
ΔS^* ($J.mol^{-1}K^{-1}$)	-0.9±3.3	6.5±3.8

NMR is seldom used for kinetic studies involving monensin but ^{23}Na NMR has been used to investigate the binding of Na^+ to monensin in either MeOH or EtOH.[139,148] Haynes et al reported that the ^{23}Na chemical shift in MeOH of the complexed Na^+ by monensin was not shifted sufficiently enough to observe a difference between it and the chemical shift of the free sodium cation. They were able to demonstrate fast exchange between the sodium sites for all of the ionophores in their study except monensin. (Lasalocid was not in the study.) Degani did not use an approach which required a large difference in chemical shifts in order to work.[139] Her study on monensin used ^{23}Na relaxation rates and was more fruitful. Both the rates for formation and dissociation were determined and are given in Table XV.

The weak field instrument (15.9 MHz cw, rather than today's 79.35 MHz FT) was certainly a limiting factor.

Table XV: The (NaMon) system in MeOH. T= 298K.

	formation	dissociation
k (s^{-1})	6.3×10^{7}	63
$\Delta H^{\ddagger}$ ($kJ.mol^{-1}$)	-3.3	43.1
$\Delta S^{\ddagger}$ ($J.mol^{-1}.K^{-1}$)	-16	-66.1

The slow dissociation rate of NaMon reflects the specificity of monensin to sodium.[139] The dissociative mechanism predominates.

Sodium is not the highest in a ranking of the selectivity of monensin. Gertenbach and Popov used four nuclei (^{1}H, ^{13}C, ^{23}Na, ^{7}Li) for NMR studies to determine the stability constants of NaMon and complexation titrations with other cations to determine its selectivity to be $Ag^{+} > Na^{+} > K^{+} > Rb^{+} > Cs^{+} > Li^{+} \sim NH_4^{+}$ in MeOH.[149] They also focussed on the sodium binding with the acidic form of monesin (MonH) which is fairly strong in MeOH. The structure of the complex thus formed would be quite different from the one for the "normal" NaMon which is prepared in basic solution.

A ranking of metal-monensin complex stabilities, as determined by potentiometry[150], was reported before Gertenbach and Popov published their selectivity rankings, but this was in EtOH rather than MeOH. The ranking of the stability of LiMon relative to KMon was not determined but both are less stable than NaMon. The rankings, though of different factors, are identical. Formation rate constants were reported and increase with cation diameter. The AgMon has an extremely high formation rate (3.5×10^{10} $M^{-1}s^{-1}$) which is approaching diffusion control. The rate of formation of NaMon in EtOH is faster than what Degani[139]

reported ((1.1±0.2)×10^9 as compared to 6.3×10^7 $M^{-1}s^{-1}$). The rate of dissociation is slower (2.2±0.2 as compared to 6.3 s^{-1})[150]. The use of different techniques and the inherent limitations in both would probably account for these differences.

Amat et al determined rate constants for the exchange reactions of sodium cations with sodium monensin (NaMon) in MeOH using ^{23}Na NMR spin-lattice relaxation rates (T_1^{-1}).[151] The dissociation of the NaMon is the rate-determining one in non-aqueous solvents. Any addition of water increases the dissociation rate, suggesting the participation of a protonated complex where possible. This would be logical based on earlier results where the (MonH-Na^+) complex was shown to be quite strong.[149] Further work showed that in highly acidic media, $NaMonH^+$ is the intermediate as NaMon is converted to MonH, though it is much less stable than Mon^-.[152]

Hoogerheide and Popov determined the entropy and enthalpy of complexation from formation constants for NaMon which were determined at several temperatures.[153] $\Delta H°$ was -22.9 $kJ.mol^{-1}$ while $\Delta S°$ was 52±3 $J.mol^{-1}.K^{-1}$. At 298K $\log(K_f)$ is 6.72±0.05.

^{23}Na, ^{39}K, and ^{7}Li NMR have been used to study the transport of these cations, mediated by monensin, across phospholipid bilayers.[26,27,154] The rate of exchange of Li^+ as measured by ^{7}Li NMR suggests that each monensin molecule transports one lithium ion.[26] Similar studies were done with ^{39}K and ^{23}Na where once again, one monensin molecule transports one ion. In competitive situations Na^+ is tranported preferentially because it forms the more stable complex, though K^+ on its own is tranported more rapidly.[27] Shungu and Briggs report exchange rate constants for both the "in" and the "out" processes.[154] At 293K, Riddell et al[27] report a rate of 10.7 s^{-1}. This study gives k(out → in) = 10.3 s^{-1} and k(in → out) = 68.5 s^{-1} at 294K.[154]

7.1.3 The (Na^+-18C6A_4) System

Since 18C6 has been shown to complex Na^+, substituted 18C6 molecules have also been studied. These compounds have the advantage that the substituents may render the

molecule more suitable for certain environments than it might otherwise be. Many crown ethers have been derived from tartaric acid and its derivatives,[155] for example the 2,3,11,12-tetracarboxylic acid-18C6 (18C6A_4)(A= -COOH) and 2,3,11,12-tetracarboxamide -27C9 (27C9$(COX)_4$)(X= -$CONMe_2$). The 18C6A_4 (see Figure 43), which incorporates two (R,R)-tartaric acid residues, has much more affinity for cations than 18C6, forming very stable complexes, even in aqueous media. Knowledge of the geometry of the 18C6A_4, both complexed and uncomplexed, is a benefit when predicting and understanding its interactions with other molecules.[156] Stabilities of K^+ and NH_4^+ with differently substituted 18C6$(COX)_4$, where X=OH for the 18C6A_4, have been determined. The nature of the interactions was examined and it was shown that for (X=O^-) the most stable complexes are formed. This stability is comparable to cryptate-alkali metal cation complexes and $(K\text{-}18C6)^+$ is 4000 times less stable.[157] Electrostatic interactions are present here so they do dominate the binding strength. Other factors which contribute to binding strength include lipophilic interactions, shielding and central and/or lateral discrimination.

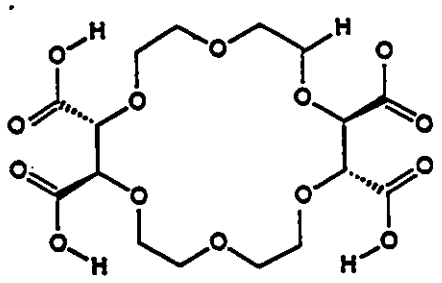

Figure 43: The tetra-carboxylic acid substituted 18C6: 18C6A_4.

In water the pH determines which species form. ($H_2$18C6A_4^{-2}) is the predominant protonated species over a range of pH centred near 3.5. The second protonation of each tartaric residue requires more acidic conditions.[158,159] If the pH is greater than 7, the

predominant form will be $18C6A_4$, so this will be the molecule available to complex the Na^+ in solution.[160] Refer to Table XVI.

Table XVI: Concentrations of the different species present at pH=8 for different ρ values

$[Na^+]_T = 20mM$

ρ	$[Na^+]$	$[Na^+\text{-}18C6A_4]$	$[(18C6A_4)^{-4}]$
0.1	1.80×10^{-2}	2.00×10^{-3}	3.51×10^{-6}
0.5	1.00×10^{-2}	1.00×10^{-2}	3.14×10^{-5}
1.0	7.80×10^{-4}	1.92×10^{-2}	7.79×10^{-4}
1.1	2.74×10^{-4}	1.97×10^{-2}	2.27×10^{-3}

At pH =7 the concentrations of the different species are not significantly different. The computer program used to calculate these values gives at least ten decimal places, and the differences occur in the third decimal place.[160]

In aqueous media there are three types of interactions which may occur for these complexes: interaction with the crown ether cavity alone, coulombic metal - ligand interaction and cooperative interaction of the crown ether bound cation with carboxylate. Na^+-$18C6A_4$ was found to be 68% coulombic interaction, and only 3% crown ether cavity interaction. With K^+, cooperative interaction (49%) is the most prevalent with 18% crown ether cavity interaction. It can be seen that the K^+ fits the cavity better, an expected result.[134] Eyring and co-workers established the equation which relates free energy changes of complexation in terms of contributions from different interactions between the crown ether, its carboxylate group and the cation.[161]

By studying $18C6A_4$ in non-aqueous media it was hoped to see evidence for complexation and exchange. Depending on the behaviour of the system, there was the possibility that any interactions similar to those observed in aqueous media might also be identified under non-aqueous conditions.

7.2 Results

7.2.1 The (Na^+-Las) system

One of the differences between lasalocid A and 18C6 is that the former may serve the function of both ionophore and counter anion. The sodium salt of lasalocid A was used for these studies, so in solution it dissociates to Las^- and Na^+. The negative charge is at the carboxylic acid function of the aromatic ring. The oxygen atoms coordinate with the Na^+ ion and a hydrogen bond closes the ring about the ion. Monensin A was not used because pure compound was not available and it was felt that while lasalocid A could be used after drying, monensin A would require more extensive purification.

Lasalocid A is not soluble in NM and AN. It is soluble in PY, a highly donating solvent of lower dielectric constant or permittivity. In 1981 Farber and Petrucci reported the kinetics of complexation of 18C6 with $LiClO_4$ in low dielectric solvents.[162] They felt that, "kinetic investigations in media of low permittivity (resembling the membrane of biological cells) between electrolytes and macrocyclic ligands as crown ethers are lacking.", and that there was a "need for knowledge of the processes occurring in nonaqueous medium during cation transport." The two solvents chosen for their study were 1,3-dioxolane and 1,2-dimethoxyethane whose dielectric constants are 6.95 and 7.05 respectively (at 25°C). As shown in Table VI, the dielectric constant for pyridine is 12.91, slightly higher than the other two solvents but distinctly lower than the 78.304 value for water.

Titration series were run for (Na-Las) at three temperatures: 253K, 274K and 300K. None of the series consists exclusively of Lorentzian plots, so full lineshape analyses were

used for all samples, regardless of whether they appeared to be Lorentzian or not. At 274K, the stacked plots of ^{23}Na spectra show clearly the introduction of a second peak (see Figure 44), which grows as ρ increases. $[Na^+]_T$ was maintained at ~20mM through the addition of $NaBPh_4$. The total concentration of anion was therefore $[BPh_4^-] + [Las^-] \sim 20mM$. The use of the sodium salt of lasalocid precluded the study of samples where $\rho > 1$ so the presence of stoichiometry greater than 1:1 could not be established nor shown to be absent. Chemical shift data and T_1^{-1} relaxation rates are not used in the evaluation of the data when exchange is slow, and the non-Lorentzian T_2 peaks yield little useful information for this analysis approach.

A concentration study was run on the (Na^+-Las) system at 274K. As the concentration of $[Na^+]_T$ increases ($k_A + k_B$) does increase but not in the "clean" manner which is seen for $NaBPh_4$ - 18C6 in PY (see Figure 29). For a dissociative mechanism parallel lines would be expected but that is not clearly visible for this system. The scatter in the data is such that the determination of alternatives are not feasible. The pseudo-first order rate constants for three temperatures (252.6K, 274.2K, 300.0K) were determined and are shown in graphical form in Figure 45 as a function of $(1-\rho)^{-1}$. More conclusive information is not possible here. Despite greater scatter in these points than those for the $(Na\text{-}18C6)^+$ systems, it can be seen that, as the temperature increases, the rate of dissociation k_{-1} also increases.

7.2.2 The (Na^+-18C6A_4) system

The exchange for (Na^+-18C6A_4) in H_2O at pH >8 at 277K is too fast for the ^{23}Na NMR timescale. The difference in chemical shifts for the free and complexed Na^+ is only ~1.3ppm. In MeOH:H_2O solutions at the same temperature the difference in chemical shifts shrinks to ~0.9ppm. Neither system was suitable so the use of non-aqueous solvents was investigated. Low solubility in AN prevented the use of that solvent but PY was suitable.

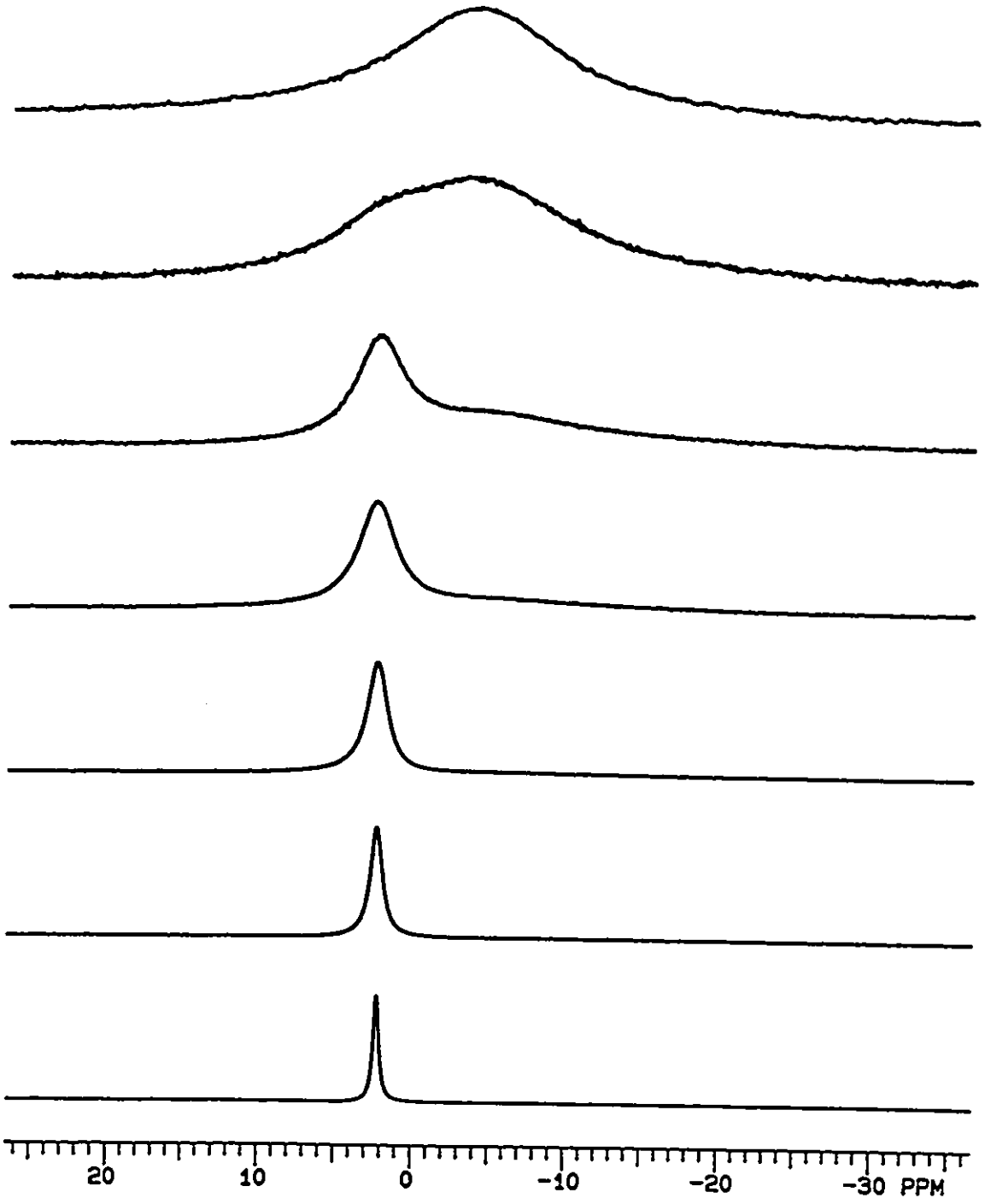

Figure 44: ^{23}Na NMR spectra of $NaBPh_4$-lasalocid in PY with varying ρ values. $[Na^+]_T$=21.5mM. T= 274K. Top to bottom: ρ = 1.00; 0.92; 0.75; 0.59; 0.37; 0.12; 0.00.

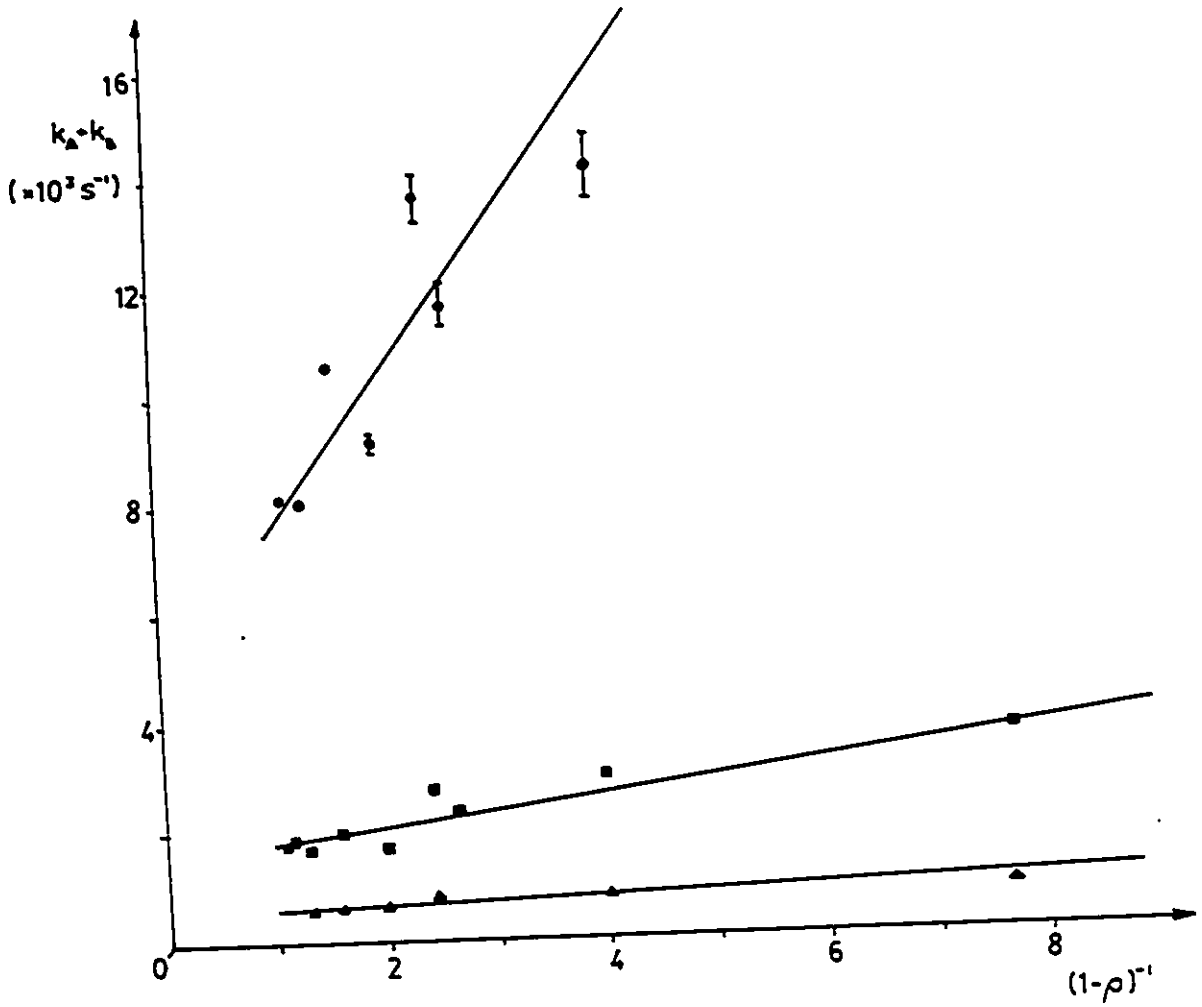

Figure 45: $k_A + k_B$ as a function of $(1-\rho)^{-1}$ for (Na^+-Las) in PY at 252.6K (▲); 274.2K (■); and 300.0K (●). $[Na^+]_T = 21.5mM$.

Since PY has been used to study the (Na^+-Las) system, its use again is totally acceptable as, depending on the results, comparisons might be possible.

A titration curve for the ($NaBPh_4$-$18C6A_4$) in PY at 300K was studied. The signals are not truly Lorentzian and the resulting errors on the estimated chemical shifts are large. From the stack plot of the ^{23}Na NMR spectra (see Figure 46) it can be seen that the narrow peak at $\rho = 0$ broadens immediately upon the addition of $18C6A_4$. The chemical shift becomes more negative for $\rho = 0$ to $\rho = 0.7$ and then becomes more positive. Once more the system is not a simple 1:1 complex formation but a more complicated one. The range in chemical shifts is ~14ppm. It is interesting to note that, while the signal broadens when $18C6A_4$ is first added, the chemical shift hardly varies until $\rho > 0.4$. Linewidths are typically 1kHz for $\rho > 1$ and too broad to measure accurately in the $0.5 < \rho < 1.0$ range. Full lineshape analysis does not yield satisfactory results.

7.3 Discussion

The approach used for both the study and the analysis of the data for the (Na^+-Las) system was similar to that used for the $(Na\text{-}18C6)^+$ system. The complication of having the lasalocid capable of being ionophore and counter anion is not negligible, and it appears that the roles may be less mutually distinct than hoped. The scatter in the experimental data cannot be attributed solely to poor technique since the technique was not changed when the transition from $(Na\text{-}18C6)^+$ systems to (Na^+-Las) systems was made. Dimers have been observed for Lasalocid A[131] so there is also the possibility that the lasalocid molecule may be interacting with itself rather than the Na^+. This would yield a system containing other interactions. Unlike the complications which the use of the ion-pairing SCN^- ion introduced, these are less identifiable and less separable. The model for the study of this system was possibly oversimplified. None the less, comparisons are still possible from the data which was obtained.

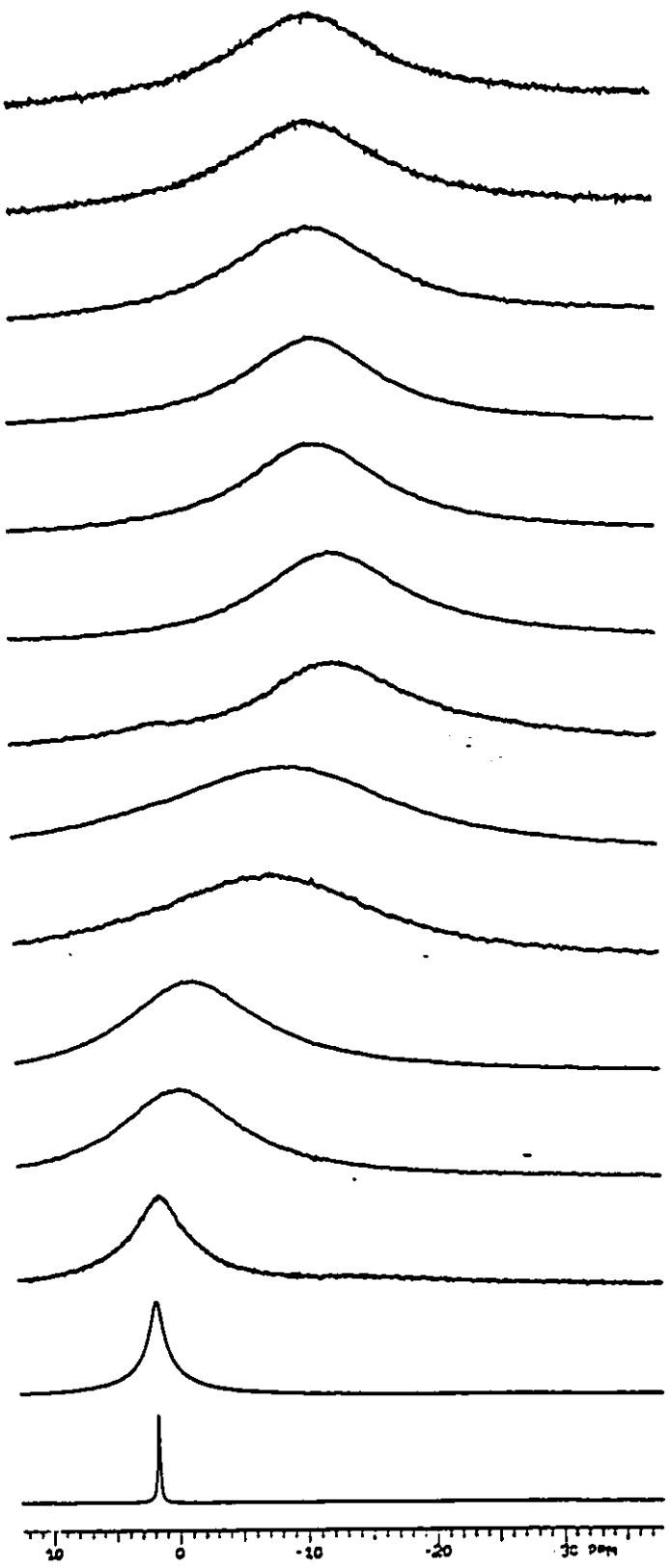

Figure 46: ^{23}Na NMR spectra of $NaBPh_4$-18C6A_4 in PY with varying ρ values. $[Na^+]_T$=20mM. T=300K. Top to bottom: ρ= 1.89; 1.51; 1.32; 1.21; 0.94; 0.90; 0.70; 0.60; 0.51; 0.41; 0.40; 0.35; 0.20; 0.00.

$18C6A_4$, with four carboxylic arms, has the capabilities of being in many conformations which would yield many different Na^+ environments, and the exact participation of these arms is not clear. Since several conformations, which would not be expected to have the same ^{23}Na chemical shifts, are possible, K_f determinations were not made.

In retrospect, the (Na^+-$18C6A_4$) system was complicated by having four substituent acid groups and minimal symmetry. In water there are three possible interactions for each substituent.[134,135] There is no guarantee that in PY that there are still three possibilities and that each substituent does not "do its own thing", changing rapidly amongst the three conformations. $18C6A_6$, with six carboxylic acid groups, might be simpler because of its symmetry.

7.3.1 Comparisons between (Na-Las) and $(Na\text{-}18C6)^+$ in Pyridine

Lasalocid and 18C6 were both studied in PY. Table XVII summarizes the kinetic parameters for the two systems. The pseudo-first order rate constants are an order of magnitude slower for 18C6 than for lasalocid and the dissociative rate constant is slower by the same amount at ~300K. The enthalpies of activation are comparable but the entropies of activation are quite different. For 18C6 the negative ΔS^* value is the result of the increased order in the system when it dissociates. This may initially appear to be contradictory but it must be remembered that this value refers to entropy on an overall level, where all molecules (18C6, $NaBPh_4$, PY) are considered. There is more order on a "global" level even though the entropy would be expected to increase when only the products of the decomplexation of $(Na\text{-}18C6)^+$ are considered. With (Na-Las) the net change in entropy is much closer to zero, suggesting that while the entropy may increase for certain system participants, such as Na^+ and Las, there are sufficient decreases in entropy in the solvent that the change is barely positive. It is of interest to note that while ΔG^* is smaller for (Na-Las) in PY than it is for $(Na\text{-}18C6)^+$ in PY, it is the same as for $(Na\text{-}18C6)^+$ in AN.

Table XVII: Kinetic Parameters for the $NaBPh_4$:18C6 and $NaBPh_4$:Lasalocid systems in Pyridine

	18C6	Lasalocid
$k_A + k_B$ (s^{-1}) [A]	$(1.47\pm0.05)\times10^{3}$ [B]	$(1.13\pm0.02)\times10^{4}$ [C]
k_{-1} (s^{-1})	$(5.3\pm0.2)\times10^{2}$ [B]	$(4.0\pm0.5)\times10^{3}$ [C]
$\Delta H^{\ddagger}$ $(kJ.mol^{-1})$	49±4	54±1
$\Delta S^{\ddagger}$ $(J.mol^{-1}.K^{-1})$	-30±10	4±3
$\Delta G^{\ddagger}_{301.5}$ $(kJ.mol^{-1})$	58.1±0.1	53±2

A: $\rho = 0.50$

B: T= 301.5±0.5K

C: T= 300.0±0.5K

7.4 Conclusions

When a compound has the ability to be both counter anion and ionophore, such as lasalocid A, the study of the decomplexation of its complex with Na^+ is not as straight forward as for ionophores with one capability. The (Na^+-Las) system did demonstrate that it follows the dissociative mechanism but other mechanisms must also be operative. Some suggestion of ion-pairing is seen through the data but quantitative analysis, the identification and separation of the different contributions, was not feasible.

The wide range of possible interactions between $18C6A_4$ and Na^+ yielded a system which was much more complex than could be handled adequately. Possibly the hexa-acid 18C6 might be a better choice for further studies, a system where the proximity of the acid functions and additional symmetry may reduce the motions of the individual substituents and should simplify the interpretation of the results. It would probably be a good idea to investigate the possibility of using another solvent. The high donating ability of PY may be introducing even more possibilities.

Chapter 8
The (Ca^{++}-18C6) System

^{43}Ca will never be called a "gifted" nucleus! Despite its low sensitivity and abundance (see Table III) the decision was made to attempt studies with ^{43}Ca to see what could be learned about its complexation by 18C6. If these had been successful, more complicated ionophores might have been investigated.

8.1 Background

The ionic diameters of Ca^{++} and Na^{+} are similar, which suggests that, neglecting the effect of a doubly-charged cation, the ions would fit into similarly sized cavities. The disordered $Ca(SCN)_2$ complex of 18C6 has hexagonal bipyramidal coordination, with the thiocyanate nitrogen atom completing it.[164] The NaSCN complex of 18C6 is a distorted pentagonal bipyramid.[113] In 1969 ^{43}Ca NMR was the first proposed as a useful tool for studying protein-bound calcium at physiological concentrations.[164] Bryant examined the binding of Ca^{++} by ATP using an enriched sample.[164] These biologically-related studies continued and such systems were the main reason that use of this technique was pursued. High resolution spectra of Ca^{++}-EDTA complexes were reported in 1981.[165] Further information about ^{43}Ca NMR is in Section 1.5.5.

Farmer and Popov's study was more basic in nature. They looked at the ^{43}Ca resonance as a function of solvent, counter-anion concentration and total salt concentration.[45] With calcium nitrate a gradual upfield shift is observed for increasing concentrations of methanol, but in DMF chemical shifts are independent of concentration. Qualitative correlation between the solvating abilities, as given by the Gutmann Donicity numbers, and the estimated values of the chemical shifts at infinite dilution can be seen. The linewidths are broader in non-aqueous solvents than in aqueous media. 0.5M calcium nitrate in DMSO has a linewidth of ~15Hz, 50Hz in ethylene glycol and 56Hz in TMG. This does not illustrate a direct correlation with the solvents' viscosities. James and Cutler investigated the

dependence of ^{43}Ca NMR linewidths upon concentration for $Ca(ClO_4)_2$ in water. The linewidth of the ^{43}Ca NMR signal increases from 2Hz to 15Hz as the concentration increases from 0.15M to 4M.[166]

Alkaline-earth cations complexed with cryptands and other small synthetic ionophores have been studied by various techniques. One use of these studies was to help in the interpretation of ^{43}Ca NMR data from other complexes. Drakenberg determined ^{43}Ca QCC values for Ca^{++}-EDTA and Ca^{++}-EGTA complexes using a technique analogous to the one discussed in Chapter 6. The complex with EDTA was the more symmetrical of the two.[167]

Cox's group has made use of stopped-flow methods in their studies of alkaline-earth metal complexes.[102,168-171] Calcium-diaza-18C6 complexes in MeOH dissociate at a rate of 80.3 s^{-1} at 298K, which is faster than dimethyl-diaza-18C6 (k_d =38.4 s^{-1}). Complexes with Sr^{++} and Ba^{++} dissociate more slowly again and have higher formation constants.[168] The dissociation of $(Ca\text{-}C2_B22)^{++}$ is practically independent of the choice of anion (Br^- or ClO_4^-) but Cl^- does accelerate the rate. In contrast $(Ca\text{-}C2_B2_B2)^{++}$ is less influenced. This suggests that dissociation rates may be catalyzed but the structure of the ligand plays a role. The anion must be free to approach the cation or else the catalysis may be suppressed.[102] They have also determined stability constants for calcium ion - cryptate complexes in a variety of solvents, including: MeOH[169], H_2O, DMSO, DMF and PC; using direct potentiometry.[170] The rates of formation and dissociation, determined conductimetrically, were reported for the same five solvents. The results suggest that in these systems complexation involves the stepwise replacement of solvent by ligand donor atoms.[169] Stability constants and dissociation rates in AN/H_2O mixtures were reported later.[171]

The three steps for the complexation of alkaline-earth metals and C222 in H_2O were identified in 1986.[172] The fastest step is the initial conformational change of the cryptand. This is followed by the replacement of the coordinating solvent molecules about the cation by the cryptand. The actual inclusion of the ion is the slowest step. Studies of the entropies and

enthalpies of complexation for alkaline-earth-C222 complexes have identified $(Ca\text{-}C222)^{++}$ as an exception.[173,174] It is believed that Ca^{++} is more strongly desolvated upon complex formation than the other cations in this family because the C222 is in a rigid conformation and surrounds the Ca^{++} more fully.

Studies of Ca^{++} interactions with protein and other biologically-related molecules continued to emerge as the NMR of ^{43}Ca was developed further. Forsén and Drakenberg, along with numerous co-workers have been quite active in this field. In 1982, their results for the binding of Ca^{++} to three proteins (calmodulin, parvalbumin and troponin C) were published.[175,176] Using isotropically enriched samples they found that the Ca^{++}-binding sites are relatively rigid. T_1 and T_2 measurements were made and the quadrupolar coupling constants and correlation times were determined. The ^{43}Ca QCC values were within the range 1.2±0.2MHz. Another study on Ca^{++}-calmodulin solutions examined the effects of the presence of other compounds such as glucagon. The Ca^{++} bound more tightly to low-affinity sites in their presence.[177]

Ca^{++}-lasalocid complexes have been the subject of a few studies.[178-182] Potentiometric methods were used to study complex formation in MeOH. Two species were shown to form: AM^+ and A_2M; though the amount of A_2M is small.[178] With alkali metal - lasalocid complexes AM is believed to be predominant over AHM^+.[179] In MeOH the enthalpies of reaction become more negative as alkaline-earth cation size increases. When the complex with Mg^{++} forms, the lasalocid backbone is not very involved. When Sr^{++} and Ba^{++} are complexed, the pseudo-crown ether form is adopted. The Ca^{++} complex is in an intermediary position.[180] Overall, in MeOH and PC the alkaline-earth complexes with lasalocid are stronger than the alkali metal complexes.[181] The transport of Ca^{++} across a liquid membrane (H_2O pH=5.0 / $CHCl_3$ / H_2O pH=9.0) is negligible at pH <6, but at pH >7.8 the maximum flow rate is attained when lasalocid is present.[182]

Other technologies, such as potentiometry and stopped-flow methods, continue to be more efficient probes into the kinetics of complex formation between Ca^{++} and cryptands,

crown ethers, and related compounds.[169,183] Despite this, the study of crown ethers is a logical progression because lariat ethers and cryptates have been examined. Lower solubility of calcium salts in nonaqueous solvents may make ^{43}Ca NMR studies in these solvents more challenging but, with the higher field spectrometers, the calcium signal is more easily seen.

8.2 Results

18C6 was studied in 50:50 AC:H_2O (by volume) because of solubility problems with calcium nitrate in neat acetone. A titration series was run where the amount of 18C6 increased from ρ =0 to ρ =2.5, so there was the possibility of observing sandwich complexes if they were to occur. Figure 47 shows the stacked ^{43}Ca NMR spectra. The observed transverse relaxation rates and chemical shifts are in Table XVIII.

Table XVIII: Summary of ^{43}Ca NMR results

ρ	T_2^{-1} (±10%)(Hz)	δ (±0.5)(ppm)
0.00	7.6	5.6
0.22	47	0.4
0.42	76	-3.5
0.54	100	-6.5
0.60	105	-7.2
0.79	129	-12.5
0.87	126	-13.6
1.05	142	-16.3
1.24	186	-19.9
1.57	181	-24.0
1.97	166	-25.1
2.48	178	-26.2

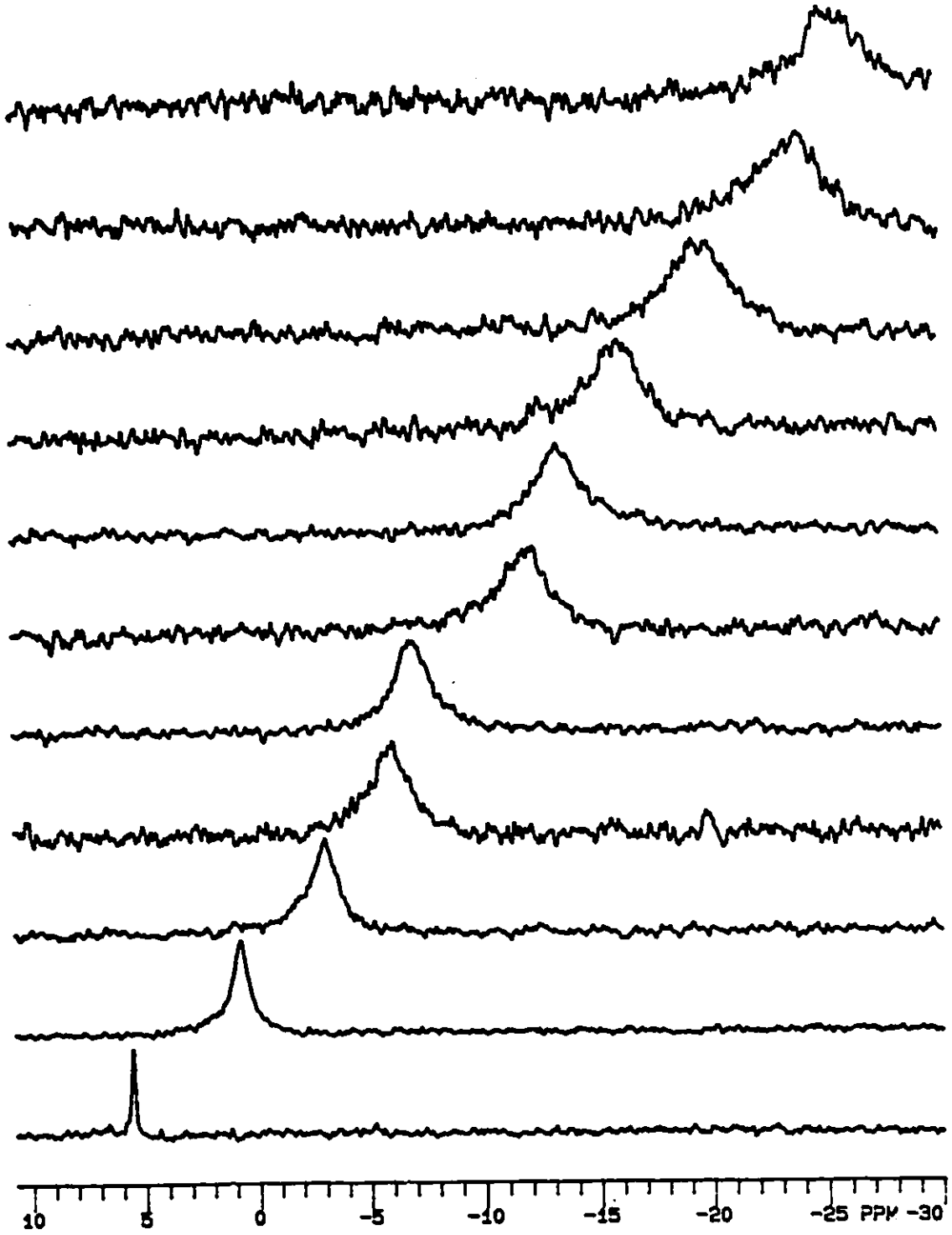

Figure 47: ^{43}Ca NMR spectra of $Ca(NO_3)_2$-18C6 in 50:50 AC:H_2O with varying ρ values. $[Ca^{++}]_T$=20mM. T=300K. Top to bottom: ρ= 1.97; 1.57; 1.24; 1.05; 0.87; 0.79; 0.60; 0.54; 0.42; 0.22; 0.00.

The range in chemical shifts is ~30ppm. No plateau is observed for $\rho > 1$ but the graph of ^{43}Ca chemical shift as a function of ρ (see Figure 48) shows that the relationship is approximately linear for $0 < \rho < 1$ and then curves. If more samples where $\rho > 2$ were run, a plateau might be observed. This suggests that a 1:1 complex forms with $K_f < 10^4$. The possibility of 2:1 complexes cannot be ruled out. The K_f was evaluated by doing a computer regression on the chemical shift data and consequently the K_f value was used to determine the transverse relaxation rates and the chemical shifts for the free and complexed calcium cations. Table XIX summarizes these results. The errors are given by the regression. These results seem logical but the value for K_f is lower than what was predicted. Even if the error on K_f is under-estimated, it is clear that $K_f < 10^2$.

Table XIX: The characteristics of Ca^{++} and (Ca^{++}-18C6) in 50:50 AC:H_2O

$K_f = 10 \pm 3$

	free	complexed
T_2^{-1} (s^{-1})	19±12	241±10
δ (ppm)	7±1	-35±3

8.3 Discussion

In MeOH Ca^{++}-18C6 has a reported chemical shift of -40ppm with respect to an aqueous Ca^{++} reference.[44] In 50:50 AC:H_2O the most negative chemical shift was -26ppm for $\rho = 2.5$. Here is another suggestion that the Ca^{++} cations are not all bound to the 18C6. The chemical shift of calcium nitrate is 6ppm. The ^{43}Ca chemical shift for (Ca^{++}-18C6(COO^-)$_4$) is ~ -20ppm. The chemical shifts have been shown to be at lower frequencies if only oxygen atoms are coordinating, rather than if nitrogen atoms also coordinate.[44] In MeOH slow exchange is observed for solvated Ca^{++} and Ca^{++}-18C6.[45] Dale and Kristiansen confirmed this with ^1H NMR.[184] In this system only one signal, the weighted average of the sites, is observed.

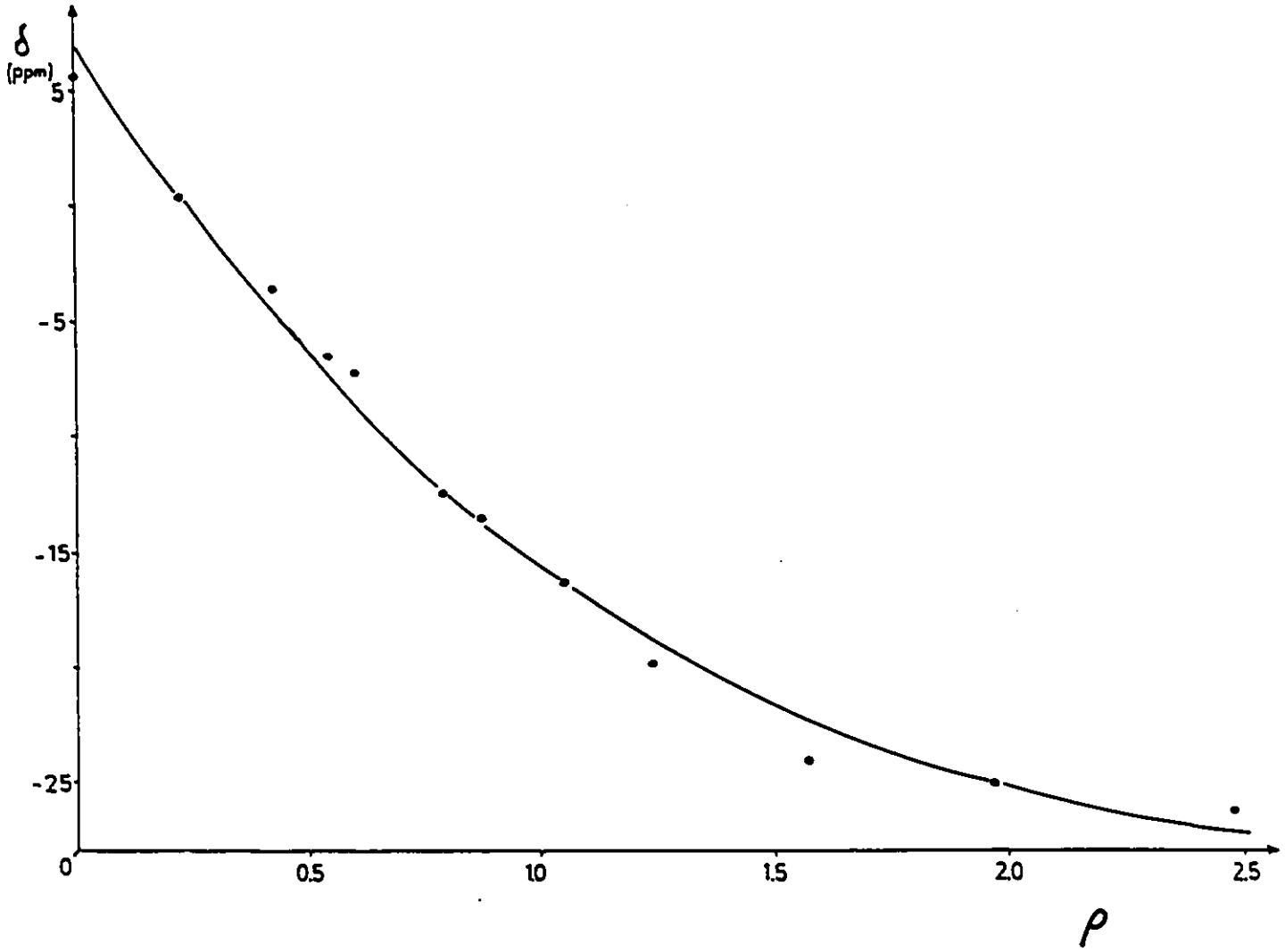

Figure 48: ^{43}Ca chemical shifts of $Ca(NO_3)_2$-18C6 in 50:50 AC:H_2O as a function of ρ. T=300K. The data points are experimental, and the curve is calculated from the values given in Table XIX.

8.4 Conclusions

^{43}Ca NMR experiments on un-enriched samples are time-consuming. Unfortunately this nucleus did not lend itself to a detailed mechanistic and kinetic study but it did provide a glimpse of the (Ca^{++}-18C6) complex which was not previously available. For $(Na\text{-}18C6)^{+}$ complex formation is quantitative but the K_f for (Ca^{++}-18C6) was calculated to be 10±3.

Chapter 9
Experimental Methods and Procedures

9.1 Experimental Details

9.1.1 Salts

$NaBPh_4$ was purchased from Aldrich (99+%, ACS reagent) and was recrystallized from cyclohexane with minimal ethanol. NaSCN was purchased from Fisher (99.5%, ACS reagent) and was recrystallized from acetonitrile in minimal cyclohexane. Bu_4NBPh_4 (99%),$NaPF_6$ (98%), and Bu_4NPF_6 (98%) were purchased from Aldrich. All were vacuum dried over phosphorous pentoxide for at least 24 hours at 50°C prior to use. $Ca(NO_3)_2.4H_2O$ (99%) was purchased from Aldrich and was vacuum dried for at least 24 hours prior to use.

9.1.2 Solvents

Pyridine (BDH assured), acetonitrile (BDH assured), acetone (Fisher, 99.5% spectranalyzed), and nitromethane (Aldrich 96%, Gold label) were dried under reflux, over calcium hydride for at least 2 hours, distilled under N_2, and stored under argon. Propylene carbonate (Burdick & Jackson, water content 0.012%) was dried over molecular sieves 4Å. Water was pyrolitically, doubly-distilled and was kindly supplied by B.E. Conway's lab here in the Chemistry Department of the University of Ottawa.[185] Deuterated AN(99.5 %D), NM(99 %D), and PY(99 %D) were purchased from Aldrich. Deuterated AC(99.9 %D) was purchased from MSD Isotopes (a division of Merck Frosst).

9.1.3 Crown Ethers

18C6 was purchased from Aldrich (99%) and was recrystallized following the procedure described by Gokel et al[186], and vacuum dried over P_2O_5 for a minimum of 24 hours at 50°C. The complete removal of acetonitrile from the recrystallized crown was confirmed by ^1H NMR. DB24C8 was purchased from Aldrich (98%) and was vacuum dried just prior to use over P_2O_5 for a minimum of 24 hours.

9.1.4 Lasalocid

The sodium salt of lasalocid was purchased from Sigma (99%). It was vacuum dried over P_2O_5 for a minimum of 24 hours.

9.1.5 $18C6A_4$

This compound was the gift of T.M. Fyles from the Chemistry Department at the University of Victoria. It was used as received.[187]

9.1.6 Sample Preparation

Samples were prepared by weighing appropriate amounts of crown ether directly into volumetric flasks and filling up with stock solutions of the desired sodium salt concentration. In a series where the concentration of the sodium salt varied, dilutions were done. This was also done to avoid having to weigh out quantities <0.001g. All handling was done rapidly in air.

9.1.6.1 ^{23}Na NMR samples

4ml of solution in 10 mm o.d. tubes were sealed with Parafilm under argon. All spectra were recorded within 48 hours of preparation of the samples.

9.1.6.2 ^{13}C NMR samples

0.5 ml of solution was placed in 5 mm o.d. tubes which were sealed under vacuum after careful degassing by at least three freeze-pump-thaw cycles. The exception was in the case of PY where the sample of complexed crown ether was run without degassing.

9.1.6.3 ^{43}Ca NMR samples

8 ml of solution in 16 mm o.d. tubes was sealed with Parafilm under argon.

9.1.7 Spectrometer related Details

9.1.7.1 ^{23}Na NMR spectra

^{23}Na NMR spectra were run, unlocked, on a Varian XL-300 spectrometer at 79.35 MHz; 90° pulse widths were typically 17 μs (PC), 27 μs (PY), 31 μs (AC), 24 μs (NM), and 31 μs (AN). They were measured before each set of experiments. Temperature measurements were made with a thermocouple submerged in mineral oil in a non-spinning 10 mm o.d. NMR tube. The temperature calibration was verified at regular intervals over the range 245K - 300K. It was also established prior to when temperatures from 300K to 330K were used. The temperature of the sample was deemed to be reliable to ±0.5 K. The signal-to-noise ratio was at least 100.

The chemical shifts were referenced to ^{23}NaCl 0.1M in H_2O and were corrected for bulk magnetic susceptibility. (See Table XX) In the case of PC, the correction was done from the measurement of ^{23}Na chemical shifts in two different geometries on a Varian XL300 and a Varian FT80.

In solenoid magnets, where the magnetic field lines run parallel to the long axis of the NMR tube, such as for the XL300, the correction on the observed chemical shift for bulk magnetic susceptibility is:

$$\delta_{TRUE} = \delta_{OBS} + \left(\frac{4\pi}{3}\right)(\chi_{ref} - \chi_{sample}) \qquad \text{(XL-300, 79.35MHz) equation 69}$$

For electomagnets, where the magnetic field lines run perpendicular to the long axis of the NMR tube, such as for the FT80, the corresponding relationship is:

$$\delta_{TRUE} = \delta_{OBS} + \left(\frac{2\pi}{3}\right)(\chi_{ref} - \chi_{sample}) \qquad \text{(FT-80, 21.04MHz) equation 70}$$

Table XX: Corrections for Bulk Magnetic Susceptibility

solvent	XL300 (ppm)	FT80 (ppm)
AC	-1.085	
AN	-0.775	+0.387
NM	-1.374	+0.687
PC	-1.127	+0.563
PY	-0.452	+0.226

T_1 measurements were done using the inversion-recovery 180°-τ-90° pulse sequence and were obtained from a nonlinear regression analysis. At least nine points were used for each determination. T_2^{-1} measurements were obtained directly from the linewidth when the lineshape was lorentzian, and were corrected for inhomogeneity (equation 38).

9.1.7.2 ^{13}C NMR spectra

^{13}C T_1 measurements were made on a Varian XL300 under proton-noise-decoupling conditions by the inversion-recovery technique. A waiting time of at least five times the longest relaxation time was used in each case.

NOE enhancements ^{13}C-{^1H} were measured on either a Varian XL300 or a Varian Gemini 200. Several samples were run on both instruments to ensure that the results would be comparable.

9.1.7.3 ^{43}Ca NMR spectra

^{43}Ca spectra were run, unlocked, on a Varian XL-300 spectrometer at 20.185 MHz; 90° pulse width was 90 μs. It was measured by maximum height rather than determining the 360° pulse. The pulse width for acquisition was 52.5 μs. The chemical shifts were referenced to $^{43}Ca(NO_3)_2$ 2.07M in H_2O/D_2O. The 16mm probe was tuned to $^{133}CsCl$, whose linewidth is 0.1Hz, before tuning to ^{43}Ca.

9.1.8 Pulse Sequences

The pulse sequences used in these experiments are shown schematically in Figures 49 - 52. Figure 49 shows the standard ^{23}Na pulse. The number of transients (NT) varied, depending on the concentration of the sample and how broad a signal might be expected. The pulse sequence for the ^{13}C-{^{1}H} NOE experiments (see Figure 50) shows that fewer transients were required and a delay has been added. The decoupler mode (DM) is given underneath. Figure 51 shows the pulse sequences for the ^{23}Na and ^{13}C T_1 experiments. ^{23}Na relaxes very quickly so no delay (D1) is required. The number of transients for the ^{23}Na experiment did vary and were usually lower than that needed for the T_2 experiment since the signal to noise ratio is less crucial. The pulse sequence for ^{43}Ca experiments (see Figure 52) is identical to that used for the ^{23}Na T_2 experiments except that many more transients are needed before a signal rises above the noise floor.

9.1.9 Computer Programmes

Full lineshape analyses:

Two different procedures were followed for full lineshape analyses for two-site exchange to derive the pseudo-first order rate constants for non-Lorentzian lineshapes. A Simplex fitting procedure was used with manually transferred coordinates. A more efficient method was subsequently established. This was used on all lineshapes, both Lorentzian and non-Lorentzian. The coordinates were transferred via an IBM-clone PC and Kermit software, and subsequently a Sytek line to the university mainframe where they were analysed using SAS. The SAS program can be found in Appendix A. A program, written by H.D. Dettman, using Varian "magical' software digitized the data and sent it to the pc.[188] For the case of moderately rapid exchange, Lorentzian lineshapes could be analysed using the equation derived by Woessner.[68]

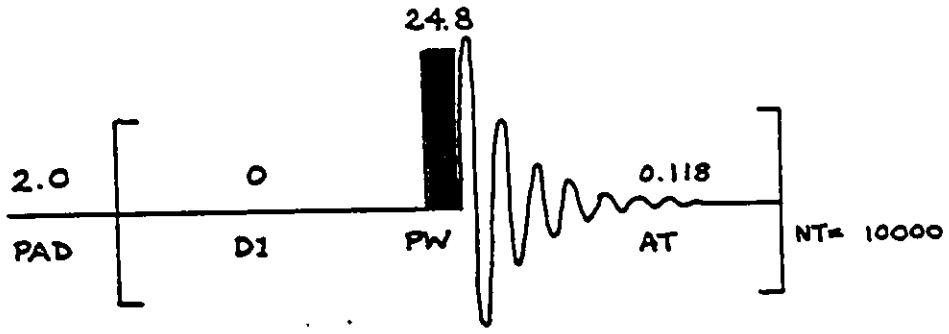

Figure 49: The ^{23}Na NMR S2PUL pulse sequence.

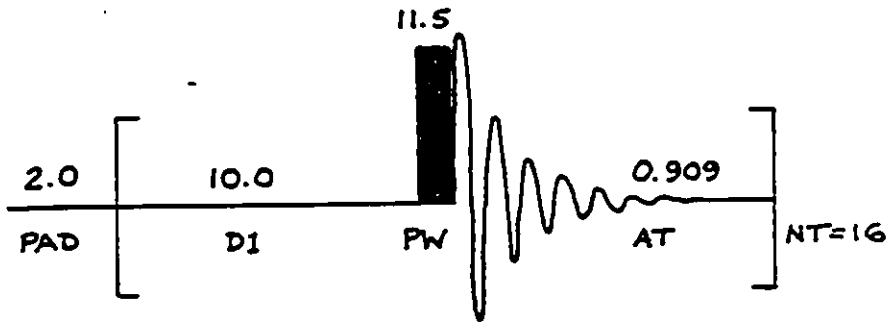

DM ARRAY
1 YYY
2 NNY

Figure 50: The pulse sequence for the ^{13}C-{^{1}H} NOE experiment.

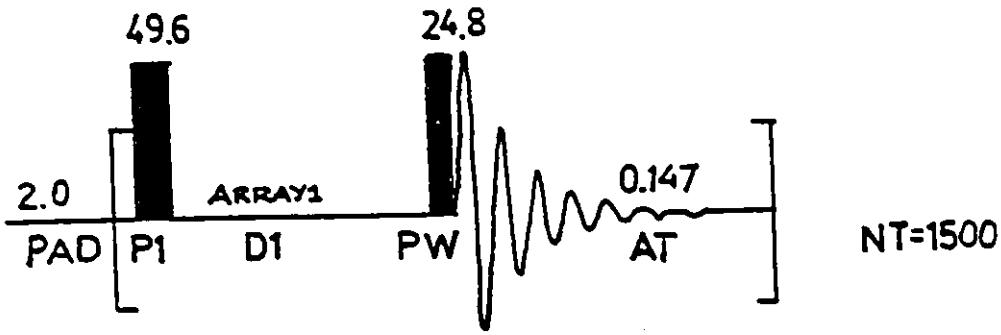

Figure 51: The pulse sequences for the T_1 experiments.

(a) ^{23}Na; (b) ^{13}C.

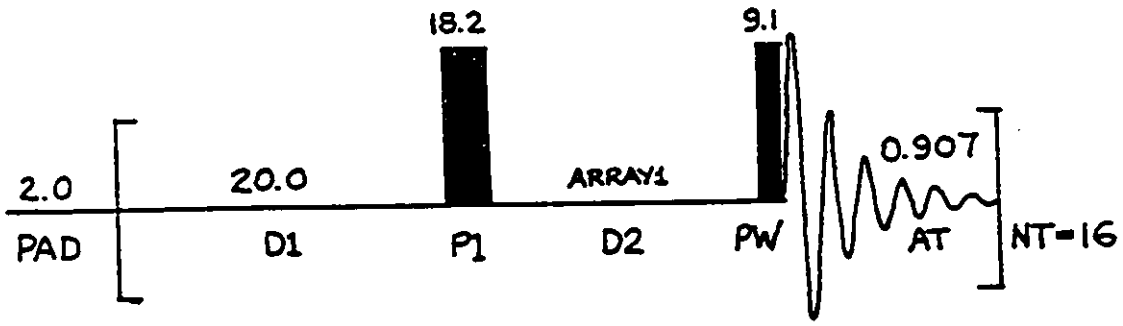

DMM= ON

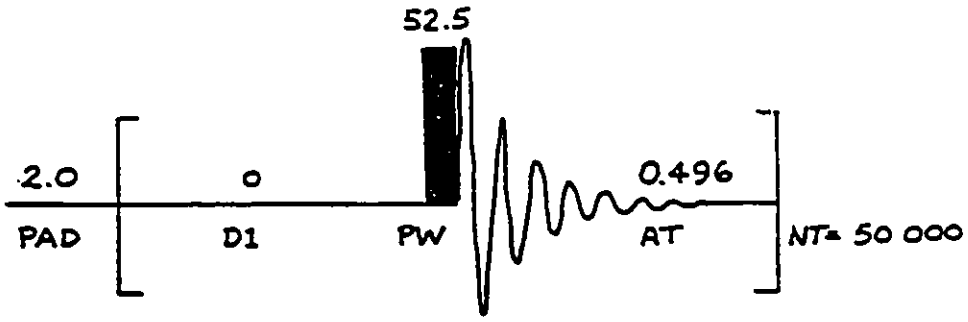

Figure 52: The pulse sequence for the ^{43}Ca experiments.

9.2 Errors and Error Determination

9.2.1 Errors on $\nu_{\frac{1}{2}}$, T_1 and T_2 measurements

Errors on the ^{23}Na linewidths at half-height were measured for each solvent. ^{13}C T_1 measurements were run at least twice. Errors were calculated and given by the computer.

9.2.2 Errors on the NOE measurements

Errors on the NOE enhancement are standard deviations of at least three trials.

9.2.3 Errors on ρ, [M⁺]/[crown]

The value of ρ is deemed to be accurate within ±0.01. Where Lorentzian peaks were observed the plot of δ vs. ρ would show clearly any errors in ρ. Where the determination of $(k_A + k_B)$ was done by SAS it was possible to give ρ as a variable, thus exposing potential errors in ρ.

9.2.4 Errors on $(k_A + k_B)$

The errors on $(k_A + k_B)$ were obtained from the experimental errors on T_2^{-1} and T_1^{-1}, in the case of the moderately rapid exchange. A full lineshape analysis for two-site exchange[189] using a Simplex fitting procedure[190] was used to derive the pseudo-first order rate constants for non-Lorentzian lineshapes. In that case errors were estimated from the rms of the regression. When the analyses were performed using SAS, the computer gave an error.

9.2.5 Errors on k_{-1} and k_2

The errors on k_{-1} and k_2 are the standard deviations on the slope and the y-intercept of the linear regressions of $(k_A + k_B)$ as a function of $(1-\rho)^{-1}$. In many cases the linear regression was made taking into account the errors on each value included.

9.2.6 Errors on $\Delta H^{\ddagger}$, $\Delta S^{\ddagger}$ and $\Delta G^{\ddagger}$

The errors on $\Delta H^{\ddagger}$ and $\Delta S^{\ddagger}$ are the standard deviations of the linear regressions on the Eyring plots. The errors on $\Delta G^{\ddagger}$ have been calculated from the corresponding errors on k_{-1} and k_2 at 301.5 K.[191]

$$\frac{\Delta\Delta G^{\ddagger}}{\Delta G^{\ddagger}} = \frac{\left\{\left[\frac{\Delta T}{T}\left(\ln\frac{k_B T}{h k}+1\right)\right]^2+\left(\frac{\Delta k}{k}\right)^2\right\}^{\frac{1}{2}}}{\ln\left(\frac{k_B T}{h k}\right)} \qquad \text{equation 71}$$

Summary and Conclusions

NMR is a useful tool for studying the dissociation of cation complexes with ionophores. In this study two mechanisms were shown to be operative for the different systems which were investigated. The principal cation used was $^{23}Na^+$, and crown ethers were the most widely used ionophores. The $(Na\text{-}18C6)^+$ system was studied in great detail in order to examine the roles of each component and factor: the solvent, the counter anion and the temperature. Other systems were studied where the ionophore or the cation were changed.

^{23}Na NMR was used to study the role of the counter anion (BPh_4^- or PF_6^-) in the dissociation of $(Na\text{-}DB24C8)^+$ which forms quantitatively ($K_f > 10^5$). This system follows the metal associative interchange "M_{ai}" mechanism. When the concentrations of the cation and counter anion are varied the M_{ai} mechanism is operative. When the concentration of the counter anion is maintained while the concentration of the cation is diminished, the same mechanism prevails. The presence of high concentrations of ions slightly accelerates the operative dissociative mechanism rather than changing it.

The $(Na\text{-}18C6)^+$ complex in AC, when BPh_4^- is the counter anion, decomplexes exclusively by the dissociative mechanism. For the same system in AN, PC and PY there is competition between the two mechanisms. The rate constants have been determined for these systems and the kinetic parameters for the dissociative mechanism have been calculated, except for PC where both sets of kinetic parameters were accessible. In NM the small difference in chemical shifts between the solvated and complexed sodium precludes the study of this system. In these systems an entropy - enthalpy compensation effect is observed.

The influence of the counter anion was examined on the $(Na\text{-}18C6)^+$ in AC. This solvent was chosen because when BPh_4^- was used the decomplexation was effected exclusively via the dissociative mechanism. Ion-pairing must be taken into consideration when SCN^- is the counter anion. The four species present $((Na^+)_s$, $(Na^+,SCN^-)_s$, $(Na\text{-}18C6)^+$

and ($Na\text{-}18C6^+$,SCN^-)) were characterized in terms of chemical shifts and relaxation rates. The ion-pairing constants for both the free and complexed sodium cations (K_{IP} and K_{CIP}) were determined. The observed rate of dissociation ($k_{-1,obs}$) was separated into the contributions from the dissociation of the complex (k_{-1}) and the ion-paired complex (k_{-1}'). The energetics of SCN^- ion-pairing were then fully described. The rate of dissociation increases upon the introduction of SCN^- to replace BPh_4^-. No change in mechanism is observed.

Access to the ^{23}Na quadrupolar coupling constants (χ) was made based on the assumption that the τ_{eff} from ^{13}C NMR of the 18C6 is equivalent to the τ_c of the $^{23}Na^+$ in the complex. In AC, AN and PC the environment around the Na^+ is quite symmetrical. In PY the highly donating solvent competes with crown ether oxygens and in NM the high internal pressure of the solvent both lead to distortions of the complex from high symmetry and higher χ values result.

The (Na^+-Lasalocid) system is more complicated than the systems with crown ethers because this naturally-occurring ionophore can serve both as ionophore and counter anion. The dissociative mechanism is operative, but the treatment used was probably oversimplified so the identification of other interactions and mechanisms was not realized. There is a wide range of possible interactions between $18C6A_4$ (A= -COOH) and Na^+. Interactions were observed between the two by ^{23}Na NMR but were not identified.

The ^{43}Ca nucleus did not lend itself to a detailed mechanistic and kinetic ^{43}Ca NMR study, but it did provide a glimpse of the (Ca^{++}-18C6) complex which was not previously available. The formation constant (K_f) for (Ca^{++}-18C6) was calculated to be 10±3.

Claims to original research

^{23}Na NMR experiments show that the $(Na\text{-}DB24C8)^+$ complex in NM dissociates by the metal associative interchange "M_{ai}" mechanism. No dissociative mechanism, even one involving the counter anion, could account for these experimental results. The concentration of the counter anion was maintained constant and the concentration of Na^+ was reduced, resulting in a reduction of the exchange rate of sodium between the complexed and solvated sites. The same is viewed when BPh_4^- is replaced by PF_6^-. This is an unambiguous demonstration of the plausibility of an associative (M_{ai}) mechanism in cation - crown ether complex systems in solution. This is a mechanism where the charge repulsion between the cations is overcome. Despite the proximity of the cations the M_{ai} mechanism is still operative.

^{23}Na NMR was used to observe that in AC the $(Na\text{-}18C6)^+$ complex dissociates exclusively by the dissociative mechanism. In AN, PY and PC both the metal associative interchange (M_{ai}) and dissociative mechanisms are operative. The kinetic parameters for the dissociative mechanism were determined in all four solvents. In PC it was possible to determine the kinetic parameters for both mechanisms.

The observed dissociative rate constant for the $NaBPh_4$/NaSCN-18C6 system in AC was separated into the contributions from the dissociation of the ion-paired and the solvated complexes. The presence of SCN^- accelerates the rate of dissociation. The energetics for the ion-pairing of SCN^- in AC were determined completely. A study of such depth has not been previously achieved.

The ^{23}Na quadrupolar coupling constants were determined for $(Na\text{-}18C6)^+$ in five solvents. In AC, AN and PC the $^{23}Na^+$ environment is quite symmetrical (χ ~1.0-1.2 MHz). In NM and PY the $^{23}Na^+$ is less symmetrical.

The (Na-Las) complex dissociates by the dissociative mechanism in PY though this is not the only operative one. In PY there are interactions between Na^+ and $18C6A_4$ (A = -COOH) as observed by the ^{23}Na NMR.

Exploratory ^{43}Ca NMR experiments were undertaken, and demonstrated the potential of this method. The formation constant for (Ca^{++}-18C6) complex was determined. K_f = 10±3.

Appendix A

SAS program

```
DATA TWO;
        CMS FILEDEF TWO DISK INPAR DATA A;
        INFILE TWO;
        INPUT TF VF TB VB PF PB TEMP;
PROC PRINT;
DATA ONE;
        CMS FILEDEF ONE DISK H000 NMR A;
        INFILE ONE;
        INPUT NO X Y;
        IF N=1 THEN SET TWO;
        PI=3.14159;
PROC NLIN METHOD=DUD;
        PARMS CO=1E5 KAB=1E3;
        BOUNDS 1<CO<1E6, 0<KAB<5E7;
        TA=1/KAB;
        DV=(VF-VB);
        DELV=0.5*(VF-VB)-X;
        P=TA*(TF*TB-4*PI**2*DELV**2+PI**2*DV**2)+PF*TF+PB*TB;
        O=TA*(2*PI*DELV-PI*DV*(PF-PB));
        R=2*PI*DELV*(1+TA*(TF+TB))+(PI*DV*TA*(TB-TF))+PI*DV*(PF-PB);
        YCAL=CO*(P*(1+TA*(PB*TF+PA*TB))+O*R)/(P**2+R**2);
        MODEL Y=CO*(P*(1+TA*(PB*TF+PA*TB))+O*R)/(P**2+R**2);
        DER.CO=(P*(1+TA*(PB*TF+PA*TB))+O*R)/(P**2+R**2);
        ID YCAL;
PROC PLOT DAT=PUT;
        PLOT Y*X='O' YCAL*X='+'/OVERLAY;
```

Notes:

TF= $T_{2,obs}^{-1}$ of the solvated Na^+.

VF= δ (Hz) of the solvated Na^+.

TB= $T_{2,obs}^{-1}$ of the complexed Na^+

VB= δ (Hz) of the complexed Na^+.

PF= population of solvated Na^+.

PB= poplulation of complexed Na^+.

H000 NMR is the file of (x,y) coordinates from the spectrometer.

References

1) Dobler, M.; Ionophores and Their Stuctures, John Wiley & Sons Inc., New York, 1981.

2) (a) Kimball, J.W.; Biology, 4th edition, Addison-Wesley, Reading, Mass., 1978, 857 pages.
(b) Lehninger, A.L.; Biochemistry, Worth Publishers, N.Y., U.S.A., 1970, 833 pages.

3) (a) Whang, R.; Potassium: Its Biologic Significance, CRC Press, Florida, U.S.A., 1983, 163 pages.
(b) Hille, B.; Ionic Channels of Excitable Membranes, Sinauer Associates Inc., Massachusetts, U.S.A., 1984, 426 pages.
(c) Oiki, S.; Danho, W.; Montal, M.; Proc. Natl. Acad. Sci. USA, 1988, 85, 2393-2397.
(d) Oiki, S.; Danho, W.; Madison, V.; Montal, M.; Proc. Natl. Acad. Sci. USA, 1988, 85, 8703-8707.
(e) Montal, M.; Montal, M.; Tomich, J.M.; Proc. Natl. Acad. Sci. USA, 1990, 87, 6929-6933.
(f) Hill, J.A. Jr.; Coronado, R.; Strauss, H.C.; Biophys. J., 1989, 55, 35-46.

4) Pedersen, C.J.; J. Am. Chem. Soc., 1967, 89, 7017-7036.

5) Pedersen, C.J.; Angew. Chem. Int. Ed. Eng., 1988, 27, 1021-1027.

6) Ullman's Encyclopedia of Industrial Chemistry, E. Weber ed., VCH Verlagsgesellschraft, 1987, A8, 91-97.

7) Gokel, G.W.; Dishong, D.M.; Diamond, C.J.; J. Chem. Soc., Chem. Commun., 1980, 1053-1054.

8) Lehn, J.-M.; Angew. Chem. Int. Ed. Eng., 1988, 27, 89-112.

9) (a) Dietrich, B.; Lehn, J.-M.; Sauvage, J.-P.; Tet. Lett., 1969, 2885-2888.
(b) Dietrich, B.; Lehn, J.-M.; Sauvage, J.-P.; Tet. Lett., 1969, 2889-2892.

10) Cram, D.J.; Angew. Chem. Int. Ed. Eng., 1988, 27, 1009-1020.

11) (a) Cram, D.J.; Cram, J.M.; Science, 1974, 183, 803-809.
(b) Kyba, E.P.; Siegel, M.G.; Sousa, L.R.; Sogah, G.D.Y.; Cram, D.J.; J. Am. Chem. Soc., 1973, 95, 2691-2692.
(c) Kyba, E.P.; Koga, K.; Sousa, L.R.; Siegel, M.G.; Cram, D.J.; J. Am. Chem. Soc., 1973, 95, 2692-2693.

12) Albrecht-Gary, A.-M.; Dietrich-Buchecker, C.O.; Saad, Z.; Sauvage, J.-P.; J. Am. Chem. Soc., 1988, 110, 1467-1472.

13) Dietrich-Buchecker, C.O.; Sauvage, J.-P.; Angew. Chem. Int. Ed. Eng., 1989, 28, 189-192.

14) Dietrich-Buchecker, C.O.; Sauvage, J.-P.; Chem. Rev., 1987, 87, 795-810.

15) Sarges, R.; Witkop, B.; Biochem., 1965, 4, 2491-2494.

16) Hughes, M.N.; The Inorganic Chemistry of Biological Processes, 2nd edition, John Wiley & Sons, Chichester, U.K., 1985, 270-271.

17) Spisni, A.; Khaled, M.A.; Urry, D.W.; F.E.B.S. Lett., 1979, **102**, 321-324.

18) Urry, D.W.; Trapane, T.L.; Venkatachalam, C.M.; Prasad, K.U.; Can. J. Chem., 1985, **63**, 1976-1981.

19) Urry, D.W.; Trapane, T.L.; Brown, R.A.; Venkatachalam, C.M.; Prasad, K.U.; J. Magn. Reson., 1985, **65**, 43-61.

20) Urry, D.W.; Trapane, T.L.; Venkatachalam, C.M.; J. Membrane Biol., 1986, **89**, 107-111.

21) Hinton, J.F.; Koeppe, R.E. II; Shungu, D.; Whaley, W.L.; Paczkowski, J.A.; Millett, F.S.; Biophys. J.; 1986, **49**, 571-577.

22) Hinton, J.F.; Whaley, W.L.; Shungu, D.; Koeppe, R.E. II; Millett, F.S.; Biophys. J.; 1986, **50**, 539-544.

23) Dietrich, B.; J. Chem. Ed., 1985, **62**, 954-964.

24) Riddell, F.G.; Arumugam, S.; Brophy, P.J.; Payne, M.C.H.; Southon, T.E.; J. Am. Chem. Soc., 1988, **110**, 734-738.

25) Dulyea, L.M.; Fyles, T.M.; Whitfield, D.M.; Can. J. Chem., 1984, **62**, 498-506.

26) Riddell, F.G.; Arumugam, S.; Cox, B.G.; J. Chem. Soc. Chem. Commun., 1987, 1890-1891.

27) Riddell, F.G.; Arumugam, S.; Cox, B.G.; Biochimica et Biophysica Acta, 1988, **944**, 279-284.

28) Choy, E.M.; Evans, D.F.; Cussler, E.L.; J. Am. Chem. Soc., 1974, **96**, 7085-7090.

29) Behr, J.-P.; Lehn, J.-M.; Dock, A.-C.; Moras, D.; Nature, 1982, **295**, 526-527.

30) Fyles, T.M.; James, T.D.; Kaye, K.C.; Can. J. Chem., 1990, **68**, 976-978.

31) Carmichael, V.E.; Dutton, P.J.; Fyles, T.M.; James, T.D.; Swan, J.A.; Zojaji, M.; J. Am. Chem. Soc., 1989, **111**, 767-769.

32) Nakano, A.; Xie, Q.; Mallen, J.V.; Echegoyen, L.; Gokel, G.W.; J. Am. Chem. Soc., 1990, **112**, 1287-1289.

33) Andersen, O.J.; Biophys. J., 1983, **41**, 147-165.

34) Cornélis, A.; Laszlo, P.; Biochem., 1979, **18**, 2004-2007.

35) Practical Spectroscopy Series, **11**, Modern NMR Techniques and Their Application in Chemistry, edited by A.I. Popov and K. Hallenga, Marcel Dekker Inc., N.Y., U.S.A., 1991.
(a) 485-520. (b) 521-566.

36) CHM 8133, University of Ottawa, given by C. Detellier, lecture notes, 1988.

37) Harris, R.K.; Nuclear Magnetic Resonance Spectroscopy, Longman Group U.K. Ltd., Bath Press, Avon, 1986.

38) Bovey, F.A.; Nuclear Magnetic Spin Resonance, 2nd edition, Academic Press Inc., San Diego, U.S.A., 1987, 653 pages.

39) Derome, A.E.; Modern NMR Techniques for Chemistry Research, Pergamon Press, Oxford, U.K., 1988, 280 pages.

40) Brevard, C.; Granger, P.; Handbook of High Resolution Multinuclear NMR, John Wiley & Sons Inc., New York, 1981.

41) Laszlo, P.; Angew. Chem. Int. Ed. Engl., 1978, **17**, 254-266.

42) Laszlo, P.; Progress in NMR Spectroscopy, 1979, **13**, 257-270.

43) Laszlo, P.; ACS Symp. Series, 1982, **191**, 63-95.

44) NMR of Newly Accessible Nuclei, 2, Chemically and Biochemically Important Elements, edited by P.Laszlo, Academic Press, N.Y., U.S.A., 1983, 229-252.

45) Farmer, R.M.; Popov, A.I.; Inorg. Nucl. Chem. Letters, 1981, **17**, 51-56.

46) Laidler, K.J.; Pure and Appl. Chem., 1990, **62**, 2221-2226.

47) Grell, E.; Funk, T.; Eggers, F.; in "Membranes"; Eisenman, G., Ed.; Marcel Dekker, New York, 1975; **III**, 1-126.

48) Davies, C.W.; Ion Association, Butterworths, London, U.K., 1962, 95-101.

49) Eigen, M.; Winkler, R., in "Neurosciences, Second study programme"; Schmit, F.O., Ed., Rockefeller University Press, New York, U.S.A., 1970, 685-696.

50) Cox, B.G.; Schneider, H.; Pure and Appl. Chem., 1990, **62**, 2259-2268.

51) Maynard, K.J.; Irish, D.E.; Eyring, E.M.; Petrucci, S.; J. Phys. Chem., 1984, **88**, 729-736.

52) Chock, P.B.; Proc. Nat. Acad. Sci. USA, 1972, **69**, 1939-1942.

53) Chen, C.; Wallace, W.; Eyring, E.M.; Petrucci, S.; J. Phys. Chem., 1984, **88**, 2541-2547.

54) Wallace, W.; Eyring, E.M.; Petrucci, S.; J. Phys. Chem., 1984, **88**, 6353-6356.

55) Kashanian, S.; Shamsipur, M.; Inorg. Chim. Acta, 1989, **155**, 203-206.

56) Chen, C.; Wallace, W.; Eyring, E.M.; Petrucci, S.; J. Phys. Chem., 1984, **88**, 5445-5450.

57) Richman, H.; Harada, Y.; Eyring, E.M.; Petrucci, S.; J. Phys. Chem., 1985, **89**, 2373-2376.

58) Chen, C.C.; Petrucci, S.; J. Phys. Chem., 1982, **86**, 2601-2605.

59) Xu, M.; Obeid, N.; Eyring, E.M.; Petrucci, S.; J. Phys. Chem., 1989, **93**, 989-997.

60) Takeuchi, H.; Arai, T.; Harada, I.; J. Mol. Struct., 1986, **146**, 197-212.

61) van Eerden, J.; Harkema, S.; Feil, D.; J. Phys. Chem., 1988, **92**, 5076-5079.

62) Mazor, M.H.; McCammon, J.A.; Lybrand, T.P.; J. Am. Chem. Soc., 1989, **111**, 55-56.

63) Wipff, G.; Weiner, P.; Kollman, P.; J. Am. Chem. Soc., 1982, **104**, 3249-3258.

64) Hase, W.L.; Richou, M.-C.; Mondro, S.L.; J. Phys. Chem., 1989, **93**, 539-545.

65) Lockhart, J.C.; in "Advances in Inorganic and Bioinorganic Mechanisms"; Sykes, A.G., Ed.; Academic Press, New York, U.S.A., 1982, **1**, 1217-268.

66) Shchori, E.; Jagur-Grodzinski, J.; Luz, Z.; Shporer, M.; J. Am. Chem. Soc., 1971, **93**, 7133-7138.

67) Shchori, E.; Jagur-Grodzinski, J.; Shporer, M.; J. Am. Chem. Soc., 1973, **95**, 3842-3846.

68) Woessner, D.E.; J. Chem. Phys., 1961, **35**, 41-48.

69) Lin, J.D.; Popov, A.I.; J. Am. Chem. Soc., 1981, **103**, 3773-3777.

70) Jardetzky, O.; Wertz, J.E.; J. Am. Chem. Soc., 1960, **82**, 318-323.

71) Grotens, A.M.; Smid, J.; de Boer, E.; Chem. Commun., 1971, 759-760.

72) Templeman, G.J.; Van Geet, A.L.; J. Am. Chem. Soc., 1972, **94**, 5578-5582.

73) Mei, E.; Dye, J.L.; Popov, A.I.; J. Am. Chem. Soc., 1977, **99**, 5308-5311.

74) Mei, E.; Popov, A.I.; Dye, J.L.; J. Phys. Chem., 1977, **81**, 1677-1681.

75) Soong, L.-L.; Leroi, G.E.; Popov, A.I.; Inorg. Chem., 1990, **29**, 1366-1370.

76) Strasser, B.O.; Shamsipur, M.; Popov, A.I.; J. Phys. Chem., 1985, **89**, 4822-4824.

77) Smetana, A.J.; Popov, A.I.; J. Soln. Chem., 1980, **9**, 183-196.

78) Lehn, J.-M.; Sauvage, J.-P.; Dietrich, B.; J. Am. Chem. Soc., 1970, **92**, 2916-2918.

79) Live, D.; Chan, S.I.; J. Am. Chem. Soc., 1976, **98**, 3769-3778.

80) Echegoyen, L.; Kaifer, A.; Durst, H.D.; Gokel, G.W.; J. Org. Chem., 1984, **49**, 688-690.

81) Echegoyen, L.; Kaifer, A.; Durst, H.; Schultz, R.A.; Dishong, D.M.; Goli, D.M.; Gokel, G.W.; J. Am. Chem. Soc., 1984, **106**, 5100-5103.

82) Buchanan, G.W.; Khan, M.Z.; Ripmeester, J.A.; Bovenkamp, J.W.; Rodrigue, A.; Can. J. Chem., 1987, **65**, 2564-2567.

83) de Boer, J.A.A.; Reinhoudt, D.N.; Harkema, S.; van Hummel, G.J.; de Jong, F.; J. Am. Chem. Soc., 1982, **104**, 4073-4076.

84) Mosier-Boss, P.A.; Popov, A.I.; J. Am. Chem. Soc., 1985, **107**, 6168-6174.

85) Chen, Z.; Dettman, H.D.; Detellier, C.; Polyhedron, 1989, **8**, 2029-2033.

86) Boss, R.D.; Popov, A.I.; Inorg. Chem., 1985, **24**, 3660-3664.

87) Schmidt, E.; Popov, A.I.; J. Am. Chem. Soc., 1983, **105**, 1873-1878.

88) Shih, J.S.; Popov, A.I.; Inorg. Nucl. Chem. Letters, 1977, **13**, 105-110.

89) Delville, A.; Stöver, H.D.H.; Detellier, C.; J. Am. Chem. Soc., 1987, **109**, 7293-7301.

90) Stöver, H.D.H.; Detellier, C.; J. Phys. Chem., 1989, **93**, 3174-3178.

91) Stöver, H.D.H.; Delville, A.; Detellier, C.; J. Am. Chem. Soc., 1985, **107**, 4167-4172.

92) Delville, A.; Stöver, H.D.H.; Detellier, C.; J. Am. Chem. Soc., 1985, **107**, 4172-4175.

93) Strasser, B.O.; Hallenga, K.; Popov, A.I.; J. Am. Chem. Soc., 1985, **107**, 789-792.

94) Strasser, B.O.; Popov, A.I.; J. Am. Chem. Soc., 1985, **107**, 7921-7924.

95) Brière, K.M.; Detellier, C.; J. Phys. Chem., 1987, **91**, 6097-6099.

96) Brière, K.M.; Detellier, C.; New J. Chem., 1989, **13**, 145-149.

97) Lincoln, S.F.; White, A.; Hounslow, A.M.; J. Chem. Soc. Faraday Trans. I, 1987, **83**, 2459-2466.

98) Graves, H.P.; Detellier, C.; J. Am. Chem. Soc., 1988, **110**, 6019-6024.

99) Buschmann, H.-J.; J. Incl. Phen. & Mol. Rec., 1989, **7**, 581-588.

100) Inoue, Y.; Hakushi, T.; J. Chem. Soc. Perkin Trans. II, 1985, 935-946.

101) Okoroafor, N.O.; Popov, A.I.; Inorg. Chim. Acta, 1988, **148**, 91-96.

102) Phillips, R.C.; Khazaeli, S.; Dye, J.L.; J. Phys. Chem., 1985, **89**, 600-606.

103) Erlich, R.H.; Popov, A.I.; J. Am. Chem. Soc., 1971, **93**, 5620-5623.

104) Greenberg, M.S.; Bodner, R.L.; Popov, A.I.; J. Phys. Chem., 1973, **77**, 2449-2454.

105) Cox, B.G.; van Truong, N.; Garcia-Rosas, J.; Schneider, H.; Inorganica Chimica Acta, 1983, **77**, L155-L158.

106) Brière, K.M.; Ph.D. thesis, University of Ottawa, 1990.

107) Kintzinger,J.P.; Lehn, J.M.; J. Am. Chem. Soc., 1974, **96**, 3313-3314.

108) Bisnaire, M.; Detellier, C.; Nadon, D.; Can. J. Chem., 1982, **60**, 3071-3076.

109) Detellier, C.; Robillard, M.; Can. J. Chem., 1987, **65**, 1684-1687.

110) Eliasson, B.; Larsson, K.M.; Kowalewski, J.; J. Phys. Chem., 1985, **89**, 258-261.

111) Dunitz, J.D.; Dobler, M.; Seiler, P.; Phizackerley, R.P.; Acta Cryst., 1974, **B30**, 2733-2738.

112) Dunitz, J.D.; Seiler, P.; Acta Cryst., 1974, **B30**, 2739-2741.

113) Dobler, M.; Dunitz, J.D.; Seiler, P.; Acta Cryst., 1974, **B30**, 2741-2743.

114) Seiler, P.; Dobler, M.; Dunitz, J.D.; Acta Cryst., 1974, **B30**, 2744-2745.

115) Dobler, M.; Phizackerley, R.P.; Acta Cryst., 1974, **B30**, 2746-2748.

116) Dobler, M.; Phizackerley, R.P.; Acta Cryst., 1974, **B30**, 2748-2750.

117) Rogers, R.D.; Richards, P.D.; J. Incl. Phen., 1987, **5**, 631-638.

118) Rogers, R.D.; Green, L.M.; J. Incl. Phen., 1986, **4**, 77-84.

119) Rogers, R.D.; Richards, P.D.; Voss, E.J.; J. Incl. Phen., 1988, **6**, 65-71.

120) Garrell, R.L.; Smyth, J.C.; Fronczek, F.R.; Gandour, R.D.; J. Incl. Phen., 1988, **6**, 73-78.

121) Rogers, R.D.; J. Incl. Phen., 1988, **6**, 629-645.

122) Buchanan, G.W.; Kirby, R.A.; Ripmeester, J.A.; Ratcliffe, C.I.; Tetrahedron Lett., 1987, **28**, 4783-4786.

123) Rodrigue, A.; Bovenkamp, J.W.; Murchie, M.P.; Buchanan, G.W.; Fortier, S.; Can. J. Chem., 1987, **65**, 2551-2557.

124) Buchanan, G.W.; Morat, C.; Ratcliffe, C.I.; Ripmeester, J.A.; J. Chem. Soc., Chem. Commun., 1989, 1306-1308.

125) Damewood, J.R.; Anderson, W.P.; Urban, J.J.; J. Comput. Chem., 1988, **9**, 111-124.

126) Friedman, J.M.; Rousseau, D.L.; Shen, C.; Paul, I.C.; J. Chem. Soc., Chen. Commun., 1977, 684-686.

127) Riddick, J.A.; Bunger, W.B.; Sakano, T.K.; Techniques of Chemistry, vol.2: organic solvents - Properties and Methods of Purification, 4th edition, 1986, 1325 pages.

128) Berger, J.; Rachlin, A.I.; Scott, W.E.; Sternbach, L.H.; Goldberg, M.W.; J. Am. Chem. Soc., 1951, **73**, 5295-5298.

129) Johnson, S.M.; Herrin, J.; Liu, S.J.; Paul, I.C.; Chem. Commun., 1970, 72-73.

130) Maier, C.A.; Paul, I.C.; J. Chem. Soc. Chem. Commun., 1971, 181-182.

131) Bissell, E.C.; Paul, I.C.; J. Chem. Soc. Chem. Commun., 1977, 967-968.

132) Suh, I.-H.; Aoki, K.; Yamazaki, H.; Inorg. Chem., 1989, **28**, 358-362.

133) Chiang, C.C.; Paul, I.C.; Science, 1977, **196**, 1441-1443.

134) Smith, G.D.; Duax, W.L.; Fortier, S.; J. Am. Chem. Soc., 1978, **100**, 6725-6727.

135) Patel, D.J.; Shen, C.; Proc. Natl. Acad. Sci. U.S.A., 1976, **73**, 1786-1790.

136) Shen, C.; Patel, D.J.; Proc. Natl. Acad. Sci. U.S.A., 1976, **73**, 4277-4281.

137) Anteunis, M.J.O.; Bioorg. Chem., 1976, **5**, 327-337.

138) Agtarap, A.; Chamberlin, J.W.; Pinkerton, M.; Steinrauf, L.; J. Am. Chem. Soc., 1967, **89**, 5737-5739.

139) Degani, H.; Biophys. Chem., 1977, **6**, 345-349.

140) Schmidt, P.G.; Wang, A.H.-J.; Paul, I.C.; J. Am. Chem. Soc., 1974, **96**, 6189-6191.

141) (a) Haney, M.E. Jr.; Hoehn, M.M.; Antimicrobial Agents and Chemotherapy, 1967, 349-352.
(b) Stark, W.M.; Knox, N.G.; Westhead, J.E.; *ibid*, 1967, 353-358.
(c) Agtarap, A.; Chamberlin, J.W.; *ibid*, 1967, 359-362.
(d) Gorman, M.; Chamberlin, J.W.; Hamill, R.L.; *ibid*, 1967, 363-368.
(e) Shumard, R.F.; Callender, M.E.; *ibid*, 1967, 369-377.

142) Duax, W.L.; Smith, G.D.; Strong, P.D.; J. Am. Chem. Soc., 1980, **102**, 6725-6729.

143) Pangborn, W.; Duax, W.L.; Langs, D.; J. Am. Chem. Soc., 1987, **109**, 2163-2165.

144) Sankaram, M.B.; Shastri, B.P.; Easwaran, K.R.K.; Biochem., 1987, **26**, 4936-4941.

145) Shastri, B.P.; Sankaram, M.B.; Easwaran, K.R.K.; Biochem., 1987, **26**, 4925-4930.

146) Fernandez, E.; Grandjean, J.; Laszlo, P.; Eur. J. Biochem., 1987, **167**, 353-359.

147) Amat, E.; Cox, B.G.; Schneider, H.; J. Magn. Reson., 1987, **71**, 259-270.

148) Haynes, D.H.; Pressman, B.C.; Kowalsky, A.; Biochem., 1971, **10**, 852-860.

149) Gertenbach, P.G.; Popov, A.I.; J. Am. Chem. Soc., 1975, **97**, 4738-4744.

150) Cox, B.G.; van Truong, N.; Rzeszotarska, J.; Schneider, H.; J. Am. Chem. Soc., 1984, **106**, 5965-5969.

151) Amat, E.; Cox, B.G.; Rzeszotarska, J.; Schneider, H.; J. Am. Chem. Soc., 1988, **110**, 3368-3372.

152) Cox, B.G.; Firman, P.; Schneider, H.; J. Am. Chem. Soc., 1985, **107**, 4297-4300.

153) Hoogerheide, J.G.; Popov, A.I.; J. Soln. Chem., 1978, 7, 357-372.

154) Shungu, D.C.; Briggs, R.W.; J. Magn. Reson., 1988, 77, 491-503.

155) Behr, J.-P.; Girodeau, J.-M.; Hayward, R.C.; Lehn, J.-M.; Sauvage, J.-P.; Helv. Chim. Acta, 1980, **63**, 2096-2111.

156) Daly, J.J.; Schönholzer, P.; Behr, J.-P.; Lehn, J.-M.; Helv. Chim. Acta, 1981, **64**, 1444-1451.

157) Behr, J.-P.; Lehn, J.-M.; Vierling, P.; Helv. Chim. Acta, 1982, **65**, 1853-1867.

158) Dutton, P.J.; Fyles, T.M.; McDermid, S.J.; Can. J. Chem., 1988, **66**, 1097-1108.

159) Dutton, P.J.; Fyles, T.M.; Hansen, S.P.; J. Incl. Phen., 1989, 7, 173-182.

160) Private communication, T.M. Fyles.

161) Adamic, R.J.; Eyring, E.M.; Petrucci, S.; Bartsch, R.A.; J. Phys. Chem., 1985, **89**, 3752-3757.

162) Farber, H.; Petrucci, S.; J. Phys. Chem., 1981, **85**, 1396-1401.

163) Dunitz, J.D.; Seiler, P.; Acta Cryst., 1974, **B30**, 2750-2750.

164) Bryant, R.G.; J. Am. Chem. Soc., 1969, **91**, 1870-1871.

165) Bouhoutsos-Brown, E.; Murk Rose, D.; Bryant, R.G.; J. Inorg. Nucl. Chem., 1981, **41**, 2247-2248.

166) James, D.W.; Cutler, P.G.; Aust. J. Chem.; 1986, **39**, 137-147.

167) Drakenberg, T.; Acta Chem. Scand., 1982, **A36**, 79-82.

168) Cox, B.G.; Firman, P.; Schneider, H.; Inorg. Chim. Acta, 1983, **69**, 161-166.

169) Cox, B.G.; van Truong, N.; Garcia-Rosas, J.; Schneider, H.; J. Phys. Chem., 1984, **88**, 996-1001.

170) Cox, B.G.; van Truong, N.; Schneider, H.; J. Am. Chem. Soc., 1984, **106**, 1273-1280.

171) Cox, B.G.; Stroka, J.; Schneider, H.; Inorg. Chim. Acta, 1987, **128**, 207-213.

172) Kitano, H.; Hasegawa, J.; Iwai, S.; Okubo, T.; J. Phys. Chem., 1986, **90**, 6281-6284.

173) Morel-Desrosiers, N.; Morel, J.-P.; J. Phys. Chem., 1985, **89**, 1541-1546.

174) Morel-Desrosiers, N.; Morel, J.-P.; Nouv. J. Chim., 1985, **9**, 629-631.

175) Andersson, A.; Drakenberg, T.; Forsén, S.; Thulin, E.; Swärd, M.; J. Am. Chem. Soc., 1982, **104**, 576-580.

176) Forsén, S.; Andersson, A.; Drakenberg, T.; Thulin, E.; Swärd, M.; Fed. Proc., 1982, **41**, 2981-2986.

177) Shimizu, T.; Hatano, M.; Inorg. Chim. Acta, 1988, **152**, 257-260.

178) Juillard, J.; Tissier, C.; Jeminet, G.; J. Chem. Soc., Faraday Trans I, 1988, **84**, 951-958.

179) Pointud, Y.; Juillard, J.; J. Chem. Soc., Faraday Trans I, 1988, **84**, 959-967.

180) Pointud, Y.; Passelaigue, E.; Juillard, J.; J. Chem. Soc., Faraday Trans I, 1988, **84**, 1713-1722.

181) Cox, B.G.; van Truong, N.; Rzeszotarska, J.; Schneider, H.; J. Chem. Soc., Faraday Trans I, 1984, **80**, 3275-3284.

182) Bolte, J.; Demuynck, C.; Jeminet, G.; Juillard, J.; Tissier, C.; Can. J. Chem., 1982, **60**, 981-989.

183) Cox, B.G.; Firman, P.; Schneider, I.; Schneider, H.; Inorg. Chem., 1988, **27**, 4018-4021.

184) Dale, J.; Kristiansen, P.O.; Acta Chem. Scand., 1972, **26**, 1471-1478.

185) Conway, B.E.; Angerstein-Kozlowska, H.; Sharp, W.B.A.; Criddle, E.E.; Anal. Chem., 1973, **45**, 1331-1336.

186) Gokel, G.W.; Cram, D.J.; Liotta, C.L.; Harris, H.P.; Cook, F.L.; Org. Synth., 1977, **57**, 30-33.

187) Anantanarayan, A.; Carmichael, V.A.; Dutton, P.J.; Fyles, T.M.; Pitre, M.J.; Synth. Commun., 1986, **16**, 1771-1776.

188) Varian Magnetic Moments, 1987, **3**, 12.

189) Sandström, J.; Dynamic NMR Spectroscopy, Academic Press: New York, 1982.

190) Deming, S.N.; Morgan, S.S.; Anal. Chem., 1973, **45A**, 278-282.

191) Reference 189, p.109.